UNIVERSITÀ DEGLI STUDI
DI MODENA E REGGIO EMILIA

Dottorato di ricerca in Modellistica, simulazione computazionale e caratterizzazione multiscala per le scienze dei materiali e della vita

(nell'ambito della Scuola di dottorato in Modellistica, simulazione computazionale e caratterizzazione multiscala per le scienze dei materiali e della vita)

Ciclo XXVI

Study and Development of Advanced Materials for Architecture and Construction: Preparation and Characterization of TiO_2 Coatings for Building Materials

(Studio e sviluppo di materiali avanzati per l'architettura e l'edilizia: preparazione e caratterizzazione di rivestimenti di TiO_2 per materiali da costruzione)

Candidato: M. Sc. Erika Iveth Cedillo González Erika Cedillo

Relatore: Prof. Cristina Siligardi

Correlatore: Dott.ssa Monia Montorsi PhD

Coordinatore del Dottorato: Prof. Ledi Menabue

Direttore della Scuola di dottorato: Prof. Ledi Menabue

El mejor día es aquel en el que el alma tiene hambre y sed
No olvides lo aprendido, no dejes de comprender,
Rodéate de buenos y tú lo parecerás,
Rodéate de sabios y algo en ti se quedará...

La danza del fuego, Mägo de Oz

Acknowledgements

Con estas líneas quiero agradecer antes que a nadie a mi Señor, que con cada paso que he dado en esta vida me ha conducido al cumplimiento de uno de mis mayores anhelos, el de llegar a convertirme en Doctora algún día. Gracias Padre.

También a Él agradezco que me haya dado unos padres maravillosos, que me han apoyado en cada decisión que he tomado en mi camino, aún cuando éstas significaran el tenerme lejos de ellos por un largo tiempo... Gracias Pá y Má, por favor no olviden nunca que con cada una de sus porras, consejos y a veces regaños ustedes me llevaron de la mano a la realización de este nuevo evento que yo considero un éxito en mi vida.

Gracias a Danny que con sus chistes y competencias entre hermanos me ha siempre apoyado aunque él no lo sepa.

Mi más sincero agradecimiento a Italia, que a través de la Università degli Studi di Modena e Reggio Emilia me ha dado la oportunidad de estudiar un doctorado becada.

Gracias a la Prof. Cristina Siligardi y a la Prof. Monia Montorsi por recibirme en su grupo de investigación, y por darme todas esas grandes y maravillosas oportunidades de conocer el mundo y la investigación que se realiza en él. Mil gracias por compartir conmigo sus conocimientos y experiencias.

Agradezco al Dr. Paolo Falcaro por recibirme en su grupo de investigación dentro del Commonwealth Scientific and Industrial

Research Organization en Australia, y al Dr. Raffaele Riccò que me ayudó con la experimentación cuando estuve en su laboratorio. A ambos agradezco toda su ayuda y su intercambio de conocimientos conmigo.

Igualmente agradezco a la Dra. Leticia M. Torres-Martínez y al Dr. Isaías Juárez Ramírez por recibirme en el Laboratorio de Ecomateriales y Energía de la Universidad Autónoma de Nuevo Léon, México.

Gracias a los chicos del DIEF y a todas las lindas personas que he conocido en Italia y que me han ayudado a sobrellevar la nostalgia de mi hogar.

Aprovecho también esta ocasión para agradecer a una persona que ha hecho grandes aportaciones a mi vida académica desde que la conocí allá por el 2006: Dra. Bertha, mil gracias por toda su colaboración, amistad y apoyo, usted ha sido mi guía y uno de mis ejemplos durante todo este tiempo.

Finalmente, quiero expresar mi profundo agradecimiento a la persona que me ha acompañado durante estos tres años: mi amado Paolo, gracias a ti he podido cumplir uno de los sueños más grandes de mi vida, y gracias a ti también este sueño se ha cumplido con un extra: tu amor!!! Gracias amorcito.

Erika Cedillo

Febrero 9, 2014

TABLE OF CONTENTS

THESIS OUTLINE

In this work, the preparation and characterization of several kinds of anatase TiO_2 coatings was carried out with the aim of promoting the application of these materials inside the Italian building sector. One of the benefits of these materials is their so-called self-cleaning effect, which is based in two phenomena that occurs in the TiO_2 surface when irradiated with UV light: the photo-oxidation of pollutants and the superhydrophilicity. Since this self-cleaning effect can keep buildings clean effortlessly, it can reduce the amount of detergents and cleaning water needed for maintenance and improves environmental conservation. Although much research has been carried out in this field and several companies have released self-cleaning materials, their practical integration in buildings is still an open issue. The production costs associated to the existing deposition technologies and the difficulties correlated with the performance of these materials when exposed to real conditions, represent to date the main limitations to their diffusion on a large scale. In this thesis, the study and development of advanced (functional) materials for architecture and construction was carried out. Particularly, the research was divided in two principal aspects: (i) issues associated with the production of TiO_2 self-cleaning materials and (ii) limitations associated with the utilization of self-cleaning coatings at real conditions.

CHAPTER 1

INTRODUCTION

1. Introduction

Since the discovery of the phenomenon of photo-splitting of water in a titanium dioxide (TiO_2) anode photochemical cell by Fujishima and Honda [1], the fundamentals and applications of photocatalytic oxidation (PCO) reaction have received significant attention. As a consequence, the research in the photocatalysis field has derived in the development of new technologies that have proved to possess great potential in sectors such as environmental remediation or building industry [2-5]. In this latter, several semiconductor photocatalytic oxides such as titanium dioxide, zinc oxide or doped-titanium dioxide [2, 4, 6-9] have been combined with building materials with the aim of obtaining functional construction components with self-cleaning characteristics. These materials are expected not only to improve the quality of the surrounding environment by gradual degradation of pollutants, but also to keep the aesthetic characteristics of the facades of buildings for long periods of time without the need of the actual (usually expensive and dangerous) maintenance procedures.

It is clear that functional semiconductor-based building materials have a huge potential as commercial products. Indeed, some of this potential is already being realized: several self-cleaning building products prepared from semiconductor photocatalysts are currently being commercialized by multinational companies such as TOTO, Pilkington, Pittsburgh Plate Glass (PPG) Industries, Cardinal Glass Industries, Saint-Gobain, Nippon Sheet Glass (NSG), etc.

Although all these companies have released self-cleaning materials, their practical integration in buildings components is still an open issue. The high production costs associated to the existing vacuum deposition technologies, as well as the difficulties correlated with the efficiency of these materials when exposed to real conditions, represent to date the main limitations to their diffusion on a large scale [3, 10, 11]. Therefore, in this research, the study and development of advanced (functional) materials for architecture and construction was carried out. Particularly, the attention was focused on the preparation and characterization of TiO_2 coatings for building materials.

1.1. Basic principles of semiconductor photocatalysis

Semiconductors such as TiO_2, ZnO, Fe_2O_3, CdS and ZnS can act as sensitizers for light-reduced redox processes due to their electronic structure. This is characterized by a manifold of electron energy levels filled with electrons and, at higher energy, a manifold of largely vacant electron energy levels. These energy levels are called the valence band (VB) and the conduction band (CB), respectively. The energy

difference between these two bands is called the bandgap, E_g [2, 12]. **Figure 1.1** illustrates the basic electron energy features of a semiconductor material.

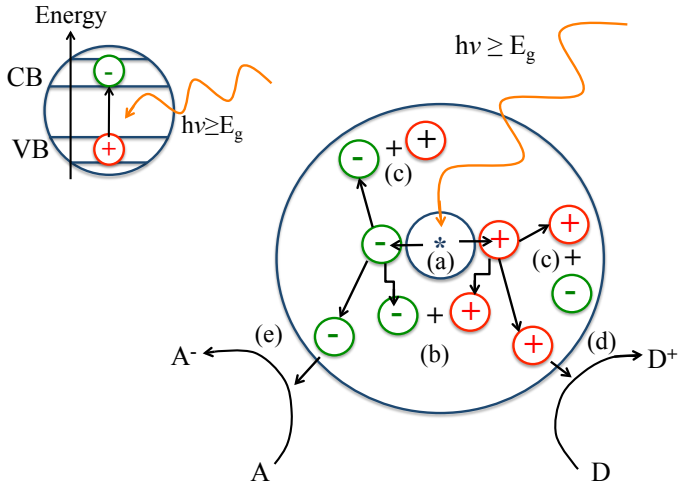

Figure 1.1. Schematic illustration of the major processes that occur on a semiconductor particle upon absorption of an ultra-bandgap light. (a) Adsorption of a photon and creation f an electron-hole pair; (b) bulk recombination; (c) surface recombination; (d) oxidation of an electron donor (D) adsorbed on the surface by the photogenerated hole and (e) reduction of an electron acceptor adsorbed on the surface by the photogenerated electron. Taken from *Mills and Lee, J. Photochem. Photobiol. A 2002;152:233-247* [2].

The adsorption of a photon of ultra-bandgap light, i.e. $h\nu \geq E_g$, promotes the transfer of an electron from the valence band to the conduction band (e^-), leaving behind a positive hole (h^+), as observed in the process (a) from **Figure 1.1**. After its generation, the electron-hole pair can recombine in the bulk or in the surface to generate heat (processes (b) and (c) in **Figure 1.1**) or interact with adsorbed surface species. If an electron donor, i.e. D, is present at the surface, then the photogenerated hole can react with it to generate an oxidised product, D^+ (process (d) in **Figure 1.1**). Similarly, if there is an electron acceptor present at the surface, i.e. A, then the

photogenerated conductance band electron can react with it to generate a reduced product, A^- (process (e) in **Figure 1.1**) [2, 4, 13, 14]. The overall reaction can be summarised as follows:

$$A + D \xrightarrow{semicinductor, hv \geq E_{BG}} A^- + D^+ \quad [1.1]$$

If the change in Gibbs free energy for **Reaction [1.1]** is positive, the overall process is an example of semiconductor photosynthesis. If, as is more usually the case, the change in Gibbs free energy is negative, then it is an example of semiconductor photocatalysis [2].

As mentioned above, semiconductor photocatalysis is currently undergoing heavy commercial exploitation [2-9]. Many of the current systems that utilise **Reaction [1.1]** employ the semiconductor photocatalyst to drive oxidation of organic pollutants by oxygen, i.e.

$$organic + O_2 \xrightarrow{semicinductor, hv \geq E_{BG}} CO_2 + H_2O + mineral\ acids \quad [1.2]$$

If organic oxidation drive by illuminated TiO_2 is completed up to obtaining carbon dioxide, water and mineral acids, the process is called photomineralisation or photocatalytic activity (PCA).

Although there are many semiconducting materials in this world, only a few are very effective as semiconductor photocatalysts. Ideally, a semiconductor photocatalyst should be chemically and biologically inert, photocatalytically active, easy to produce and use, activated by sunlight and cheap [2]. In fact, not surprisingly, no semiconductor fits this list of ideals, although one semiconductor, titanium dioxide, comes close. Then, this work was focused on the use of TiO_2 as photocatalyst semiconductor for building materials.

1.2. TiO_2 semiconductor photocatalyst

In photocatalysis, TiO_2 is by far the most widely studied semiconductor due to its high activity, desirable physical and chemical properties, low cost, and availability. Of three common TiO_2 crystalline forms, anatase and rutile forms have been investigated extensively as photocatalysts. Anatase has been reported to be more active and easy to produce as a photocatalyst than rutile [2, 15]. It large band gap, E_g ~ 3.2-3.0 eV, permits it only to absorb UV light and, as a consequence, is limited to absorbing a small fraction (ca. 5%) of the solar spectrum [2].

Despite this substantial limitation, its positive features far outweigh this one negative, and so anatase TiO_2 has become the semiconducting material to use in the field of semiconductor photocatalysis [2]. Indeed, TiO_2 photocatalysis technology can be applied even using solar light, since there exists typically several hundred W/cm^2 of UV light even in outdoor shade in the daytime. Although this is low from the viewpoint of energy density, corresponds to about 10^{15} of photons/cm^2 per

second (with a typical UV flux of 20-30 W m^{-2}) which is a huge amount compared to the number of pollutant molecules adsorbed on the surface [5, 15].

1.2.1. Photocatalytic oxidation of organics (PCO)

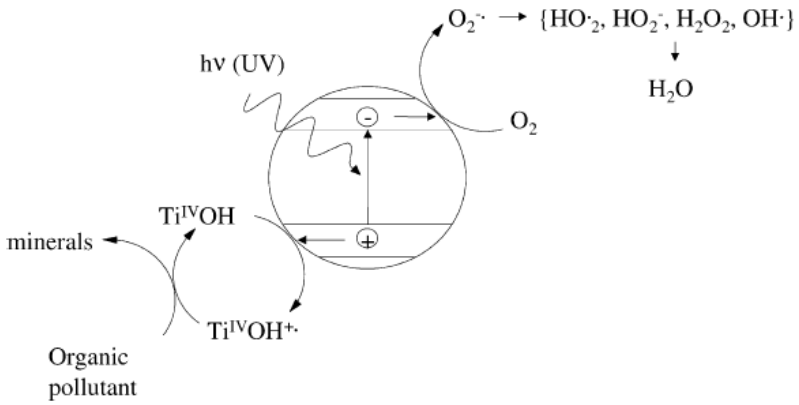

Figure 1.2. Schematic illustration of the major processes associated with the photocatalytic oxidation of organics sensitized by a TiO_2 semiconductor particle. Ultra-bandgap light generates electron-hole pairs. Photogenerated holes that make it to the surface can react with surface hydroxyl groups to generate adsorbed hydroxyl radicals ($TiOH^{\bullet+}$) which, in turn, can oxidise the pollutant to its mineral form. Photogenerated electrons that make it to the surface can react with adsorbed oxygen to generate superoxide, which can be subsequently reduced to hydrogen peroxide and then water. The intermediate species produced can act as a further source of hydroxyl radicals, OH•. Taken from *Mills and Lee, J. Photochem. Photobiol. A 2002;152:233-247* [2].

In the photooxidation of organic materials sensitised by titanium dioxide, i.e. **Reaction (1.2)**, the photogenerated electrons reduce water to oxygen and the photogenerated holes mineralise the organic. The latter process appears to involve the initial oxidation of adsorbed surface hydroxyl groups on the TiO_2 to hydroxyl radicals (OH•), which then oxidise the organic and any subsequent intermediate, or

intermediates [2]. The reduction of oxygen by the photogenerated electrons generates superoxide, O_2^- as initial reduction product. The latter specie can be further reduced to hydrogen peroxide (H_2O_2), as an intermediate in the overall reduction of oxygen to water. Hydrogen peroxide is, of course, also a possible source of hydroxyl radicals and it appears likely that during the course of **Reaction (1.2)** some of the mineralisation of organic pollutant is brought by oxidising species, such as hydroxyl radicals, generated via the reduction of oxygen by the photogenerated electrons [2]. The overall processes in the photomineralisation of organics pollutants over TiO_2 are illustrated in **Figure 1.2**.

1.2.2. Superhydrophilicity

In terms of commercial success, probably the biggest impact of semiconductor photocatalysis is in the area of semiconductor photoinduced superhydrophilicity. In this process, ultra-band gap generates an electron-hole pair that can either recombine or react with surface species. In the case of TiO_2, in the absence of any appreciable level of adsorbed competing species such as an organic, the surface species available for reaction appear to be Ti(IV) and bridging O^{2-} groups. As a consequence, hydrophilic surface Ti(III) species are generated via the reduction of the surface Ti(IV) species by the photogenerated electrons, and, oxygen vacancies are generated via the oxidation of the bridging O^{2-} species to oxygen by the photogenerated holes. Hydroxyl ions subsequently absorb and fill the oxygen vacancies, with the result that the hydrophilic nature of the surface is increased. The process is reversed, usually slowly in the dark, as the Ti(III) are oxidised back to Ti(IV) by ambient oxygen, and

the vacancies filled by the O^{2-} ions generated as a consequence of the oxidation reaction. **Figure 1.3** illustrates these major processes behind the phenomenon of superhydrophilicity, which appears to be alms exclusive to titanium dioxide [2].

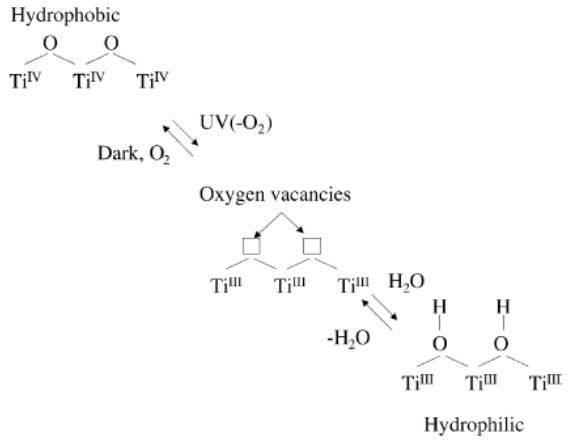

Figure 1.3. Schematic illustration of the major processes associated with the photoinduced superhydrophilic property of TiO_2. UV excitation of the semiconductor creates electron-hole pairs. The holes can oxidise bridging O^{2-} species on the surface to oxygen, thereby creating vacancies. The photogenerated electrons can reduce the Ti(IV) atoms to Ti(III). Dissociative adsorption of water onto the irradiated surface hydroxylates it and renders it considerably more hydrophilic. The process is reversed in the dark as oxygen oxidises the Ti(III) species present and the reduced oxygen fills the bridging oxygen vacancies. Taken from *Mills and Lee, J. Photochem. Photobiol. A 2002;152:233-247* [2].

As a consequence of superhydrophilicity, thin films of titanium dioxide are rendered much more wettable upon exposure to UV light. Interestingly, this process appears to have a high quantum yield at low light levels and thus can be affected by the low UV light levels found indoors (from fluorescent light strips) as well as outside (from the sun). Certainly, the component of UV light in sunlight is sufficient to render titanium

dioxide coated surfaces very wettable, i.e. the water film contact angle for a TiO_2 film falls from about 60-40° to ca. 0° upon its exposure to ultra-band gap light.

1.2.3. TiO_2 self-cleaning property

Nowadays, it is generally accepted that the self-cleaning property of TiO_2 is explained by the previous two photochemical phenomena that occur on its surface under illumination (PCO and superhydrophilicity) [3]. The self-cleaning action arises from the fact that any dirt and grime that usually collects on a surface are readily washed away on a very hydrophilic surface such as that afforded by UV-activated thin (< 30 nm), transparent nanocrystalline film of TiO_2 deposited on the surface. In addition, such thin semiconductor coatings can also destroy such organic deposits via photocatalytic oxidation, which is an additional self-cleaning action since such organic deposits usually act as sites of soot and grime to collect. Thus, a thin, transparent coating of titanium dioxide on a surface, upon exposure to sunlight, can stay cleaner longer than non photocatalyst-coated traditional surfaces. In addition, such material will no longer appear to fog, since the latter us characteristic of surfaces with high (> 20°) water contact angles [2].

1.3. Application of self-cleaning TiO_2 surfaces

Watanabe, Hashimoto and Fujishima were the firsts to demonstrate the self-cleaning concept on a titania TiO_2-coated ceramic tile in 1992 [16]. A similar idea was conceived independently by Heller in 1995 [17].

One of the first commercialized products using this technique was the self-cleaning cover glass for highway tunnel lamps in Japan. This type of lamp (often a sodium lamp in Japan) emits UV light of about 3 mW cm^{-2} at the position of the cover glass. This UV light is of no use for lighting, but it is sufficient to decompose the contamination from exhaust compounds. As a result, the cover glass can maintain transparency for long-term use [8]. Unfortunately, it is known that the efficiency of self-cleaning surfaces is dependent on the relative rates of decontamination vs. contamination. This means that the TiO_2 photocatalyst can maintain the surface clean *only* when the photocatalytic decontamination rate is greater than that of contamination. Wang et al. [18], however, observed that the self-cleaning effect of TiO_2 surfaces could be enhanced when water flow, such as natural rainfall, is applied to the surface and attributed this phenomenon to the superhydrophilic property of TiO_2 surface. Thus, this phenomenon effectively removed the limitation of the self-cleaning function of TiO_2 photocatalysis set by the number of incident photons. Even though the number of photons may be insufficient to decompose the adsorbed stain, the surface is maintained clean when water is supplied there. Thus, Wang and co-workers suggested that the best use of self-cleaning TiO_2 surfaces should be exterior construction materials, since these materials could be exposed to abundant sunlight and natural rainfall. Following this advisement, self-cleaning TiO_2 surfaces have been applied in a large number of buildings by architects. Some examples include the Cowboy Stadium in Dallas (U.S.) [19]; the Glass Tree House in MacMaster Beach (Australia) [19, 20]; the Fergammana Officies in Mantova (Italy) [21]; OLIMP Shopping Centre in Lublin (Poland) [20] and the MSV Arena in Duisburg (Germany)

[20]. However, even today, several practical limitations correlated with the obtaining of efficient products and their efficiencies at real conditions still prevent the widespread use of photocatalytic self-cleaning materials in the building sector, which is strongly commanded by the final consumers.

In this research, investigations regards these limitations were carried out with the aim of promoting a widespread use of TiO_2-based self-cleaning materials in the building industry. The research was divided in two principal aspects: (i) issues associated with the production of TiO_2 self-cleaning materials and (ii) limitations associated with the utilization of self-cleaning coatings at real conditions.

1.4. References

[1]. Fujishima, A.; Honda, K. *Electrochemical photolysis of water at a semiconductor electrode*. Nature **1972**;238:37.

[2]. Mills, A.; Lee, S.-K. *A web-based overview of semiconductor photochemistry-based current commercial applications*. J. Photochem. Photobiol. A **2002**;152:233.

[3]. Chen, J.; Poon, C.-s. *Photocatalytic construction and building materials: From fundamentals to applications*. Build. Environ. **2009**;44:1899.

[4]. Fujishima, A.; Zhand, X.; Tryk, D. A. *TiO_2 photocatalysis and related surface phenomena*. Surf. Sci. Rep. **2008**;63:515.

[5]. Hashimoto, K.; Irie, H.; Fujishima, A. *TiO_2 photocatalysis: a historical overview and future prospects*. Jpn. J. Appl. Phy.s **2005**;44:8269.

[6]. Badre., C.; Pauporté, T.; Turmine, M.; Dubot, P.; Lincot, D. *Water-repellent ZnO nanowires films obtained by octadecylsilane self-assembled monolayers.* Physica E **2008**;40:2454.

[7]. Wu, J.; Xia, J.; Lei, W.; Wang, B.-p. *Fabrication of superhydrophobic surfaces with double-scale roughness*. Mater. Lett. **2010**;64:1251.

[8]. Kesmez, Ö.; Camurlu, H. E.; Burunkaya, E.; Arpac, E. *Sol-gel preparation and characterization of anti-reflective self-cleaning SiO_2-TiO_2 double-layer nanometric films*. Sol. Energy Mater. Sol. Cells **2009**;93:1833.

[9]. Guan, K. *Relationship between photocatalytic activity, hydrophilicity and self-cleaning effect of TiO_2/SiO_2 films*. Surf. Coatings Technol. **2005**;191:155.

[10]. Cannavale, A.; Fiorito, F.; Manca, M.; Tortorici, G.; Cingolani, R.; Gigli, G. *Multifunctional bioinspired sol-gel coatings for architectural glasses*. Build. Environ. **2010**;45:1233.

[11]. Cedillo-González E. I.; Riccò, R.; Montorsi, M.; Montorsi, M.; Falcaro, P.; Siligardi, C. *Self-cleaning glass prepared from a commercial TiO_2 nano-dispersion and its photocatalytic performance under common anthropogenic and atmospheric factors*. Build. Environ. **2014**;71:7.

[12]. Hoffmann, M. R.; Martin, S. T.; Choi, W.; Bahnemann, D. W. *Environmental applications of semiconductor photocatalysis*. Chem. Rev. **1995**;95:69.

[13]. Gaya, U. I.; Abdullah, A.H. *Heterogeneous photocatalytic degradation of organic contaminants over titanium dioxide: a review of fundamentals, progress and oroblems.* J. Photochem. Photobiol. C **2008**;9:1.

[14]. Wang, S.; Ang, H. M.; Tade, M. O. *Volatile organic compounds in indoor environment and photocatalytic oxidation: state of the art*. Environ. Int. **2007**;33:694.

[15]. Ahmed, S.; Rasul, M. G.; Brown, R.; Hashib, M. A. *Influence of parameters on the heterogeneous photocatalytic degradation of pesticides and phenolic contaminant in wastewater: A short review*. J. Environ. Manage. **2011**;92:311.

[16]. Watanabe, T.; Hashimoto, K.; Fujishima, A. *1st International Conference on TiO_2 Photocatalytic Purification and Treatment of Water and Air*, **1992**.

[17]. Heller, A. *Chemistry and applications of photocatalytic oxidation of thin organic films.* Acc. Chem. Res. **1995**:28:503.

[18]. Wang, R.; Hashimoto, K.; Fujishima, A.; Chikuni, M.; Kojima, E.; Kitamura, A.; Shimohigoshi, M.; Watanabe, T. *Photogeneration of highly amphiphilic TiO_2 surfaces.* Adv. Mater. **1998**;10:135.

[19]. HYDROTEC Projects, presented by TOTO. Consulted on December 18th, **2013**. URL: http://www.toto.co.jp/hydrotect/eng/projects01.html#

[20]. Pilkington Activ™ Global Brochure. Consulted on December 18th, **2013**. URL: http://www.pilkington.com/Europe/italy/italian/products/bp/bybenefit/selfcleaning/activ/literature.htm.

[21]. SAINT-GOBAIN Project references. Consulted on December 18th, **2013**. URL: http://nordic.saint-gobain-glass.com/b2b/default.asp?nav1=re&nav2=rd&id=305.

CHAPTER 2

STATE OF THE ART

2. State of the art

As stated previously, in this work were identified two principal practical limitations that prevent the widespread use of self-cleaning TiO_2 surfaces in the building sector:

- *Issues associated to the production of TiO_2 self-cleaning materials* and
- *Limitations associated with the utilization of self-cleaning coatings at real conditions*.

Between all the types of self-cleaning materials that are being developed for the building sector (i.e., glasses, tiles, tents, panels, paints, tunnel walls, etc. [1]), in this research the attention was focused in the study of TiO_2 coatings deposited over glass substrates to develop self-cleaning glasses.

2.1. Issues associated to the production of commercial TiO_2 self-cleaning materials for the building sector

Commercial self-cleaning glasses such as Activ™ (produced by Pilkington), Bioclean (produced by Saint Gobain) and Neat Glass (produced by Cardinal Glass Industries) are produced using chemical vapour deposition [2, 3] or magnetron sputtering [3] techniques. These procedures promote the obtainment of photoactive mechanically-robust self-cleaning glasses with good optical characteristics [2]. On the other hand, other companies such as LG Electronics, Nanopac Co. Ltd., Nihon Parkerizing Co. Ltd., Sukgyung A T Co. Ltd. (Korea) [4] and COLOROBBIA S.p.A. (Italia) [5, 6] have commercialized TiO_2 photocatalysts coating dispersions that can be applied over a wide gamma of substrates. However, the production of self-cleaning glasses from these already-prepared commercial TiO_2 dispersions involves a series of difficulties that, if not considered through the production process, can affect the efficiency of the final products, limiting their successful commercialization worldwide [2, 5, 7-10]. These difficulties include:

- *the low adhesion between the coatings and the substrate (glass)* [2, 7-9]*;*
- *the use of soda-lime window glasses as substrates, since these could affect the photocatalytic activity (hereinafter PCA)* [8-10] and
- *the presence of residues from the photocatalysts dispersions that could compromise the PCA of the final products* [11].

2.1.1. Low adhesion

In contrast to nano-TiO_2 aerosols or suspensions, photocatalytic coatings present the advantage of immobilizing the nanoparticles on a support and therefore limit their spread in the environment. As immobilization is also required in most industrial applications, a considerable market has emerged for photocatalytic coatings.

It has been reported that coatings made from powder dispersions of commercial TiO_2 nanoparticles (e.g., Degussa P25) are not mechanically stable, nor highly reproducible and typically can be readily wiped off using a cloth or thumb [3, 8, 9]. This phenomenon is frequently observed also in the case of coatings made from commercial photocatalytic suspensions. Dispersion of nanoparticles through the environment due to low adhesion between the photocatalytic coatings and their substrates can bring forward damage to aquatic microorganisms by the washing out of nanoparticles from the substrate [12]. In addition, risks of health threats due to the harmful effects of nanoparticles to human health have been also well documented [13]. Thus, development of methodologies that improve the adhesion of nanoparticled photocatalyst coatings is of huge importance to the successful application of not only TiO_2-based self-cleaning materials in the building industry, but also any other kind of nanoparticled semiconductor. In addition, less need of restoration and a decrease in the maintenance costs (due to coating replacement) is another advantage of producing TiO_2 self-cleaning glasses with good adhesion.

Usually, the adhesion of photocatalytic coatings deposited over any kind of substrate is enhanced by annealing the coated material. However, heat can promote crack

formation, especially when the photocatalyst dispersion media includes large organic molecules that evaporate or decompose when heating, leaving behind cracks over the entire film [14]. Moreover, in the case of glass substrates, alkaline ion migration from the glass to the photocatalytic film has also been reported when subjecting the coated glasses to annealing [8-10]. As will be explained in **Section 2.1.2**, these alkaline ions can negatively affect the PCA of the TiO_2 coated-glasses [8-10].

In this research, improvements of the adhesion between TiO_2 coatings from a commercial dispersion and soda-lime glasses were reached through roughness modifications of the glasses. This approach was chosen since it has been reported to successfully increase the adhesion of Au nanoparticles over soda-lime glasses [15] and also because it does not consider annealing procedures. Contrary to the procedure reported by Ramos and co-workers [15], in which particle accelerators are used to induce roughness, in this work chemical treatments of the glasses were carried out with the aim of modifying the glass roughness. This alternative methodology did not only facilitate the experimental procedure, but also it was found to decreased the concentration of Na^+ from the glass surface, avoiding reductions on the PCA of the final products due to alkaline ion contamination.

2.1.2. Substrates that affect the PCA

As stated in **Section 2.1.1**, alkaline and alkaline earth ions such as Na^+ and Ca^{2+} that migrate from soda-lime glass substrates to the photocatalyst coating can negatively affect the PCA of the coated materials [8-10]. This problem has been partially

resolved by applying a protective silicon oxide layer prior photocatalyst deposition between the glass substrate and the TiO_2 coating. The task of this SiO_2 protective layer is to avoid ion diffusion [2, 16, 17]. On the other hand, chemical treatments of freshly deposited TiO_2 coatings with 0.2M HCl and 1M H_2SO_4 have also proved to promote sodium ion exchange between the TiO_2 coating and the acid solution, removing the alkaline ion from the final self-cleaning materials [10, 18]. Furthermore, this approach also enhances the PCA of the acid-treated glasses due to an increase in the adsorbed hydroxyl content on the surface of the TiO_2 films.

In this work, the chemical treatments at which the glass substrates were subjected before TiO_2 deposition (**Section 2.1.1**) accomplished a dual function: enhanced the adhesion of the coatings and decreased the surface sodium concentration in the glass surface, which further avoided reductions on the PCA of the final products due to alkaline ion contamination. Then, no treatment of the self-cleaning glasses to avoid alkaline or alkaline earth contamination from the glass were needed.

2.1.3. Residues from the catalyst synthesis that affects the PCA

It has been well documented that contamination of photocatalytic self-cleaning coatings with residues from the semiconductor synthesis [11] or reaction intermediates build up from the degradation of complex or inorganic-substituted organic pollutants [11, 19-21] bring forwards the gradual deterioration of the PCA. This effect has been frequently attributed to a phenomenon of competition between the original target pollutant and these contaminate species [22, 23]. In these cases, it

has been observed that some moisture can improve the PCA since additional reactions of water with residual species or intermediates can contribute to enhance the overall reaction rate [11, 20]. Moreover, water molecules can block the cation sites preventing the bonding of intermediates to the TiO_2 surface and also promote facile reaction of the target pollutant with hydroxyl radicals [11, 19].

In this work, it was found that sodium chloride, which is used as stabilization agent in dispersions containing nanoparticles [24], affect the PCA of the self-cleaning glasses prepared from a commercial TiO_2 nanodispersion. This task was overcome by treatments of the as-prepared products with deionized water (to increase the hydroxyl content in the TiO_2 surface) and with diluted HCl (to remove the NaCl).

2.2. Limitations associated to the utilization of TiO_2 self-cleaning coatings at real conditions

Although the initial efficiency of TiO_2 building materials is an important aspect for their successful commercialization, the efficiency during the life cycle is also a crucial factor. In normal household conditions, photocatalytic building materials are subjected to both anthropogenic and atmospheric factors that affect their efficiency. These variables may greatly differ depending on geographical zone or the season of the year. In this work, the principal limitations considered regards the utilization of TiO_2 self-cleaning coatings at real conditions were:

- *weathering;*
- *the changes in the PCA associated to the relative humidity and*
- *the changes in the PCA associated to the substrate temperature.*

Furthermore, since the surface characteristics of the photocatalyst coating also influence the photocatalytic efficiency of the final self-cleaning materials, three types of TiO_2 coatings -namely, nanoparticled, mesoporous and non-porous- were investigated.

2.2.1. Weathering

Even if different kinds of self-cleaning building materials are already commercially available [1, 4] and they may experience severe weathering in most of their application, little work has been done to investigate its effects comprehensive way [5, 25-29]. Indeed, throughout production, shipping and usage lifetime, self-cleaning materials are typically exposed to a variety of environmental conditions such as humidity, rain, acid rain, temperature variations, etc. Such conditions can accelerate the deterioration of the photocatalytic coatings, changing their characteristics and thus affecting the self-cleaning properties of these materials [28]. Therefore, evaluating the changes in the photocatalytic efficiency due to weathering is a crucial factor in the self-cleaning field that must be considered for proper commercialization.

Some authors have reported the changes of PCA of self-cleaning glasses after weathering. Chabas and co-workers [25, 26] investigated the behaviour of Pilkington and Saint-Gobain self-cleaning glasses in urban atmosphere (centre of Paris) during 2 years. They do not found weathering phenomena on the TiO_2-coated self-cleaning glasses after the 24 months of exposure. Guo et al. [27] investigated the photocatalytic activities of a Degussa P25 TiO_2-coated glass subjected to weathering, in terms of NO removal and *Escherichia coli* inactivation. Three types of weathering were evaluated: a normal weathering condition (no treatment was applied to the samples); a weathering condition by deionized water (rain) and an abrasive weathering condition by scraping the samples with a cotton towel. Authors found that after abrasive weathering, the TiO_2-coated glass almost completely lost the NO removal efficiency. Mellott and colaborators [28] investigated the chemical durability of two commercial and one laboratory-prepared self-cleaning glasses after their immersion in neutral, acid and basic aqueous solutions for 1 month. Authors found that these treatments not only cause changes in the surface composition and roughness of the films, but also an increase in the PCA of the coatings versus stearic acid.

As it can be expected, weathering not only affects the PCA of TiO_2-coated self-cleaning materials, but also promote the release of nanoparticles -due to weakening of the adhesion between coating and substrate-, being dangerous for the environment [12, 30-35] or the human health [13]. In most of the works dealing with self-cleaning materials, the adhesion of the coating to the substrate is usually evaluated directly after preparation or after a few cycles of use, and thereby is only representative of

relatively new materials. Conversely, photocatalytic coatings are likely to experience severe weathering specially in outdoor applications. Hence, it is critical to figure out how immobilized TiO_2 will endure weathering and if it will keep bound to the substrate over time [29].

Regards the release of TiO_2 nanoparticles from self-cleaning coatings, Kaegi et al. reported that natural weathering of painted exterior facades promotes emission of titania nanoparticles to the aquatic environment, suggesting that a similar release may occur on photocatalytic coatings [36, 37]. Olabarrieta et al. [29] investigated the aging of Pilkington Activ^{TM} and experimental TiO_2 self-cleaning glasses under water flow. They observed deactivation after prolonged immersion and alteration of the mechanical properties accompanied by TiO_2 emissions as high as 150.5 μgL^{-1}. Their results suggested that the use of photocatalytic coatings with surface bound nanoparticles in environmental applications might entail new entries of nanomaterials into aqueous medium.

In the present work, TiO_2 thin films were exposed to weathering (using model solutions that simulate environmental and domestic weathering such as rain, acid rain and cleaning agents) and the changes in the physicochemical, structural and electronic characteristics were studied in order to evaluate the effect of this phenomenon on the PCA. Furthermore, TiO_2 releases from the coatings subjected to weathering were also measured.

2.2.2. Relative Humidity

When exposed to moisture, the surface of TiO_2 becomes hydroxylated as a result of dissociative chemisorption of water into the Ti^{4+} sites [19; 38, 39]. These hydroxyl groups or water molecules behave as hole traps [22], forming surface adsorbed hydroxyls radicals, according with **Equations [2.1]** and **[2.2]** [39].

$$TiO_2 + h\nu \rightarrow e^- + h^+ \quad \textbf{[2.1]}$$

$$H_2O + h^+ \rightarrow OH\bullet + H^+ \quad \textbf{[2.2]}$$

It is generally accepted that these hydroxyls are adsorption sites acting as the primary oxidants of organics [19, 38, 39] and therefore, their presence is critical to the PCA. In general, low and in some cases medium humidity levels increase the PCA of TiO_2, while high levels decrease it, as shown in **Figure 2.1**.

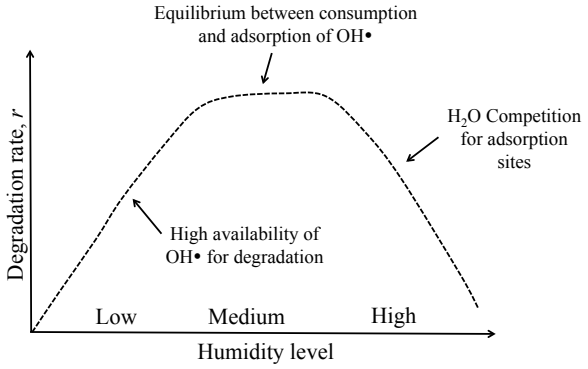

Figure 2.1. General effect of humidity on the photocatalytic degradation rate of pollutants using TiO_2.

The behaviour of the degradation rate of pollutants reported in **Figure 2.1** has been principally attributed to a major availability of hydroxyl radicals at low or moderate moisture levels [38, 39]. This permits the increase in the degradation of the organic pollutants adsorbed on the well-hydrated TiO_2. On the other hand, there exists a suitable equilibrium between adsorption and consumption of hydroxyl radicals to keep a stable photocatalytic degradation rate. If the water vapour content in the reaction mixture is raised, such equilibrium can be destroyed and the increase of adsorption of water molecules on the catalyst surface will conduct to a decrease in the overall degradation rate [40, 41] principally due to competition between the water and the pollutant molecules for the TiO_2 adsorption sites [21, 22, 38, 39, 42].

Many reports have attributed the changes in the PCA of TiO_2 when varying humidity to the previous phenomena [21, 40, 41, 43-47]. However, the changes in the PCA of TiO_2 coatings not only depend on the level of moisture, but also on other several factors that strongly influence its overall effect on the PCA. These factors include:

- *The presence of an initial quantity of adsorbed water on the catalyst surface* [2, 22, 48, 50, 51];
- *The level of humidity*: which can promote the increase in degradation rate [21, 40, 41, 43-47] or e^--h^+ recombination [22,50];
- *The pollutant adsorption process affected by water competition* [22, 23, 39-41, 45, 52, 54-63]: these in turn are affected by the pollutant affinity to the hydroxylated catalyst surface [19, 21, 23, 38, 55, 62, 64, 65] and the changes in the pollutant adsorption modes [61];

- *The nature of the pollutant molecule* [55, 64, 66-68]: water can be necessary for stoichiometry [22] or promote additional degradation paths [23, 44, 55, 69]. Indeed, the nature of the target molecule can define if water is or is not necessary for photocatalytic degradation, since the direct attack of pollutant by the photogenerated holes [70, 71] or the pollutant self-generation of hydroxyl radicals [40, 41, 67] have been proposed as explanations to the continuous degradation of pollutants in absence of water;

- *The presence of residues and reaction intermediates from incomplete degradation* [11, 19-21]: they can promote competition between the intermediates and the original pollutant for the TiO_2 adsorption sites [22, 23] or can be degraded by water [11, 20] re-generating the catalyst [40, 41, 50, 56, 62, 72];

- *The reaction temperature:* it promotes water desorption from the catalyst surface [42, 65];

- *The texture and surface characteristics of the TiO_2 sample* [19, 73].

Figure 2.2 presents a general summary of how the overall effect of humidity on the PCA of TiO_2.

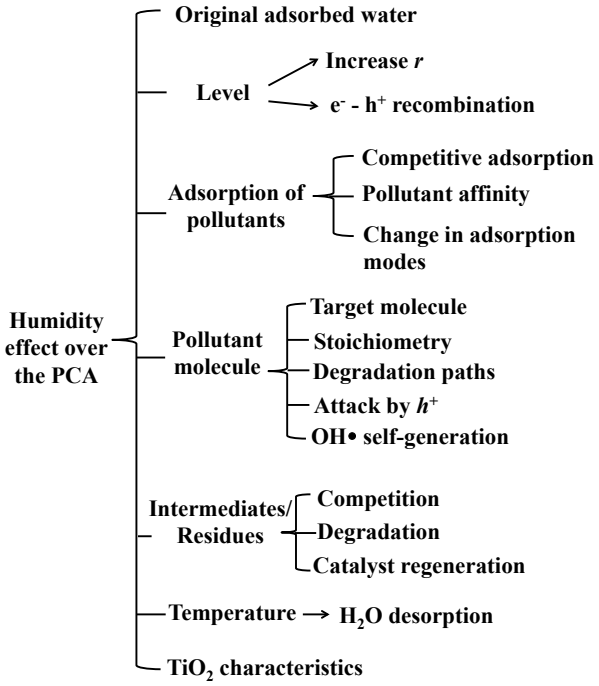

Figure 2.2. Variables that influence the overall effect of humidity on the photocatalytic activity of TiO_2.

As explained above, humidity has a huge influence in the photocatalytic self-cleaning performance of TiO_2 coatings. Even though the effect of humidity on the self-cleaning performance of TiO_2 coatings has been widely investigated for gaseous pollutants [19, 20, 38, 39, 42, 65], the same information using solid pollutants is of great importance for the building sector, since it is expected that self-cleaning materials not only decontaminate the round ambient but also maintain the aesthetic image of building materials such as glasses or tiles.

Regards this aspect, several authors have investigated the effect of humidity on the self-cleaning performance of TiO_2 coatings using stearic acid (SA) as solid pollutant model [2, 48, 51]. Unfortunately, these reports do not specify whether the pollutant

adsorption process over the coating was carried out at controlled humidity. This detail is of great importance as it has been established that the effect of humidity on the self-cleaning performance of TiO_2 is stronger at the pollutant adsorption stage and depends on the humidity level [19, 38, 39].

In this research, the effect of four relative humidity levels on the self-cleaning performance of TiO_2 coatings was evaluated using SA as a solid pollutant model. Since conditions at which pollutants are deposited over self-cleaning surfaces are an important factor in the overall self-cleaning process, coatings were pre-conditioned at the target humidity *prior* SA deposition.

2.2.3. Substrate temperature

Another important environmental variable that has proved to affect the PCA of TiO_2 is the reaction temperature (or thermal energy). Moreover, since self-cleaning building materials could be also exposed to outdoor environments where temperatures may be variable and in some cases extreme, temperature is factor that may significantly affect the performance of these materials and therefore it should be considered when assessing the proprieties of TiO_2-coated building materials.

The impact of the reaction temperature on the photocatalytic decomposition of pollutants over TiO_2 coatings has not been widely investigated as that of humidity. However, some trends in the photocatalytic rate when varying temperature (or when

increasing temperature) have been reported and the phenomena correlated to these behaviours have been discussed.

In most of these studies, it has been observed that the increase in reaction temperature generally enhances the photocatalytic degradation rate [48, 65 74]. This enhancement has been mainly attributed to (i) the change of water adsorption affinity and its resultant desorption from the TiO_2 surface [42, 65]; (ii) the easier degradation of reaction intermediates [75] and (iii) the major availability of TiO_2 active sites for oxidation, as a consequence of the desorption of both reaction intermediates [48] and reaction products [63]. On the other hand, in some cases it has been observed that photocatalytic degradation rates reach a maximum at a fixed temperature value (which depends of the specific target pollutant) and that higher values generally promote a decrease in reaction rate [43, 40, 76]. This decrease has been explained by the limited adsorption of pollutants over the TiO_2 surface when increasing reaction temperature [40, 43, 63, 76]. **Figure 2.3** presents a general overview of the degradation rate of pollutants over TiO_2 coatings, when varying temperature.

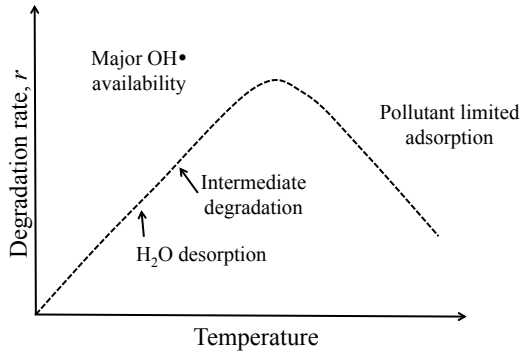

Figure 2.3. General effect of reaction temperature on the photocatalytic activity of TiO_2.

Thermal energy applied to photocatalytic degradation of pollutants can not only promote water desorption and intermediate degradation, but also can facilitate another secondary effects that, as water desorption, are more correlated to physical phenomena than to photochemical degradation. In fact, it has been reported that evaporation of small or simple organic pollutants at high reaction temperatures [77, 78] and deaggregation of TiO_2 particles inside the coating [79] can have an influence on the overall photocatalytic degradation of pollutants. **Figure 2.4** shows an overview of the effects of temperature on the overall PCA of TiO_2 coatings.

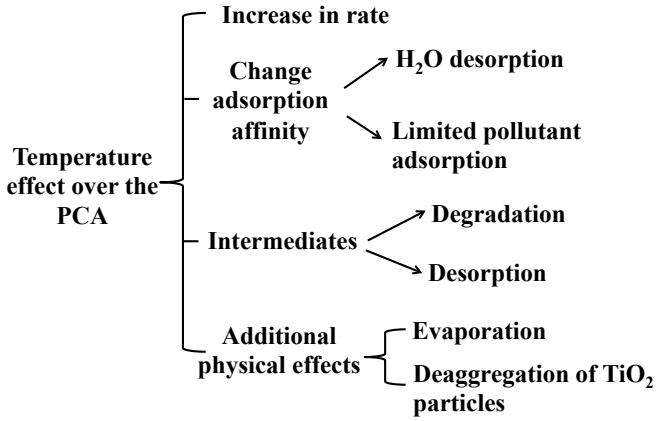

Figure 2.4. Effects of temperature or thermal energy on the photocatalytic activity of TiO_2.

As observed in **Figure 2.3**, most research of the effect of temperature on the PCA of TiO_2 coatings has been focused only in the influence of increasing temperature [42, 77, 78, 80, 81] and fewer reports deals with the influence of relatively low temperatures, i.e., ≤ 20 °C [2, 5, 48, 65, 74]. Moreover, practically all the works that reports the relationship between photocatalytic degradation of organics and temperature involve gaseous or liquid phase contaminants [40, 42, 65, 74, 80, 81]

and few works deal with the temperature effects on solid phase contaminants [2, 5, 48, 75, 77, 78].

As in the case of humidity, information about the performance of photocatalyst-coated building materials using solid pollutants -*as representative models of stains*- becomes of great importance for the building sector. Therefore, in this work, the influence of common ambient temperatures over a year (for example, 0-30 °C in West Europe) on the PCA of TiO_2 coatings was investigated using stearic acid.

2.2.4. Surface characteristics of the coatings

It is know that the efficiency of photocatalytic coatings is intimately linked to the material content, chemical composition, structure and morphology of the oxide layer.

For an efficient reagent distribution (i.e. the organic pollutant and the oxidizing hydroxyl radicals), the surface area of the film must be large. On flat surfaces, although they could be composed of very small particles (and hence have large surface areas), only few monolayers of the organic pollutant can efficiently participate in the photo-oxidation process. Furthermore, interaction of the outer monolayers of the pollutant is conditioned not only to *complete degradation* of the inner pollutant layers (those in direct contact with the TiO_2 surface) but also to the release of reaction products. On the other hand, the large surface of porous materials not only increases the photocatalytic active area for pollutant adsorption and frees up active sites for further pollutant adsorption, but at the same time favours the

production of active oxygen species [82]. Furthermore, light penetration over highly scattering porous coatings results in multiple light reflections and consequently in higher light harvesting than that from non-porous coatings [83]. To provide information about the correlation between the morphology of the film and its influence in domestic weathering, three different coating morphologies, nanoparticled, mesoporous and non-porous were evaluated.

All the information collected in this work permitted to establish the optimal conditions at which each one of these materials present better performances. In addition, the proposal of some guidelines for an adequate choosing of the kind of TiO_2 coating depending on their specific performance at determinate conditions and the target application make these materials even more interesting for the building sector from both commercial and practical point of views.

2.3. References

[1]. Chen, J.; Poon C.-s. *Photocatalytic construction and building materials: from fundamentals to applications*. Building and Environment **2009**;44:1899-1906.

[2]. Mills, A.; Lepre, A.; Elliott, N.; Bhopal, S.; Parkin, I. P.; O'Neill, S. A. *Characterisation of the photocatalyst Pilkington Activ^{TM}: a reference film photocatalyst?* Journal of Photochemistry and Photobiology A **2003**;160:213.

[3]. Self-cleaning glass. Wikipedia. Consulted on December 12th, 2013. URL: http://en.wikipedia.org/wiki/Self-cleaning_glass

[4]. Mills, A.; Lee, S.-K. *A web-based overview of semiconductor photochemistry-based current commercial applications.* Journal of Photochemistry and Photobiology A **2002**;152:233-247.

[5]. Cedillo-González, E. I.; Riccò, R.; Montorsi, M.; Montorsi, M.; Falcaro, P.; Siligardi, C. *Self-cleaning glass prepared from a commercial TiO_2 nano-dispersion and its photocatalytic performance under common anthropogenic and atmospheric factors*. Building and Environment **2014;**71:7-14.

[6]. Ce.Ri.Col.-PARNASOS® COLOROBBIA Italia S.p.A. Consulted on December 12th, 2013. URL: http://test.cericol.com/parnasos_cericol.html

[7]. Cedillo-González, E. I.; Montorsi, M.; Mugoni, C.; Montorsi, M.; Siligardi, C. *Improvement of the adhesion between TiO_2 nanofilm and glass substrate by roughness modifications.* Physics Procedia **2013**;40:19.

[8]. Paz, Y.; Luo, Z.; Rabenberg, L.; Heller, A. *Photooxidative self-cleaning transparent titanium dioxide films on glass.* Journal of Materials Research **1995**;10:2842.

[9]. Paz, Y.; Heller, A. *Photo-oxidative self-cleaning transparent titanium dioxide films on soda lime glass: The deleterious effect of sodium contamination and its prevention.* Journal of Material Research **1997**;12:2759.

[10]. Yu, J.; Zhao, X. *Effect of surface treatment on the photocatalytic activity and hydrophilic property of the sol-gel derived TiO_2 thin films*. Materials Research Bulletin **2001**;36:97-107.

[11]. Österlund, L; Štengl, V.; Mattsson, A.; Bakardjieva, S.; Andersson, P. O.; Opluštil, F. *Effect of sample preparation and humidity on the photodegradation rate*

of CEES on pure and Zd doped anatase TiO_2 nanoparticles prepared by homogeneous hydrolysis. Applied Catalysis B **2009**;88:194.

[12]. Ju-Nam, Y., Lead, J. R. *Manufactured nanoparticles: an overview of their chemistry, interactions and potential environmental implications*. Science of the Total Environment **2008**;400:396.

[13]. Ostiguy, C., Soucy, B., Lapointe, G., Woods, C., Ménard, L., Trottier, M., *Health effects of nanoparticles – 2nd Edition*, Studies and Research Projects/Report R-589, Montreal IRSST, **2008**.

[14]. Dineshram, R.; Subasri, R.; Somaraju, K. R. C.; Jayaraj, K.; Vedaprakash, L.; Ratnam, K.; Joshi, S. V.; Venkatesan, R. *Biofuling studies on nanoparticle-based metal oxide coatingns on glass coupons exposed to marine environment.* Colloids and Surfaces B **2009**;74:75-83.

[15]. Ramos, S. M. M.; Canut, B.; Benyagoub, A.; Toulemonde, M. *Can a thin film to be pinned at the surface by hollows?* Nuclear Instruments and Methods in Physics Research B **2002**;191:456.

[16]. Fujishima, A.; Narasinga Rao, T. *Recent advances in heterogeneous TiO_2 photocatalysis.* Journal of Chemical Sciences **1997**;109:471.

[17]. Zita, J.; Maixner, J.; Krysa, J. *Multilayer TiO_2/SiO_2 thin sol-gel films: Effect of calcination temperature and Na^+ diffusion.* Journal of Photochemistry and Photobiology A **2010**;216:194. 3rd International Conference on Semiconductor Photochemistry, SP-3, April 2010, Glasgow UK.

[18]. Yu, J. C.; Yu, J.; Zhao, J. *Enhanced photocatalytic activity of mesoporous and ordinary TiO_2 thin films by sulphuric acid treatment*. Applied Catalysis B **2002**;36:31-43.

[19]. Coronado, J.M.; Zorn, M. E.; Tejedor-Tejedor, I.; Anderson, M. A. *Photocatalytic oxidation of ketones in the has phase over TiO_2 films: a kinetic study on the influence of water vapor.* Appl. Catal. B. **2003**, 43, 329.

[20]. Ibusuki, T.; Takeuchi, K. *Toluene oxidation on U.V..-irradiated titanium dioxide with and without O_2, NO_2 or H_2O at ambient temperature*. Atmospheric Environment **1986**;20:1711.

[21]. Peral, J; Ollis, D. F. *Heterogeneous photocatalytic oxidation of gas-phase organics for air purification: acetone, 1-butanol, butyraldehyde, formaldehyde and m-xylene oxidation*. Journal of Catalysis **1992**;136:554.

[22]. Dibble, L. A.; Raupp, G. B. *Kinetics of the gas-solid heterogeneous photocatalytic oxidation of trichloroethylene by near UV illuminated titanium dioxide*. Catalysis Letters **1990**;4:345.

[23]. Jacoby, W. A.; Nimlos, M. R.; Blake, D. M. *Products, Intermediates, Mass Balances, and Reaction Pathways for the Oxidation of Trichloroethylene in Air Via Heterogeneous Photocatalysis.* Environmental Science and Technology **1994**;28:1661.

[24]. Jiang, J.; Oberdörster, G.; Biswas, P. *Characterization of size, surface charge and agglomeration state of nanoparticle dispersions for toxicological studies*. Journal of Nanoparticle Research **2009**;11:77.

[25]. Chabas, A.; Lombardo, T.; Cachier, H.; Pertuisot, M. H.; Oikonomou, K.; Falcone, R.; Verità, M.; Geotti-Bianchini, F. *Behaviour of self-cleaning glass in urban atmosphere.* Building and Environment **2008**;43:2124-2131.

[26]. Chabas, A.; Gentaz, L.; Lombardo, T.; Sinegre, R.; Falcone, R.; Verità, M.; Cachier, H. *Wet and dry atmospheric deposition on TiO_2 coated glass*. Environmental Pollution **2010**;158:3507-3512.

[27]. Guo, M.-Z.; Ling, T.-C.; Poon, C.-S. *Nano-TiO_2-based architectural mortar for NO removal and bacteria inactivation: influence of coating and weathering conditions*. Cement and Concrete Composites **2013**;36:101.

[28]. Mellot, N. P.; Durucan, C.; Pantano, C. G.; Guglielmi, M. *Commercial and laboratory prepared titanium dioxide thin films for self-cleaning glasses: photocatalytic performance and chemical durability.* Thin Solid Films **2006**;502:112.

[29]. Olabarrieta, J.; Zorita, S.; Peña, I.; Rioja, N.; Monzón, O.; Benguria, P.; Scifo, L. *Aging of photocatalytic coatings under a water flow: long run performance and TiO_2 nanoparticles release*. Applied Catalysis B **2012**;124-124:182.

[30]. Chen, H.-W.; Su, S.-F.; Chien, C.-T.; Lin, W.-H.; Yu, S.-L.; Chou, C.-C.; Chen, J. J. W.; Yang, P.-C. *Titanium dioxide nanoparticles induce emphysema-like lung injury in mice*. FASEB Journal **2006**:20:2393.

[31]. Warheit, D. B.; Webb, T. R.; Reed, K. L.; Frerichs, S.; Sayes, C. M. P*ulmonary toxicity study in rats with three forms of ultrafine-TiO_2 particles: differential responses related to surface properties.* Toxicology **2007**;230:90.

[32]. Inoue, K.-I.; Takano, H.; Ohnuki, M.; Yanagisawa, R.; Sakurai, M.; Shimada, A.; Mizushima, K.; Yoshikawa, T. *Size effects of nanomaterials on lung inflammation and coagulatory disturbance*. International Journal of Immunopathology and Pharmacology **2008**:21:197.

[33]. Federici, G.; Shaw, B. J.; Handy, R. D. *Toxicity of titanium dioxide nanoparticles to rainbow trout (Oncorhynchus mykiss): gill injury, oxidative stress and other physiological effects.* Aquatic Toxicology **2007**;84:415.

[34]. Ramsden, C. S.; Smith, T. J.; Shaw, B. J.; Handy, R. D. *Dietary exposure to titanium dioxide nanoparticles in rainbow trout, (Oncorhynchus mykiss): No effect on growth, but subtle biochemical disturbances in the brain.* Ecotoxicology **2009**:18:939.

[35]. Hartman, N. B.; Von der Kammer, F.; Hofmann, T.; Baalousha, M.; Ottofuelling, S.; Baun, A. *Algal testing of titanium dioxide nanoparticles – Testing considerations, inhibitory effects and modification of cadmium bioavailability.* Toxicology **2010**;269:190.

[36]. Kaegi, R.; Ulrich, A.; Sinnet, B.; Vonbank, R.; Wichser, A.; Zuleeg, S.; Simmler, H.; Brunner, S.; Vonmont, H.; Burkhardt, M.; Boller, M. *Synthetic TiO_2 nanoparticle emission from exterior facades into the aquatic environment*. Environmental Pollution **2008**;156:233.

[37]. Kaegi, R.; Sinnet, B.; Zuleeg, S.; Hagendorfer, H.; Mueller, E.; Vonbank, R.; Boller M., Burkhardt, M. *Release of silver nanoparticles from outdoor facades*. Environmental Pollution **2010**;158:2900.

[38]. Obee, T. N.; Brown, R. T. *TiO_2 Photocatalysis for Indoor Air Applications: Effects of humidity and trace contaminants levels on the oxidation rates of formaldehyde, toluene and 1,3-butadiene*. Environmental Science and Technology **1995**;29:1223.

[39]. Raillard, C.; Héquet, V.; Le Cloirec, P.; Legrand, J. *Kinetic Study of Ketones Photocatalytic Oxidation in gas Phase Using TiO_2-Containing Paper: Effect of Water Vapor.* Journal of Photochemistry and Photobiology A **2004**;163:425.

[40]. Kim, S. B.; Hwang, H. T.; Hong, S. C. *Photocatalytic degradation of volatile organic compounds at the gas-solid interface of a TiO_2 photocatalyst.* Chemosphere **2002**, 48, 437.

[41]. Kim, S. B.; Hong, S. C. *Kinetic study for photocatalytic degradation of volatile organic compounds in air using thin film TiO_2 photocatalyst.* Applied Catalysis B **2002**, 35, 305.

[42]. Fu, X.; Clark, L. A.; Zeltner, W. A., Anderson, M. A. *Effects of reaction temperature and water vapor content on the heterogeneous photocatalytic oxidation of ethylene.* Journal of Photochemistry and Photobiology A **1996**, 97, 181.

[43]. Bauer, R.; Hager, S. *Heterogeneous photocatalytic oxidation of organics for air purification by near UV irradiated titanium dioxide.* Chemosphere **1999**;38:1549.

[44]. Falconer, J. L.; Muggli, D. S. *Parallel pathways for photocatalytic decomposition of acetic acid on TiO_2*. Journal of Catalysis **1999**;187:230.

[45]. Ku, Y.; Wang, W. *Photocatalytic degradation of gaseous benzene in air streams by using an optical fiber photoreactor*. Journal of Photochemistry and Photobiology A **2003**;159:47.

[46]. Wang, W.; Chiang, L.-W.; Ku, Y. *Decomposition of Benzene in Air Streams by UV/TiO_2 Process.* Journal of Hazardous Materials **2003**;B101:133.

[47]. Zhang, P.; Liu, J. *Photocatalytic degradation of trace hexane in the gas phase with and without ozone addition: kinetic study*. Journal of Photochemistry and Photobiology A **2004**;167:87.

[48]. Guillard, C.; Herrmann, J. M.; Puzenat, E.; Peruchon, L. *Photocatalytic efficiencies of self-cleaning glasses. Influence of physical factors.* Photochemical and Photobiological Sciences **2009**;8:1040.

[50]. Park, O.-H.; Kim, C.-S. *Experimental study on the treatment of volatile organic compound vapors using a photoreactor equipped with photocatalyst-coated fabrics*. Journal of Applied Polymer Science **2004**;91:3174.

[51]. Sitkiewitz, S.; Heller, A. *Photocatalytic oxidation of benzene and stearic acid on sol- gel derived tio₂ thin films attached to glass*. New Journal of Chemistry **1996**;20:233.

[52]. Alberici, R. M.; Mendes, M. A.; Jardim, W. F.; Eberlin, M. N. *Mass spectrometry on-line monitoring and ms^2 product characterization of TiO_2/UV photocatalytic degradation of chlorinated volatile organic compounds*. Journal of the American Society for Mass Spectrometry **1998**;9:1321.

[54]. Alfano, O. M.; Iboberdorf, G. E.; Irazoqui, H. A.; Cassano, A. E. *Photocatalytic degradation of tetrachloroethylene in gas phase on TiO_2 films: a kinetic study*. Industrial & Engineering Chemistry Research **2005**;44:6075.

[55]. Amama, P. B.; Itoh, K.; Murabayashi, M. *Photocatalytic oxidation of trichloroethylene in humidified atmosphere.* Journal of Molecular Catalysis A **2001**;176:165.

[56]. Einaga, H.; Futamura, S.; Ibusuki, T. *Heterogeneous photocatalytic oxidation of benzene, toluene, ciclohexene and cyclohexane in humidified air: comparison of decomposition behaviour on photoirradiated TiO_2 catalyst*. Applied Catalysis B **2002**;38:215.

[57]. Kim, S. D., Lim, T. H. *Trichloroethylene degradation by photocatalysis in annular flow and annulus fluidized bed photoreactors.* Chemosphere **2004**, 54, 305.

[58]. Kim, J. S.; Lee, T. K. *Effect of humidity on the photocatalytic degradation of trichloroethylene in gas phase over TiO_2 thin films treated by different conditions*. Korean Journal of Chemical Engineering **2001**;18:935.

[59]. Kutsuna, S.; Ebihara, Y.; Nakamura, K.; Ibusuki, T. *Heterogeneous photochemical reactions between volatile chlorinated hydrocarbons (trichlotoethene and tetrachloroethene) and titanium dioxide*. Atmospheric Environment **1993**;27A:599.

[60]. Lichtin, N. N.; Sadeghi, M. *Oxidative photocatalytic degradation of benzene vapor over TiO_2.* Journal of Photochemistry and Photobiology A **1998**;113:81.

[61]. Sivachandiran, L.; Thevenet, F.; Gravejat, P.; Rousseau, A. *Isopropanol saturated TiO_2 surface regeneration by non-thermal plasma: influence of air relative humidity*. Chemical Engineering Journal **2013**;214:17.

[62]. Wang, K.-H.; Tsai, H.-H.; Hsieh, Y.-H. *The kinetics of photocatalytic degradation of trichloroethylene in gas phase over TiO_2 supported on glass bead.* Applied Catalysis B **1998**;17:313.

[63]. Yu, H.; Zhang, K.; Rossi, C. *Experimental study of the photocatalytic degradation of formaldehyde in indoor air using a nano-particulate titanium dioxide photocatalyst.* Indoor and Built Environment **2007;**16:529.

[64]. Cao, L.; Gao, Z.; Suib, S. L.; Obee, T. N.; Hay, S. O.; Freihaut, J. D. *Photocatalytic oxidation of toluene on nanoscale TiO_2 catalysts: studies of deactivation and regeneration*. Journal of Catalysis **2001**;196:253.

[65]. Obee, T. N.; Hay, S. O. *Effects of moisture and temperature on the photooxidation of ethylene on titania*. Environmental Science and Technology **1997**;31:2034.

[66]. Ollis, D. F.; Luo, Y. *Heterogeneous photocatalytic oxidation of trichloroethylene and toluene mixtures in air: kinetic promotion and inhibition, time-dependent catalyst activity*. Journal of Catalysis **1996**;163:1.

[67]. Palau, J.; Penya-Roja, J. M.; Gabaldón, C.; Álvarez-Hornos, F. J.; Sempere, F.; Martínez-Soria, V. *UV photocatalytic oxidation of paint solvent compounds in air using an annular TiO_2-supported reactor*. Journal of Chemical Technology and Biotechnology **2011**;86:273.

[68]. Augugliaro, V.; Coliccia, S.; Loddo, V.; Marchese, L.; Martra, G.; Palmisano, L.; Schiavello, M. *Photocatalytic oxidation of gaseous toluene on anatase TiO_2 catalyst: mechanistic aspects and FT-IR investigation*. Applied Catalysis B **1999**;20:12.

[69]. Mariñas, B. J.; Hung, C.-H. *Role of water in the photocatalytic degradation of trichloroethylene vapor on TiO_2 films*. Environmental Science and Technology **1997**;31:1440.

[70]. Choi, W.; Ko, J. Y.; Park, H.; Chung, J. S. *Investigation on TiO_2-coated optical fibers for gas-phase photocatalytic oxidation of acetone*. Applied Catalysis B **2001**;31:209.

[71]. Zahraa, O.; Doucet, N.; Bouchy, M. *Kinetics of the photocatalytic degradation of benzene*. Catalysis Today **2007**;122:168.

[72]. Raupp, G. B.; Ameen, M. M. *Reversible catalyst deactivation in the photocatalytic oxidation of dilute o-xylene in air.* Journal of Catalysis **1999**;184:112.

[73]. Suárez, S.; Arconada, N.; Castro, Y.; Coronado, J. M.; Portela, R.; Durán, A.; Sánchez, B. *Photocatalytic degradation of TCE in dry and wet air conditions with TiO_2 porous films*. Applied Catalysis B **2011**;108-109:14.

[74]. Hofstadler, K.; Bauer, R.; Novalic, S.; Heisler, G. *New Reactor Design for Photocatalytic Wastewater Treatement with TiO_2 Immobilized on Fused-Silica Glass Fiber: Photomineralization of 4-Chlorophenol.* Environ. Sci. Technol. **1994**:28:670.

[75]. Minabe, T.; Tryk, D. A.; Sawunyama, P.; Kikuchi, Y.; Hashimoto, K.; Fujishima, A. *TiO_2-mediated photodegradation of liquid and solid organic compounds*. Journal of Photochemistry and Photobiology A **2000**;137:53.

[76]. Wu, J.-F.; Hung, C.-H.; Yuan, C.-S. *Kinetic model of promotion and inhibition of temperature on photocatalytic degradation of benzene vapor*. Journal of Photochemistry and Photobiology A **2005**;170:299.

[77]. Costacurta, S.; Dal Maso, G.; Gallo, R., Guglielmi, M.; Brusatin, G.; Falcaro, P. *Influence of temperature on the photocatalytic activity of sol-gel TiO_2 films*. ACS Applied Materials & Interfaces **2010**;2:1294.

[78]. Falcaro, P.; Zaccariello, G.; Stoyanova, V.; Benedetti, A.; Costacurta, S. *Temperature matters: An infrared spectroscopic investigation on the photocatalytic efficiency of titania coatings*. Sci. Adv. Mater. 2014;6:1.

[79]. Mendive, C. B.; Hansmann, D.; Bredow, T.; Bahnemann, D. *New insights into the mechanism of TiO_2 photocatalysis: thermal process beyond the electron-hole creation*. Journal of Physical Chemistry C **2011**;115:19676.

[80]. Lozano, A., Garcia, J., Domènech, X., Casado, J., *Heterogeneous photocatalytic oxidation of manganese (II) over TiO_2.* Journal of Photochemistry and Photobiology A 1992;69:237.

[81]. Trillas, M., Peral, J., Domènech, X., *Photo-oxidation of phenoxyacetic acid by TiO_2 illuminated catalyst*. Applied Catalysis B **1993**;3:45.

[82]. Innocenzi, P.; Malfatti, L. *Mesoporous thin films: properties and applications*. Chemical Society Reviews **2013**;42:4198.

[83]. Kalyanasundaram, K.; Grätzel, M. *Applications of functionalized transition metal complexes in photonic and optoelectronic devices*. Coord. Chem. Rev. **1998**;177:247.

CHAPTER 3

DESIGN OF EXPERIMENTS

In this thesis, the Design of Experiments (DOE) approach was used to investigate the factors that affect the roughness of soda-lime glasses, with the aim to determine what kind of roughness promotes an improvement of the adhesion between glass substrates and anatase TiO_2 coatings made from commercial nano-suspensions. Therefore, this chapter presents a general overview of the DOE methodology, as well as an introduction of a special kind of experimental design derived from the DOE technique, the D-optimal design.

3.1. Introduction

Experiments are used in nearly every area to solve problems in an effective way. Indeed, experimentations can be found both in daily life and in advanced scientific areas. It is obvious that if experiments are performed randomly the result obtained will be also random. Therefore, it is necessary to plan the experiments in such a way that the interesting information can be obtained [1]. Experimental design is a tool

that is used to systematically examine different types of problems that arise within, e.g., research, development and production.

3.2. Definitions

3.2.1. Experiment

An experiment is an observation that provides characteristic information about a studied object. The classical purpose for such an observation is a hypothesis that has to be verified or falsified with an investigation. In a classical approach, the experimental setup is chosen for the specified problem statement and the experimenter tests if the hypothesis is true or false [2].

3.2.2. Design of experiments

This branch of applied statistics deals with *planning*, conducting, analysing and interpreting controlled tests to evaluate the factors that control the value of a parameter or group of parameters [3].

Contrary to the traditional One-Factor-at-a-Time (or OFAT) approach, where certain factors are kept constant and only the level of one variable is altered during every single experiment, in DOE, a strategically planned and executed experiment provides a great deal of information about the effect on a response variable due to one or more

factors [3]. Moreover, traditional OFAT experimentation frequently reduces itself to no methodology whatsoever – just trial and error and reliance on common sense. In contrast, the systematic DOE approach provides information about the interaction of variables and the way the total experimental system works, something generally not attainable through the OFAT approach [4].

Considering the costs for a single experiment, minimizing the amount of performed experiments is always an aim. With DOE, a maximum of information is gained from a minimum of experiments [1].

3.2.3. Factors and Responses

Figure 3.1. A process or a system can be manipulated by one or more different input factors. These modifications affect the responses that can be measured. Taken from *Triefenbach, F. Design of Experiments: The D-optimal Approach and its Implementation as a Computer Algorithm. Bachelor Thesis in Information and Communication Technology, 2008* [2].

There are always two types of variables when performing experiments in the field of DOE: responses and factors. The responses provide information about the investigated system, while factors are used to manipulate it, as shown in **Figure 3.1**.

A response can either have a continuous or a discrete value. However, discrete values are hard to process and thus it is always recommended to use a continuous scale if possible [2].

Normal factors can be set to two or more values and have a defined range. Factors can be divided into three groups, depending on different criteria [2]:

- ***Controllable and uncontrollable factors:*** The controllable factors are normal process factors that are easy to monitor and investigate. By contrast, an uncontrolled factor is hard to regulate because it is mostly a disturbance value or an external influence. This latter type of factors can have a high impact on the response and consequently should always be considered during the experimentation [2, 5].

- ***Quantitative and qualitative factors:*** The values of a quantitative factor have a given range and a continuous scale, whereas qualitative factors have only distinct values [2].

- ***Process and mixture factors:*** Process factors can be changed independently and do not influence each other. They are normally expressed by an amount or level. Mixture factors stand for the amount of ingredients in a mixture. They are all part of a formulation and add up to a value of 100%. A mixture factor cannot be changed independently, so special designs are needed to lead with this type of factors [2, 5].

3.3. Basic principles of DOE

As stated above, experimental plans were traditionally designed changing the value of one separate factor at time until no further improvement was accomplished [5]. **Figure 3.2** illustrates how difficult can be finding the optimum with this approach. During experimentation, it is not easy to find at which value the changes of factor x_1 should be stopped because a further improvement cannot be observed. However, finding the exact value is very important when considering it in combination with the later adjusted factor x_2 [2].

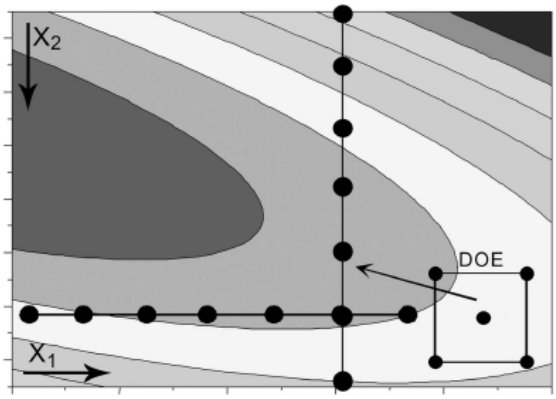

Figure 3.2. Changing all factors simultaneously, as shown in the lower right corner, gives better information about the optimum than the traditional OFAT approach where all factors are changed successively. Taken from *Eriksson, L.; Johansson, E.; Kettaneh-Wold, N.; Wikström, C.; Wold. S. Design of Experiments, Principles and Applications. Umetrics Academy, Sweden 2008* [5].

The given situation from **Figure 3.2** can also be investigated with the use of DOE. In this case, we create a special set of experiments around a so-called center-point. As shown in the lower right corner of the **Figure 3.2**, we use a uniform set of

experiments that allows obtaining a direction for a better result. This basic example clearly show the advantages of changing all relevant factors at the same time and consequently show the importance of DOE [2, 5].

3.3.1. Empirical models

It is reasonable to assume that the outcome of an experiment is dependent on the experimental conditions. This means that the result can be described as a function based on the experimental variables [1]:

$$y = f(x) \quad \textbf{[3.1]}$$

The function $f(x)$ is approximated by a polynomial function and represents a good description of the relationship between the experimental variables and the responses within a limited experimental domain.

Three types of polynomial models are here discussed and exemplified with two variables, x_1 and x_2 [1]. Although a model is never 100% right, it simple helps to transport the complexity of the reality into an equation that is easy to handle [2,5].

The simplest polynomial model contains only linear terms and describes only the linear relationship between the experimental variables and the responses [1, 2]. In a linear model, the two variables x_1 and x_2 are expressed as:

$$y = b_0 + b_1x_1 + b_2x_2 + \text{residual} \quad \textbf{[3.2]}$$

The next level of polynomial model contains additional terms that describe the interaction between different experimental variables [1]. Thus, a second order interaction model contains the following terms:

$$y = b_0 + b_1x_1 + b_2x_2 + b_{12}x_1x_2 + \text{residual} \quad \textbf{[3.3]}$$

The two models above are used to investigate the experimental system, i.e., with screening studies, robustness tests or similar.

To be able to determine an optimum (maximum or minimum) quadratic terms have to be introduced in the model. By introducing these terms in the model, it is possible to determine non-linear relationships between the experimental variables and responses [1]. The polynomial function below describes a quadratic model with two variables:

$$y = b_0 + b_1x_1 + b_2x_2 + b_{11}x_1^2 + b_{22}x_2^2 + b_{12}x_1x_2 + \text{residual} \quad \textbf{[3.4]}$$

In the polynomial functions described above, b_0, b_1 and b_2 represent the regression coefficients and the residual the difference between the calculated and the experimental result [1, 2]. This latter is assumed to be normally distributed with mean 0 and variance σ^2 [2].

3.3.2. Experimental objective

The term experimental objective is generally understood as the purpose for the creation of a design and can be divided into three significant types of designs [2].

3.3.2.1. Screening

Screening is normally performed at the beginning of an investigation to characterize a process, i.e., determining the main factors and investigating the changes in the response when varying each factor [1, 2]. Due to its characteristic of identifying significant main effects rather than interaction effects, screening designs are often used to analyse designs with a large number of input factors. This identification of the critical process factors can be very useful for further optimization processes because only a subset of the factors has to be considered [2].

3.3.2.2. Optimization

This kind of design not only provides detailed information about the influence of the factors on the response but also determines the combination of factors that leads to the best response. In other words, this design permits to find the optimal experimental point by predicting response values for all possible factor combinations [2]. This kind of design is usually performed after a screening study of the same process has been carried out.

3.3.2.3. Robustness Test

Normally a robustness test is the last design that is created before a process is brought to completion. Its aim is to figure out how factors must to be adjusted to guarantee robustness, i.e., to guarantee that small fluctuations of the factors do not affect the response in a distinct way [2, 5].

3.4. Experimental designs (for regular experimental domains)

Besides the experimental objectives, a statistical experimental design must be chosen based in the type of factors and experimental domain to investigate.

3.4.1. Experimental domain

The term *experimental domain* refers to the experimental "area" that will be investigated and is defined by the variation of the experimental variables [1]. The single type of each factor, their space and the total amount of factors influence the shape of the area (or domain) [2]. Thus, the experimental domain can be regular or irregular [5].

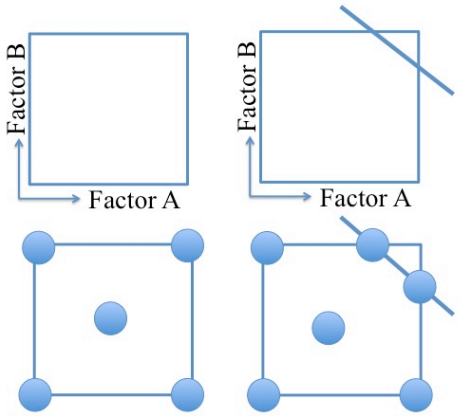

Figure 3.3. Regular and irregular experimental domains. The four squares represent an experiment with two factors. The first column shows a regular experimental domain. The second column has a constraint in the upper right corner, and therefore the experimental domain becomes irregular. Taken from *Eriksson, L.; Johansson, E.; Kettaneh-Wold, N.; Wikström, C.; Wold. S. Design of Experiments, Principles and Applications* ***2008*** [5].

Regular experimental domains lead to designs with uniform geometrical forms such as squares or cubes and makes them easy to handle. As observed in **Figure 3.3**, a squared experimental domain has no restriction in the problem formulation. A restriction means that a part of the domain is not accessible for experimentation. These kinds of restrictions lead to irregular domains, as observed in the **Figure 3.3**. Some reasons for these restrictions include the prevention of special factor combinations or the influence of outside factors [2, 5].

3.4.2. Statistical designs for regular experimental domains

3.4.2.1. Full factorial design

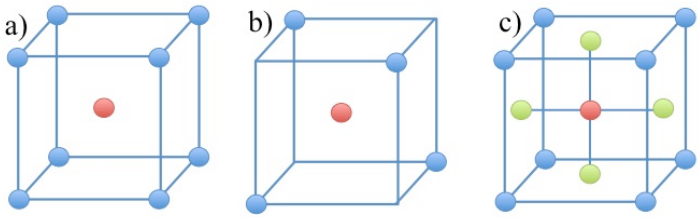

Figure 3.4. Comparison of Statistical Designs. (a) An example of full factorial design where all possible corners are investigated. (b) A fractional factorial design that considers only a fraction of all design points. (c) A composite design which has additional six axial experiments. Taken from *Eriksson, L.; Johansson, E.; Kettaneh-Wold, N.; Wikström, C.; Wold. S. Design of Experiments, Principles and Applications* ***2008*** [5].

It is called *full* because the whole cube - including all its corners - is investigated. In addition to this, some replicated center-point experiments are also investigated. **Figure 3.4a** shows a full factorial design. The factors have two levels of investigation, so for k factors we need 2^k design runs [2, 5].

3.4.2.2. Fractional factorial design

A fractional design does not consider all possible corners and reduces the number of design runs by choosing only a fraction of the 2^k runs of the full factorial design. **Figure 3.5b** shows an example, where only four of the possible eight points are investigated [2, 5].

3.4.2.3. Composite design

The composite design combines the investigations done by a factorial design, the corners and replicated center-points, with the use of axial experiments. The right-hand cube in **Figure 3.4c** shows an example of three factors where axial experiments are placed on the six squares. The factors normally have three or five levels of investigation and due to this, quadratic models are used [2, 5].

Beside the previous design families, there are other design alternatives that are useful in certain situations. In the present work, a D-optimal design was used and then, a brief introduction to this special experimental design is presented in the next section.

3.5. D-Optimal Design

3.5.1. Uses

D-optimal designs are required when [2, 5]:

- *the experimental region is irregular,*
- *already performed experiments have to be included,*
- *qualitative factors have more than two levels,*
- *the number of design runs have to be reduced,*
- *special regression models must be fitted,*
- *or process and mixture factors are used in the same design.*

3.5.1.1. Irregular Experimental Regions

There are two ways to handle the irregular experimental domains such as those of the second column of **Figure 3.3**. The easiest is to shrink down the area until it has a quadratic form again, but this would distort the whole investigation and is not recommended.

A more effective solution is the creation of a computer aided D-optimal design. As we can see in the bottom right of the four squares in **Figure 3.3**, the D-optimal algorithm chooses two points on the border of the constraint instead of the excluded corner. This increases the number of designs runs but is essential to deal with the complexity of the constricted experimental region. In addition to this, the center-point is manipulated [2, 5].

3.5.1.2. Inclusion of already performed experiments

With the application of D-optimal designs, there is the possibility to include additional runs as a part of the design and consider them during the creation [2, 5].

3.5.1.3. The use of qualitative factors

It has been previously stated that a qualitative factor has only discrete values and non a continuous scale. If the number of these discrete steps becomes higher than two, the number of runs for a normal design increases drastically. **Figure 3.5** shows an

investigation with two qualitative and one quantitative factor. With three and four discrete values for the both qualitative factors, a full factorial design would need 4 × 3 × 2 = 24 design runs to solve this problem.

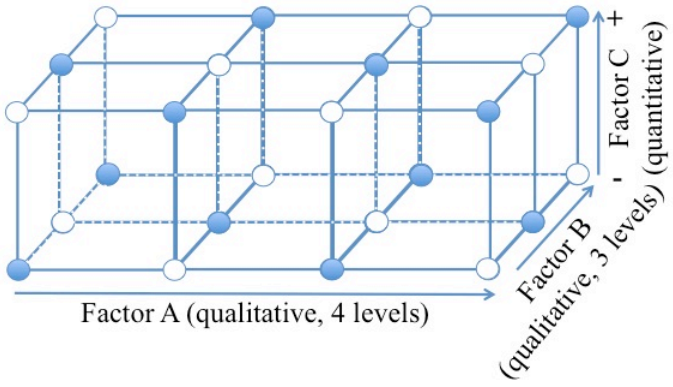

Figure 3.5. Design with multi-level qualitative factors. Factors A and B are qualitative and have three or four discrete levels. Factor C is a normal quantitative factor with values between -1 and +1. The filled cicles represent the point chosen by a D-optimal algorithm. A full 4 × 3 × 2 factorial design would select all 24 points. Taken from *Eriksson, L.; Johansson, E.; Kettaneh-Wold, N.; Wikström, C.; Wold. S. Design of Experiments, Principles and Applications* ***2008*** [5].

The D-optimal approach reduces the number of design runs to only 12 experiments. These experiments, shown in **Figure 3.5** as filled circles, are chosen to guarantee a balanced design that is spread over the whole experimental region [2, 5]. A balanced design has the same number of runs for each level of a qualitative factor [5].

3.5.1.4. Reducing the number of experiments

The classical designs are very inefficient if the number of factors increases. The needed runs for a D-optimal design are always lower and do not increase as fast as the classical design with a growing number of factors as shown in **Table 3.1** [2, 5].

Table 3.1. Minimum number for design runs for screening design.

Factors	Full factorial	Fractional factorial	D-optimal
5	32	16	16
6	64	32	28
7	128	64	35
8	256	64	43
9	512	128	52

3.5.1.5. Fitting of special regression models

D-optimal designs provide the possibility to modify the underlying model in different ways. As **Equation 3.5** shows, it is possible to delete selected terms if the experimenter knows that they are unimportant for the responses. This allows reducing the number of runs without having big influence on the investigation [2].

$$y = b_0 + b_1x_1 + b_2x_2 + b_3x_3 + b_{12}x_{12} + \cancel{b_{13}x_{13}} + b_{23}x_{23} + \text{residual} \qquad \textbf{[3.5]}$$

The second possible model modification is the addition of single higher order terms. With classical designs it is only possible to change the whole model, i.e., from an interaction to a quadratic model. In contrast to this, D-optimal designs allow the

addition of independent model terms [2]. The following equation gives an example of a linear model with an additional interaction term.

$$y = b_0 + b_1x_1 + b_2x_2 + b_3x_3 + b_{23}x_{23} + \text{residual} \quad \textbf{[3.6]}$$

3.5.2. The D-optimal approach

A D-optimal design is a computer aided design which contains the best subset of all possible experiments. Depending on a selected criterion and a given number of design runs, the best design is created by a selection process [2, 5].

3.5.2.1. Candidate set

The candidate set is a matrix that contains all theoretically and practically possible experiments. For a simple investigation with two factors, x_1 and x_2, the candidate set has two columns and four rows. **Equation 3.7** shows a candidate in the extended notation. We get four rows because we only consider the 2^k experiments that have a minimum or maximum value for the factors (-1 and 1, respectively).

$$\xi_4 = \begin{bmatrix} -1 & -1 \\ -1 & 1 \\ 1 & -1 \\ 1 & 1 \end{bmatrix} \quad \textbf{[3.7]}$$

In the candidate set of **Equation 3.7**, each row represents an experiment and each columns a variable. This so-called matrix of candidate points has *N* rows and is presented by ξ_N [2].

3.5.2.2. Design matrix

The design matrix is a $n \times p$ matrix that depends on a model with *p* coefficients. The number of rows *n* can be chosen by the experimenter and represent the number of experiments in the design. With a given model and a candidate matrix, the construction of the design matrix is easy. Each column contains a combination of the factors from the candidate set, depending on the terms in the model [2].

We use the earlier candidate set ξ_4 and the model from **Equation 3.8** for a simple example with $n = 4$ design runs.

$$y = b_0 + b_1x_1 + b_2x_2 + b_{12}x_{12} + \text{residual} \quad \textbf{[3.8]}$$

As a result, we have a model matrix with four rows and four columns, where all candidates from ξ_4 are used in the design. Normally, the candidate set contains much more experiments and the model matrix is only a small subset [2].

$$X = \begin{bmatrix} 1 & -1 & -1 & 1 \\ 1 & -1 & 1 & -1 \\ 1 & 1 & -1 & -1 \\ 1 & 1 & 1 & 1 \end{bmatrix} \quad \textbf{[3.9]}$$

The first column of X represents the constant term b_0, so it only contains ones. Columns two and three are the model terms for the investigated factors, x_1 and x_2, taken from the candidate set ξ_4. The last column of X represents an interaction between the both factors. Hence, we have to multiply the two columns from the candidate set.

With a bigger candidate set, the number of possible subsets of ξ_N increases and the selection of the design matrix has to be done depending on a special criterion. The best combination of these points is called optimal and the corresponding design matrix is called optimal design matrix X^* [2].

3.5.2.3. Information and Dispersion Matrix

To use the later described criteria for the selection of the best design, it is necessary to define other two types of matrices. The first one is the so-called information matrix ($X'X$). This matrix is the multiplication of the transpose of the design matrix X' and X itself. The dispersion matrix $(X'X)^{-1}$ is the inverse matrix of this calculation [2].

3.5.3. Criteria for the best D-optimal design

In the following section, it is discussed the different criteria for a D-optimal design. All of them belong to the group of information-based criteria because they try to maximize the information matrix ($X'X$).

3.5.3.1. D-optimality (Determinant)

The D-Optimality is the most common criterion that seeks to maximize $|X'X|$, the determinant of the information matrix ($X'X$) of the design. This means that the optimal design matrix X^* contains the n experiments which maximizes the determinant of ($X'X$). Or in other words, the n runs span the largest volume possible in the experimental region [2].

3.5.3.2. A-Optimality (Trace)

Here, the design matrix is considered as A-optimal when the trace of the dispersion matrix $(X'X)^{-1}$ is minimum. Minimizing the trace of the matrix is similar to minimizing the average variance of the estimated coefficients [2].

3.5.3.3. V-optimality (Average Prediction Variance)

With the selection of a V-optimal design, the chosen candidates have the lowest average variance of prediction [2, 6].

3.5.3.4. G-optimality (Maximum Prediction Variance)

In this criterion, the selected optimal design matrix is chosen to minimize the highest variance of prediction in the design.

3.5.3.5. G-Efficiency

In most cases, the G-criterion is not used to find the best design during the selection process but is applied to choose between several similar designs which were created with another criterion, such as D-optimality. For this comparison the so-called G-efficiency is used [2].

3.5.3.6. Condition number

The condition number (CN) is an evaluation criteria such as the G-efficiency and is used to rate an already created D-optimal design. It evaluates the sphericity and the symmetry of the D-optimal design by calculating the ratio between the largest and smallest singular values of X [5].

3.5.4. Fitting the Model

The described above D-optimal approach is always model-dependent. Hence, the selection of the model is an important step of the problem formulation. For the D-optimal design, the linear, interaction and quadratic model described in **Section 3.3.1** can be applied.

3.5.5. Number of design runs

In order to fit an optimality criterion, it has to be defined the number of experiments to have in the design. The selection of the factor *n* is essential because changing the number of the design runs alters the model matrix and consequently, another optimal design is chosen. There are no rules to define this number, but the minimum is model-dependent. A model with *p* coefficients can only be investigated with a D-optimal design that has at least *p* runs. In most cases, it is useful to create different designs that differ in the number of runs and compare the efficiency of the designs. A design with a few more or less design runs that the desired one can have a higher determinant and hence is the best design to perform [2].

3.6. Statistical analysis of the obtained data

In this work, the experimental results were analysed through statistical calculations and multiple regressions using the MODDE 9.0 software [7].

The statistical analysis was carried out following three steps: (a) evaluation of the raw data; (b) regression analysis and (c) interpretation of the model.

3.6.1. Evaluation of the raw data

The evaluation of the raw data was focused on a general appraisal of regularities and peculiarities in the data.

3.6.2. Regression analysis

The regression analysis involves the calculation of the model, linking the input factors to the measured responses. In this work, the Multiple Linear Regression (MLR) method was used to explore the dependence of the responses on varied factors. For each response, the regression model was selected based on the analysis of the following parameters: the *goodness of fit* (R^2), which measures how the regression model fit the data; the *goodness of predictions* (Q^2), which estimates the predictive power of the model; the *model validity*, that measures the validity of the model and the *reproducibility*, which represents the variation of the response of different tests performed at the same operative conditions, compared with the total variation of the response. The values of the previous parameters allow getting an overview of the regression model: R^2 could vary from 0 to 1, where 1 indicates a perfect model and 0 no model at all; Q^2 must have a value higher than 0.5. Moreover, R^2 should not exceed Q^2 more than 0.2-0.3 [5]. A value larger than 0.25 for the model validity indicates that there is no lack of fit in the data and the model error is in the same range that the pure error. Finally, a reproducibility value close to 1 indicates a high reproducibility [5].

Another tool used to determine the goodness of the model was the analysis of the residuals, since a good model should be characterized by normally distributed errors. This tool permitted to verify the normal behaviour of the residuals and detect deviating experiments.

3.6.3. Interpretation of the model

During the interpretation of the model, it was determined whether the model could be used or eventually, pruning. The analysis of the regression coefficients and their confidence intervals permitted finding out the real effect of the factors on the measured responses. The study of the interaction between factors permitted to describe how the influence of one factor on the response depends on the level of another factor. In other words, there could be experimental cases in which the factor A has a positive effect on the response for a given level of factor B, while in a different level of B, the effect of A on the response is negative [8]. To determine the effect of interaction on the responses, interaction plots were used, which displays the levels of one factor in the X axis and have a separate line for the means of each level of the other factor. The Y axis is the response.

3.7. References

[1]. Lundstedt, T.; Seifert, E.; Abramo, L.; Thelin, B.; Nyström, A.; Pettersen, J.; Bergman, R. *Experimental Design and Optimization*. Chemom. Intell. Lab. Syst. **1998**;42:3.

[2]. Triefenbach, F. *Design of Experiments: The D-optimal Approach and its Implementation as a Computer Algorithm*. Bachelor Thesis in Information and Communication Technology. Umea University (Sweden); South Westphalia University of Applied Sciences (Germany). January **2008**.

[3]. ASQ. *Design of Experiments*. Consulted on January 9th, **2014**. URL: http://asq.org/learn-about-quality/data-collection-analysis-tools/overview/design-of-experiments.html

[4]. Anderson, M. J.; Whitcomb, P. J. *Design of experiments*. John Wiley & Sons, Inc., **1974**.

[5]. Eriksson, L.; Johansson, E.; Kettaneh-Wold, N.; Wikström, C.; Wold. S. *Design of Experiments, Principles and Applications*. Umetrics Academy, Sweden **2008**.

[6]. de Aguiar, P. F.; Bourguignon, B.; Khots, M. S.; Massart, D. L.; Phan-Than-Luu, R. *D-optimal Designs*. Chemom. Intell. Lab. Syst. **1995**;30:199.

[7]. MODDE – Design of Experiments 9.0, UMETRICS.

[8]. Walpole, R. E.; Myers, R. H.; Miyers, S. L. *Probabilidad y Estadística para Ingenieros* 6ª Ed. Prentice-Hall Hispanoamericana, México **1999**.

CHAPTER 4

EXPERIMENTAL METHODOLOGY

As stated in **Chapters 1 and 2**, the research was divided in two principal aspects:

- *Issues associated to the production of commercial TiO_2 self-cleaning materials for the building sector*
- *Limitations associated with the utilization of self-cleaning coatings at real conditions.*

4.1. Issues associated to the production of commercial TiO_2 self-cleaning materials for the building sector

4.1.1. Low adhesion

The first part of the research consisted in the design of a methodology for improving the adhesion between photocatalytic coatings and window glasses by the modification of the roughness of the glass substrates. The roughness modifications were made by chemical treatment of the glasses before coating, using a D-optimal

design to plan the experiments. Finally, scratch measurements were carried out using glasses with representative roughness values and coated with TiO_2 to evaluate the adhesion.

4.1.1.1. Experimental design

The experimental procedure for the glass roughness modifications throughout chemical treatments was planned using the Design of Experiments (DOE) technique, with the goal of not only improve the adhesion by means of the roughness approach, but also accurately investigate the variables that influence the changes of glass roughness. Furthermore, by the DOE was also possible to determine at what levels those variables must be kept to get either rough or smooth surfaces.

The control factors (i.e., the input variables) were chosen based on a literature analysis [1, 2]. Then, the kind of chemical solution, its concentration, and the treatment time were identified here as control factors. Since one of these factors constitute a categorical o qualitative variable (e.g., the chemical solution), a D-optimal design was chosen to plan the experiments because this kind of design could deal easily with qualitative factors.

The construction of an experimental plan through D-optimal design consists in [3]:

1) Define the control factors and their levels,

2) Selection of the model that fits and

3) Choosing design points from a set of candidate points that was generated depending on the selected model

As stated above, the chemical solution, its concentration and the treatment time were chosen as the control factors. The categorical variable, e.g., the chemical solution, was varied through three levels: hydrochloric acid (HCl), acetic acid (CH_2COOH) and sodium hydroxide (NaOH). On the other hand, the concentration variable was varied through two levels, high and low. Finally, the third factor, the treatment time, was varied through three levels, 30, 120 and 240 min. **Table 4.1** shows these factors and their levels, as well as the codes that were used to identify them. In addition, **Table 4.1** shows the responses (output factors).

Table 4.1. Factors, their levels and the chosen responses.

Input factors				
Parameter	**Code**	**Levels (Coded)**		
Chemical solution	X_1	HCl (X_{1HCl})	NaOH (X_{1NaOH})	CH_3COOH ($X_{1CH3COOH}$)
Concentration [a]	X_2	A (X_{2A})	B (X_{2B})	-
Treatment time, min	X_3	30 (X_{3-30})	120 (X_{3-120})	240 (X_{3-240})
Output factors				**Code**
Rms roughness, nm				Y_1
R_{p-v} [b], nm				Y_2
Weight loss, %				Y_3

These variables and their levels were inserted in the software MODDE –Design of Experiments- 9.0 (UMETRICS) and a quadratic model was chosen. The final D-optimal experimental plan contains a total of 14 experiments including three center points. **Table 4.2** shows the final D-optimal experimental plan.

[a] A= High concentration, B = Low concentration. Concentration in % for HCl and CH_3COOH and in M for NaOH.
[b] R_{p-v} = maximum peak-to-valley distance.

Table 4.2. D-optimal experimental plan for glass roughness modifications.

Exp. No.	Run order	Factors		
		Qualitative	Quantitative	
		(X_1) Chemical solution	(X_2) Concentration	(X_3) Treatment time, min
1	14	HCl	A	30
2	8	NaOH	A	30
3	4	CH_3COOH	A	30
4	7	HCl	A	240
5	1	NaOH	A	240
6	**13**	**HCl**	**A**	**120**
7	10	CH_3COOH	A	240
8	9	HCl	B	30
9	2	NaOH	B	30
10	**3**	**HCl**	**A**	**120**
11	**12**	**HCl**	**A**	**120**
12	11	HCl	B	240
13	6	NaOH	B	240
14	5	CH_3COOH	B	240

4.1.1.2. Chemical treatments

The experiments specified in **Table 4.2** were carried out using SAINT GOBAIN soda-lime window glasses. The procedure used to perform the chemical treatments is based in that reported by Clark and Yen-Bower [4]: a Teflon® container immersed in an oil bath set at 37 °C was filled with HCl, NaOH or CH_3COOH. Once the chemical solution reached constant temperature, a glass specimen was placed on the top of the Teflon® container, as shown in **Figure 4.1**. The specimen was kept in contact with the solution for the periods of time specified in **Table 4.2**. After the treatment, the treated glass was washed with deionized water.

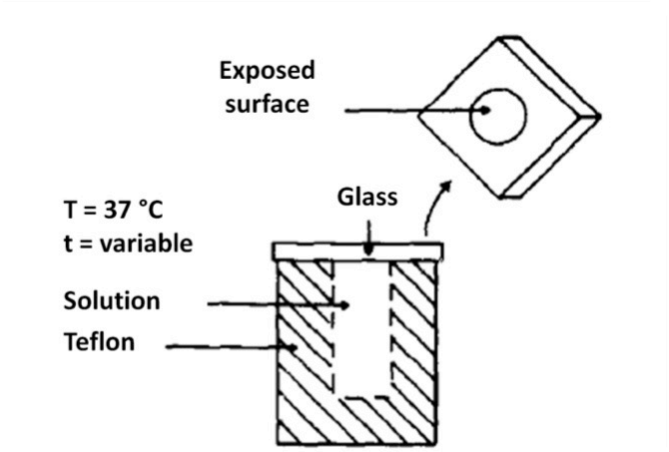

Figure 4.1. Procedure for the chemical attack of the soda-lime flat glass substrates. Taken from *Clark, D. E.; Yen-Bower, E. Lue. Corrosion of glass surfaces. Surf. Sci.* ***1980****;100:53* [4].

4.1.1.3. Glass substrates characterization

The roughness of the treated glasses was evaluated throughout Atomic Force Microscopy, AFM. Images of two different zones of each treated glass were taken with a Park Autoprobe CP, Park Scientific Instruments AFM equipment. All images were taken in non-contact mode using a 100 μm scanner, at a scan size of 5 μm. The roughness was expressed as Rms rough (root-mean-squared roughness, given by the standard deviation of the analysed data, Y_1) and R_{p-v} (referred to the maximum peak-to-valley distance within the analysed area, Y_2). The weight loss was determined measuring the weight of the glasses before and after the chemical treatment (Y_3).

4.1.1.4. Statistical analysis of the data

To determine how the chemical treatments presented in **Table 4.1** affect the roughness or the weight loss of the glass, the experimental results were analysed through statistical calculations and multiple regressions using the MODDE 9.0 [5] software, using the methodology reported in **Section 3.6** of Chapter 3.

4.1.1.5. Adhesion measurement: scratch tests

After the statistical analysis of the data and the generation and interpretation of the models for each response, some treated glasses with representative values of roughness (i.e., low, medium and high) were coated with TiO_2 to determine the correlations between roughness and adhesion.

The TiO_2 coatings were deposited from a commercial anatase TiO_2 nano-dispersion manufactured by COLOROBBIA Italia S.p.A, PARNASOS® PH000002. This dispersion contains 6.0 ± 0.5 wt. % of TiO_2 in the anatase form, with a particle size of 40 ± 2.5 nm, as reported in the Product Specifications Sheet attached to the product. The treated glasses were dip-coated using an 85 mm/min withdrawal rate. The coating procedure was carried out at 20 °C (room temperature) and 35-40% RH. After deposition, the coated glasses were dried at 110 °C for 1 hour.

The adhesion of the above samples was determined by scratch test using a CSM Open Platform with a Micro Scratch Tester. The technique involves generating a

controlled scratch with a diamond tip on the sample under examination. The tip either of diamond or sharp metal, is drawn across the coated surface under constant, incremental or progressive load [6], as shown in **Figure 4.2**. At a certain critical load the coating will start to fail. In the CSM Open Platform instrument, the critical loads are very precisely detected by means of an acoustic sensor attached to the load arm together with observations from a built-in optical microscope. The critical load data are then used to quantify the adhesive properties of different film-substrate combinations [6].

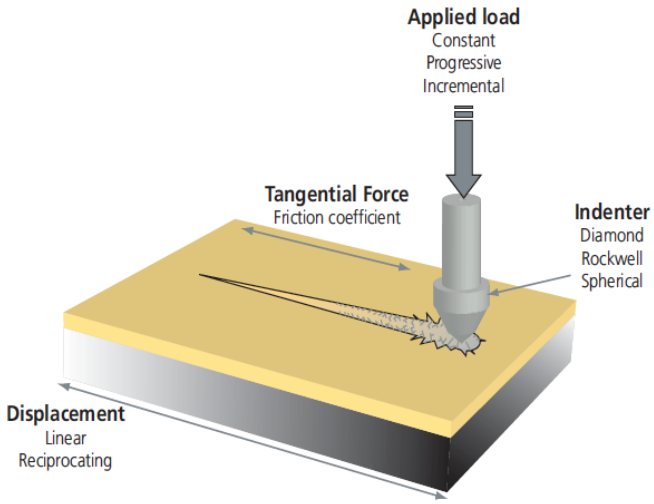

Figure 4.2. Scratch test. Taken from *CSM Scratch Tester Catalog [6]*.

The Joint Research Centre of the European Commission have defined three critical loads Lc_1, Lc_2 and Lc_3, corresponding to three particular events [7]:

Lc_1: Forward chevron cracks at the borders of the scratch track (Lc_1 shall be taken at the closest end of the event to the scratch track start);

Lc_2: Forward chevron cracks at the borders of the scratch track, with local interfacial spallation or with gross interfacial spallation (Lc_2 shall be taken at the failure event that occurs first, and at the closest end of the event to the scratch track start);

Lc_3: Gross interfacial shell-shaped spallation (Lc_3 shall be taken at the first point where the substrate can be seen at the centre of the track in a crescent that goes completely through the track).

Here, a Rockwell 209 diamond tip (200 ± 10 μm) was used. The load was gradually increased from 20 mN to 30 N, using a scanning load of 20 mN. The length of the track was 6 mm. Each measurement consisted in three steps in which the tip was scanned across the sample: the first scan with a constant load of 20 mN was performed in order to acquire the initial surface topography ("first pass"); in the second scan the increasing load was applied to the tip ("second pass"); the third scan, performed in the same way than the first, acquired the resulting scratch topography ("third pass") [8]. Three measurements were performed for each sample. In this work, only the Lc_3 values were measured and taken as the adhesion strength of the coating.

4.1.2. Preparation of TiO_2 self-cleaning glasses

Based in the results obtained from the adhesion study, samples with high adhesion were prepared for further studies. As a first step, the glass substrates were treated with concentrated acetic acid for 4 h and then dip-coated with the TiO_2 nano-

dispersion PARNASOS® PH000002 at 20 °C and 35-40% RH. After deposition, the coated glasses were dried at 110 °C for 1 hour. These samples were used for the studies of substrates that affect the PCA and the presence of residues that affect the PCA (**Sections 4.1.4** and **4.1.7**).

4.1.3. TiO_2 self-cleaning glass characterization

XRD analysis[c] was made by grazing incidence X-ray diffraction, using a Bruker D8 Advance diffractometer with Cu Kα1 radiation at the Universidad Autónoma de Nuevo León (UANL) in Monterrey, Mexico. Observations of the coatings were made using an Environmental Scanning Electron Microscopy (ESEM) FEI Quanta-200. The surface compositions of the original and acid-treated glasses coated with the TiO_2 nano-dispersion were determined by X-ray Photoelectron Spectroscopy (XPS) in an ultra-high-vacuum at a base pressure of 10^{-9} mbar. The X-ray photoemission was carried out with non-monochromatic Mg K_α photons (hv = 1253.6 eV) from a Vacuum Generators XR3 dual anode source operated at 15 kV, 18 mA and data were recorded with a double pass Perkin Elmer PHI 15-255G cylindrical-mirror electron analyser (CMA) operated at constant pass energy.

[c] **NOTE:** For data analysis convenience the XRD pattern was obtained using a silicon wafer as substrate, with the aim to avoid interferences of the glass signals with those derived of the TiO_2 film.

4.1.4. Use of substrates that affect the photocatalytic activity

The effect of the glass substrate on the PCA of TiO_2 self-cleaning glasses was determined by comparing the photocatalytic activity of a TiO_2 coating deposited over an as-received window glass and another deposited over a window glass that was treated with CH_3COOH for 4 h. The tests were carried out following the procedure reported in the next Section (**Section 4.1.5**).

4.1.5. Photocatalytic tests

All the photocatalytic tests carried out throughout this research were evaluated by the degradation of stearic acid (SA) under ultraviolet irradiation at 365 nm, using a Vilber VL-215.LC lamp (365/254 nm). SA was deposited from a solution of 0.05g SA/20 ml EtOH (ethanol) by spin coating at 1500 rpm for 30s or by dip-coating for 60 s, using a withdrawal rate of 85 mm/min. The photo-degradation was followed by Fourier-transform infrared (FTIR) spectroscopy, monitoring the disappearance of the vibrational bands between 2700-3000 cm^{-1} in the FTIR spectra, corresponding to the aliphatic C-H stretching modes. The spectra were acquired in transmission mode using a BRUKER ALPHA FT-IR Spectrometer in the studies carried out at the Commonwealth Scientific and Industrial Research Organization (CSIRO), Clayton Australia or a Vertex 70-BRUKER spectrometer in the studies carried out at the Università degli Studi di Modena e Reggio Emilia (UNIMORE), Modena, Italia, averaging in both cases 32 scans between 4000 and 400 cm^{-1} with a spectral

resolution of 4 cm^{-1}. Finally, photocatalytic efficiency plots were obtained by integrating the area under the C-H peaks.

4.1.6. Degradation rates

Depending of the trends in SA photodegradation observed in the different processes evaluated in this work, the kinetic modelling was obtained using two methods:

(i) Calculation of the degradation rate through the slope and the SA concentration, applying the reported concentration value of 3.17 x 10^{15} stearic acid molecules per cm^2 per integrated absorbance unit over the 2700-3000 cm^{-1} intervals in the FTIR spectrum [9] or

(ii) Using the pseudo first order kinetic equation proposed by Sawunyama et al. [10], which incorporates the reactivity of TiO_2 film and film disorganization phenomenon during the photodegradation process:

$$[SA]_t = [SA]_{initial}\exp(- k_{obs}t) \quad \textbf{[4.1]}$$

where $[SA]_t$ is the concentration of stearic acid at time t, $[SA]_{initial}$ is the initial concentration of stearic acid, and k_{obs} is the pseudo first order rate constant.

Since it has been widely reported that, owing to the complex mechanism of reactions, it is difficult to develop a model for the dependence of the photocatalytic

degradation rate on the experimental parameters for the whole treatment time [11], kinetic modelling of the photocatalytic processes was restricted to the analysis of the *initial rate* of photocatalytic degradation, r_i [11-13].

4.1.7. Residues that affect the PCA

The freshly prepared TiO_2 self-cleaning glasses (as stated in **Section 4.1.2**) were treated with deionized water (18 MΩ) for 19 h to remove the sodium based-salt present at the TiO_2 surface. For comparison, treatments with 0.2 M HCl were also performed. After the treatments, the PCA and the SA degradation rates of the samples were tested using the procedures specified in **Sections 4.1.5** and **4.1.6,** respectively.

4.2. Limitations associated with the utilization of TiO_2 self-cleaning coatings at real conditions

Here, three different types of TiO_2 coatings (nanoparticled, mesoporous and non-porous TiO_2) were exposed to weathering and different values of temperature and humidity in order to evaluate the effects of these phenomena on the self-cleaning property of the coatings.

4.2.1. Preparation of the TiO_2 coatings

4.2.1.1. Synthesis of the mesoporous TiO_2 coating

TiO_2 mesoporous coatings were prepared using a "*quick*" version of the EISA-derived method developed by Crepaldi and co-workers [14].

The original evaporation-induced self-assembling (EISA) method consists the preferential evaporation of a solvent (usually an alcohol) that concentrates an initial diluted solution (formed by an inorganic precursor, an alcohol and a pore-forming agent) over a non-volatile surfactant and inorganic species before equilibration with atmosphere [14, 15]. The formation of micelles organised in a liquid crystal template permits the condensation of the inorganic framework, giving rise to well-defined mesostructure hybrids [14, 15]. Finally, the extraction of the surfactant template by heat allows the obtaining of the mesoporous structure.

In EISA method, water is not considered for the synthesis of mesoporous structures. However, investigations made by Grosso's group [16-19] have demonstrated that highly organized mesoporous titania, zirconia and alumina or mesostructured mixed valence vanadium oxide-based thin films can be obtained by EISA-derived methods including controlled quantities of water [14]. Despite the similarities to the EISA method, in their approach water causes an important hydrolysis of the inorganic moieties, resulting in hydrophilic species with enhanced interactions with the polar

portion of the template. Moreover, water contributed to increase the polarity of the medium, facilitating template folding [16-19].

In the water modified EISA-method, the inorganic polymerization can be readily controlled by an acid (added or generated in situ), which is subsequently eliminated by evaporation. Besides the role of water added to the initial sol, these authors have individuated that the relative humidity of the atmosphere is a parameter of paramount importance, which plays a decisive role in the organization of the system [14, 16-19].

Here, the mesoporous titania was obtained by the slow addition of $TiCl_4$ (FLUKA Analytical) to a mixture of absolute ethanol (37% INCOFAR) and the tri-block copolymer Pluronic F-127 template (Sigma-Aldrich). Water (18 MΩ) was added drop by drop after 5 min of stirring. The molar ratio was $TiCl_4$:EtOH:H_2O = 1:40:12 and the ratio $TiCl_4$/Pluronic F-127 was 0.006. According with Crepaldi et al. [14], the addition of water causes the hydrolysis of the inorganic moieties, producing in situ ethanol and HCl, the latter being the reason for the high stability of the sols:

$$TiCl_4 + 2EtOH \rightarrow TiCl_2(OEt)_2 + 2HCl \quad \textbf{[4.2]}$$

$$TiCl_2(OEt)_2 \xrightarrow{mH_2O} [Ti(OH)_2(H_2O)_n(Z)_n]^{(2-x)+} + (\sim 2 - xHCl) + (\sim 2 - xEtOH); \quad Z = OH, Cl, OEt; \quad m > 4; \quad x < 2 \quad \textbf{[4.3]}$$

To form the coating, a silicon substrate was dip-coated at 85 mm·min^{-1} and at a relative humidity of 33%. After deposition, the film was exposed to water vapour for

30 s, contrary to the procedure reported by Crepaldi et al. [14], in which films were aged for at least 2 days at 50-60% RH. The obtained mesoporous coatings were maintained at 200°C for 24 h to stabilize the mesoporous structure. After this thermal treatment, the temperature was increased up to 500°C and kept for 3 h to crystallize the TiO_2 anatase phase.

The same mesoporous TiO_2 coatings were also prepared at CSIRO. In this case, however, the Si substrate was dip-coated at 160 $mm \cdot min^{-1}$ and at a relative humidity of 18-20 %.

4.2.1.2. Synthesis of the non-porous TiO_2 coating

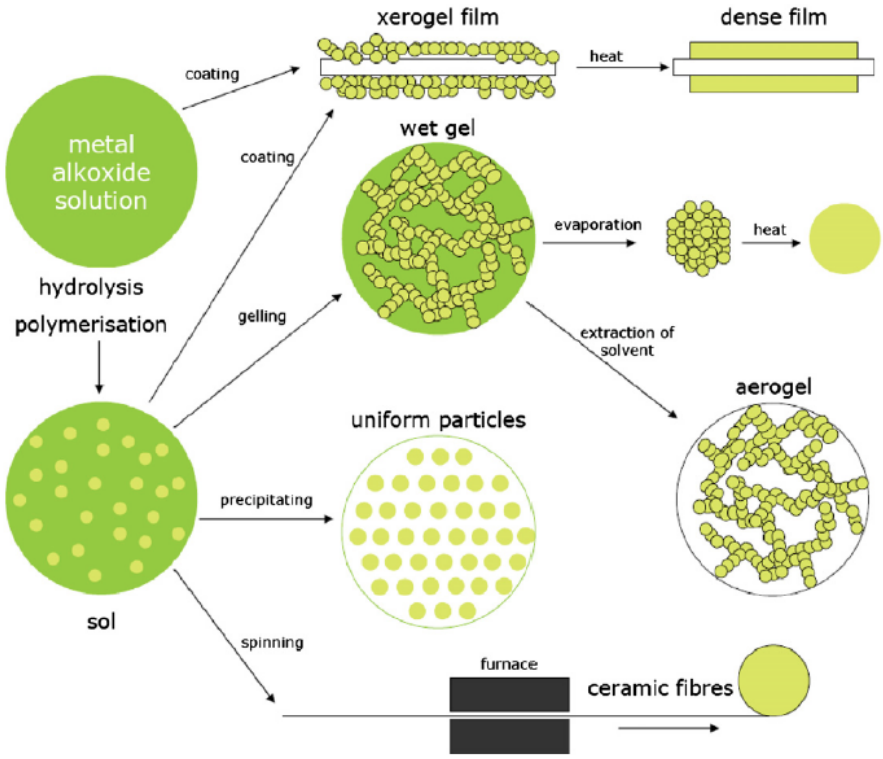

Figure 4.3. Sol-gel technology and products. Taken from *Cannavale et al. Building and Environment 2010;45,1233-1243*.

The non-porous titania was synthetized by the sol-gel process. **Figure 4.3** shows the steps of the sol-gel processing of materials and examples of the microstructures of final products.

A typical sol-gel method for fabricating materials starts with a solution consisting of metal compounds, such as metal alkoxides and acetylacetonates as source of oxides, water as hydrolysis agent, alcohol as solvent and an acidic or a basic catalysts. Metal compunds udergo hydrolysis and polycondensation at room temperature, giving rise to sol, in which polymers or fine particles are dispersed. Further reactions connect the particles, solidifying the sol into a wet gel, which still contains water and solvents. Usually, various shapes are formed during the sol to gel transformation. Vaporization of water and solvents produces a dry gel, one of the final products. Heating of gels to several hundred degrees or higher temperatures produces dense oxide materials as final products [20]. The sol-gel method is characterized by low processing temperature. Moreover, materials of various shapes and microstructures can be prepared. Bulk bodies can be made by casting the gelling sol into a mould. Fibers can be drawn from the viscous sol, whether a sol of appropriate composition is used. Coatings films can be made by dip coating or spin coating of the sol. Unsupported films can be made by synthesizing the film at the interface between alkoxide solution and water [20].

Here, the non-porous TiO_2 film was synthesized by mixing titanium isopropoxide (Sigma-Aldrich), absolute ethanol (Carlo Erba) and HCl 1M (37% INCOFAR) in the molar ratios 1:100:0.06. The sol was stirred for 1 hour before coating. A clean silicon

substrate was dip-coated in the fresh sol at a relative humidity of 11% and at the pulling rate of 85 mm·min^{-1}. Four coatings were deposited. Each coating was thermally treated at 100°C for 10 min and then 250°C for 30 min before the deposition of a successive coating. After the fourth deposition, the resultant film were thermally treated at 500°C for 3 h to favour the growth of the TiO_2 anatase crystal phase.

The same non-porous TiO_2 coatings were also prepared at CSIRO. In this case the substrate was dip-coated in the fresh sol at a relative humidity of 14-15% RH and at the pulling rate of 100 mm·min^{-1}.

4.2.1.3. Preparation of the nanoparticled TiO_2 coating

CH_3COOH-treated glass substrates were coated with the TiO_2 nano-dispersion PARNASOS® PH000002 at 20 °C and 35-40% RH. After deposition, the coating was dried at 110 °C for 1 hour.

4.2.2. Characterization of the TiO_2 coatings

Grazing incidence X-ray diffraction was used to characterize all the TiO_2 coatings using a Bruker D8 Advance diffractometer with Cu Kα1 radiation coupled with VANTEC detector (UANL, Mexico). FTIR spectra of the coatings were recorded in a Thermo Electron Nicolet 380 instrument (UANL, Mexico). By UV-Vis spectroscopy it was determined the band gap energy values, using a Perkin Elmer

Lambda 35 UV/Vis Spectrometer (UANL, Mexico). FEG-SEM images of the mesoporous and non-porous TiO_2 coatings were obtained through a FEI Nova NanoSEM 450 Field Emission SEM, in immersion lens mode. On the other hand, observations of the nanoparticled coatings were made using an Environmental Scanning Electron Microscopy (ESEM) FEI Quanta-200. Surface roughness and morphologies were evaluated by atomic force microscopy using a Digital Instruments NanoScope 3D in non contact mode, with a scanning area of 500 nm^2.

4.2.3. Weathering

4.2.3.1. Weathering treatments

To evaluate influence of the domestic weathering on the PCA, all the as-prepared coatings (nanoparticled, mesoporous and non-porous) were soaked into two model aqueous solutions that simulate common cleaning agents: a 5% isopropanol solution [21] and a detergent solution made of 2.5% propylene glycol propyl ether and 2.5 wt.% of sodium dodecylbenzenesulfonate [22].

The environmental weathering was evaluated soaking the films in 18 MΩ deionized water to simulate rain and into an aqueous acid solution to simulate acid rain (HNO_3 and H_2SO_4 pH 2-3) [23]. In addition, a quick aging test with boiling water was also performed for each morphology [24].

The treatments of the nanoparticled self-cleaning glasses were carried out at 32°C for 19 hours, since longer treatments times almost completely detach the coatings from the glasses. On the other hand, the treatments of the mesoporous and non-porous TiO_2 coatings were carried out for 1 week, since these coatings were not detached from the Si substrates during all the treatment time. **Table 4.3** shows an overview of the chemical solutions to simulate weathering of the tested materials.

Table 4.3. Chemical treatments to simulate domestic and environmental weathering.

Treatment	Objective
Boiling water	Aging test
Deionized water	Resistance to washing
Acid rain	Resistance in places with acid rain
Isopropanol 5%	Resistance to glass cleaning agents
Detergent solution	Resistance to all-purpose cleaning agents

4.2.3.2. Characterization of the TiO_2 coatings subjected to weathering

The release of TiO_2 from the self-cleaning glasses (nanoparticled) after the chemical treatments was measured by Inductively Coupled Plasma (ICP), using a Perkin Elmer ICP-OES Optima 2100 DV and a spectral line Ti 334.940 (CSIRO, Australia). The treated self-cleaning glasses were also characterized by Fourier-transform infrared (FTIR) spectroscopy. The spectra were acquired in transmission mode using a BRUKER ALPHA FT-IR Spectrometer (CSIRO, Australia). Finally, observations of all these samples were made using an Environmental Scanning Electron Microscopy (ESEM) FEI Quanta-200.

Since mesoporous and non-porous TiO_2 coatings proved to have a better resistance to weathering than the nanoparticled coatings, a more complete characterization was carried out for the these samples. Grazing incidence X-ray diffraction was used to characterize the as-prepared and treated coatings using a Bruker D8 Advance diffractometer with Cu Kα1 radiation coupled with VANTEC detector (UANL, Mexico). AFM images of all the samples were acquired using a Digital Instruments NanoScope 3D in non-contact mode (scan area of 500 nm). The initial water contact angle (WCA_i) of all the samples, i.e., the WCA of the samples before and after the chemical weathering in the dark (no UV light) was measured using a CONTACT ANGLE SYSTEM OCA. By UV-Vis spectroscopy it was determined the band gap energy value of each one the prepared coatings, using a Perkin Elmer Lambda 35 UV/Vis Spectrometer (UANL, Mexico). Furthermore, TiO_2 losses from treated films were determined by inductively coupled plasma, ICP. Finally, film adhesion of the as-prepared and treated samples was determined by scratch test using a CSM Open Platform with a Micro Scratch Tester. A Rockwell E-010 diamond tip (10 μm) was used. The load was gradually increased from 10 mN to 400 mN, using a scanning load of 10 mN. The length of the track was 6 mm. Three scratch measurements were performed and the average value of the critical load (Lc_3) is reported here.

4.2.3.3. PCA of the coatings subjected to weathering

The activity of the TiO_2 coatings subjected to weathering was evaluated using the procedure reported in **Section 4.1.5.** All the tests were performed at ambient

conditions (20 °C and 63 % RH). The initial degradation rates were obtained by applying the methodology reported in **Section 4.1.6.**

4.2.4. Effect of humidity on the PCA

4.2.4.1. Conditioning of the reactor

Humidity levels were varied through constant humidity solutions using different water-soluble salts at 20-21 °C [25]. **Table 4.4** shows the humidity levels tested.

Table 4.4. Studied relative humidity levels.

Water soluble salt	Theoretical relative humidity (%)	Measured relative humidity (%)
$LiCl \cdot H_2O$	11	12.8 ± 0.2
$MgCl_2 \cdot 6H_2O$	33	35.1 ± 0.7
$Mg(NO_3)_2 \cdot 6H_2O$	53	53.4 ± 0.6
NaCl	75	71.9 ± 1.9

4.2.4.2. Pre-conditioning of the coatings and pollutant deposition

Before pollutant deposition, all the coatings were exposed to the target relative humidity for at least 12 hours. Then, at the same humidity level, SA was deposited from a solution of 0.05g SA/20 ml EtOH (ethanol) by spin coating at 1500 rpm for 30s or by dip-coating for 60 s, using a withdrawal rate of 85 mm/min. Finally, the SA-coated TiO_2 films were kept in the darkness at the target relative humidity for 12 hours before exposure to UV light.

4.2.4.3. PCA of the coatings at different humidity values

The activity of the TiO_2 coatings at different humidity values was determined using the procedure reported in **Section 4.1.5.** All the tests were performed at ambient temperature (20 °C) and the UV lamp was turned on only when the reactor reached the target humidity value. The initial degradation rates were obtained by applying the methodology reported in **Section 4.1.6.**

4.2.5. Effect of temperature on the PCA

4.2.5.1. Experimental setup

The photocatalytic reactor consisted in a closed polystyrene container with a sensor to measure both the temperature and the relative humidity of the air. The illumination was provided by a 15W UV lamp (VILBER LOURMAT VL-215 LC) inserted in the top of the reactor. The low temperatures inside the reactor were reached using dry ice-ethylene glycol (0 °C) [26] and ice baths (10 °C). The sample-holder consisted in a Pyrex glass plate that was placed in direct contact with the bath and at 6 cm from the lamp. A thermometer directly in contact with the sample holder was used to measure the temperature of the samples. Once the low temperature was stabilized inside the reactor and the sample holder presented a constant temperature, the experiments were carried out. Since the UV lamp produces heat that can increase the substrate temperature, the cold baths were substituted by fresh ones every hour. The photocatalytic experiments made at 20 °C were carried out inside the reactor without

any bath (room temperature) and in those made at 30°C the sample holder was placed inside an oil bath set at 30 °C.

4.2.5.2. PCA of the coatings at different temperature values

The activity of the TiO_2 coatings at different temperature values was determined using the experimental setup described in the previous paragraph and the procedure reported in **Section 4.1.5.** The UV lamp was turned on only when the sample holder reached the target temperature value. The initial degradation rates were obtained by applying the methodology reported in **Section 4.1.6.**

4.3. References

[1]. Eske, L.D.; Galipeau, D.W. *Characterization of SiO_2 Surface Treatments Using AFM Contact Angles and a Novel Dewpoint Technique*. Colloids Surf. A **1999**;154:33.

[2]. Logan, B. E.; Shellenberger, K. *Effect of Molecular Scale Roughness of Glass Beads on Colloidal and Bacterial Deposition*. Environ. Sci. Technol. **2002**;36:84.

[3]. Grcic, I.; Vujevi, D.; Koprivanac, N. *The Use of D-optimal Design to Model the Effects of Process Parameters on Mineralization and Discoloration Kinetics of Fenton-type Oxidation*. Chem. Eng. J. **2010**:157:408.

[4]. Clark, D. E.; Yen-Bower, E. Lue. *Corrosion of glass surfaces*. Surf. Sci. **1980**;100:53.

[5]. MODDE – Design of Experiments 9.0, UMETRICS.

[6]. *CSM Scratch Testers Catalog*. Consulted on December 19th, **2013**. Available at: http://www.csm-instruments.com/en/Catalogs

[7]. Joint Research Centre, European Comission. *The certification of critical coating failure loads. A reference material for scratch testing according to ENV 1071-3*: **1994**.

[8]. Costacurta, S.; Falcaro, P.; Vezzù, S.; Colasuonno, M.; Scopece, P.; Zanchetta, E.; Guglielmi, M.; Patelli, A. *Fabrication of functional nanostructured coatings by a combined sol-gel plasma-enhanced chemical vapour deposition method*. J. Sol-Gel Sci. Technol. **2011**;60:340.

[9]. Paz, Y.; Luo, Z.; Rabenberg, L.; Heller, A. *Photooxidative self-cleaning transparent titanium dioxide films on glass*. J. Mater. Res. **1995**;10:2842.

[10]. Sawunyama, P.; Jiang, L.; Fujishima, A.; Hashimoto, K. *Photodecomposition of a Langmuir-Blodgett film of stearic acid on TiO_2 film observed by in situ Atomic Force Microscopy and FT-IR*. J. Phys. Chem. B **1997**;101:11000.

[11]. Kim, S. B.; Hong, S. C. *Kinetic study for photocatalytic degradation of volatile organic compunds in air using thin film TiO2 photocatalyst*. Appl. Catal. B **2002**;35:305.

[12]. Mills, A.; Lepre, A.; Elliot, N.; Bhopal, S.; Parkin, I. P.; O'Neill, S. A. *Characterisation of the photocatalyst Pilkington Activ^{TM}: a reference film photocatalyst?*. J. Photochem. Photobiol. A **2003**;160:213.

[13]. Minabe, T.; Tryk, D. A.; Sawunyama, P.; Kikuchi, Y.; Hashimoto, K.; Fujishima, A. *TiO_2-mediated photodegradation of liquid and solid organic compounds*. J Photochem. Photobiol. A **2000**;137:53.

[14]. Crepaldi, E. L.; Soler-Illia, G. J. de A.A., Grosso, D.; Cagnol, F.; Ribot, F.; Sanchez, C. *Controlled formation of highly organized mesoporous titania thin films: from mesostructured hybrids to mesoporous nanoanatase TiO_2*. J. Am. Chem. Soc. **2003**;125:9770.

[15]. Innocenzi, P.; Malfatti, L. *Mesoporous thin films: properties and applications*. Chem. Soc. Rev. **2013**;42:4198.

[16]. Grosso, D.; Soler-Illia, G. J. A. A.; Babonneau, F.; Sanchez, C., Albouy; P.-A.; Brunet-Bruneau, A.; Balkenende, A. R.. *Highly organized mesoporous titania thin films showing mono-oriented 2D hexagonal channels*. Adv. Mater. **2001**;13:1085.

[17]. Crepaldi, E. L.; Soler-Illia, G. J. A. A.; Grosso, D.; Albouy, P.-A.; Sanchez, C. *Design and post-functionalisation of ordered mesoporous zirconia thin films.* Chem. Comm. **2001**;1582.

[18]. Pidol, L.; Grosso, D.; Soler-Illia, G. J. A. A.; Crepaldi, E. L.; Sanchez, C.; Albouy, P.-A.; Amenitsch, H.; Euzen, P. *Hexagonally organized mesoporous aluminium-oxo-hydroxide thin films prepared by the template approach. In situ study of the structural formation*. J. Mater. Chem. **2002**;12:557.

[19]. Crepaldi, E. L.; Grosso, D.; Soler-Illia, G. J. A. A.; Albouy, P.-A.; Amenitsch, H.; Sanchez, C. *Formation and stabilization of mesostructured vanadium-oxo-based hybrid thin films*. Chem. Mater. **2002**;14:3316.

[20]. Cannavale, A.; Fiorito, F.; Manca, M.; Tortosici, G.; Cingolani, R.; Gigli, G. *Multifunctional bioinspired sol-gel coatings for architectural glasses*. Build. Environ. **2010**;45:1233.

[21]. Ajax Expert® Glass and Multi-Surface Cleaner, Ready-To-Use, RTU MSDS **2004**.

[22]. *Fabuloso-Lavender*® All-purpose cleaner MSDS N° 200000016032.

[23]. *EPA Method 1320*, **1986**. Multiple Extraction Procedure.

[24]. TOYOTA Rista Coat Performance tests. Consulted on September 25th, **2012**. URL: http://www.ristacoat.cn/en/index.html

[25]. Wexler, A. S. *Constant humidity solutions*. In CRC Handbook of Chemistry and Physics 87th Ed. David R. Lide, **2006-2007**.

[26]. Lee, D. W., Jensen, C. M. *Dry-Ice bath based on ethylene glycol mixtures*. J. Chem. Educ. 2000;77:629.

CHAPTER 5

ISSUES ASSOCIATED TO THE PRODUCTION OF COMMERCIAL TIO_2 SELF-CLEANING MATERIALS FOR THE BUILDING SECTOR

In this Chapter, the results and discussions regards the issues associated to the production of commercial TiO_2 self-cleaning materials are presented. As stated in the previous sections, these issues are:

- *Low adhesion*
- *Substrates that affect the PCA*
- *Residues from the photocatalyst synthesis*

5.1. Low adhesion

5.1.1. General trends of roughness and weight loss values

5.1.1.1. Roughness

The roughness and weight loss values of the treated glasses are reported in **Table**

5.1. **Figure 5.1** shows the AFM 3D images of three treated glasses with representative roughness values: high, medium and low. In addition, in **Figure 5.1** is also presented the AFM 3D image of the reference (as-received) glass. Compared with a reference glass (no treatment, Rms rough = 3.41 nm) it was observed that the chemical treatments modify the roughness, resulting in lower or higher roughness values.

Table 5.1. D-optimal experimental design with the obtained responses.

No.	Factors			Responses		
	Qualitative	Quantitative				
	(X_1) Chemical solution	(X_2) Concentration	(X_3) Treatment time, min	(Y_1) Rms rough (nm)	(Y_2) R_{p-v} (nm)	(Y_3) weight loss (%)
1	HCl	A	30	2.40	76.46	0.000
2	NaOH	A	30	2.52	45.70	0.001
3	CH_3COOH	A	30	6.00	90.84	0.000
4	HCl	A	240	2.08	54.93	0.006
5	NaOH	A	240	7.10	83.41	0.005
6	HCl	A	120	3.16	40.23	0.009
7	CH_3COOH	A	240	1.49	17.75	0.001
8	HCl	B	30	20.00	320.00	0.005
9	NaOH	B	30	3.42	43.80	0.003
10	HCl	A	120	3.84	48.37	0.003
11	HCl	A	120	13.27	126.40	0.005
12	HCl	B	240	13.60	147.00	0.002
13	NaOH	B	240	10.14	101.20	0.004
14	CH_3COOH	B	240	10.16	77.78	0.008

NOTE: Error = 0.5 nm for Y_1, 5.6 nm for Y_2 and 0.002% for Y_3.

Sample 8 shows the highest roughness value. From **Figure 5.1b** it can be observed that this surface is non-homogeneous, and from the 2D AFM image shown in **Figure 5.2** it is observed the presence of residual particles formed as consequence of the chemical attack. This was also confirmed by the highest R_{p-v} value.

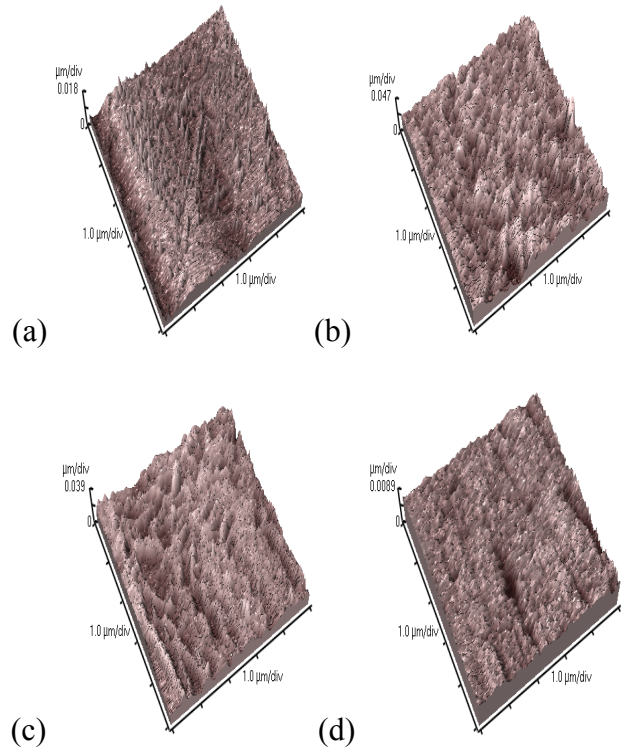

Figure 5.1. AFM 3D images of representative glass substrates. (a) Reference glass; (b) Experiment 8, highest roughness; (c) Experiment 12, medium roughness and (d) Experiment 7, lowest roughness.

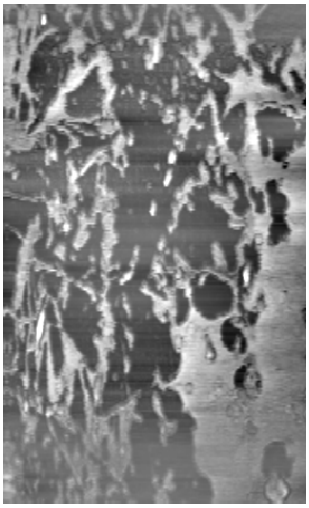

Figure 5.2. 2D AFM image of Sample 8 (roughest sample).

Experiment 12 was taken as a representative sample of "medium" value of roughness [(Highest value – Lowest value)/2]. This sample presents a more homogeneous surface than the rougher sample (**Figure 5.1c**). All the other samples with similar roughness values shown also similar homogeneous surfaces.

Finally, sample 7 presents the lowest values of roughness. This surface was the most homogeneous (**Figure 5.1d**). In both samples (13 and 7) there are no traces of residual particles.

From these AFM observations, it was concluded that the chemical treatments that induce high roughness also promote the formation of residual particles, which contribute to increase the roughness of the surface. Furthermore, the attacked surfaces of these samples are not homogeneous. This could be a problem during the deposition of nanofilms, since a non-homogeneous surface decrease the adhesion of the coating. On the other hand, the chemical treatments that induce low roughness generate homogenous smooth surfaces, without the deposition of residual particles.

5.1.1.2. Weight loss

The weight loss of the glass substrates after the chemical treatment is shown in **Table 5.1**. Correlating this data with that of roughness, it was observed that low concentrations promote higher weight losses as a consequence of the increase of the glass roughness.

5.1.2. Statistical analysis and interpretation

5.1.2.1. Y_1, Rms roughness

The analysis of the raw data for Y_1 – Rms roughness - revealed high experimental reproducibility but a non-normal distribution, for this reason, a logarithmic transformation was applied. **Equation 5.1** shows the obtained regression model, which is characterized by meaningful values of R^2, Q^2, model validity and reproducibility (**Table 5.2**).

Table 5.2. Summary of fit of the regression model for Y_1, Rms rough.

Parameter	Value
R^2	0.98
Q^2	0.90
Model validity	0.41
Reproducibility	0.99

$$Y_1 = 0.8824 + 0.0667X_{1HCl} - 0.4802X_{1NaOH} + 0.4135X_{1CH3COOH} - 0.0004X_3 - 0.3154X_{2A} + 0.3154X_{2B} - 0.0002X_{1HCl}X_3 + 0.0026X_{1NaOH}X_3 - 0.0025X_{1CH3COOH}X_3 - 0.1197X_{1HCl}X_{2A} + 0.2354X_{1NaOH}X_{2A} - 0.2354X_{1NaOH}X_{2B} - 0.1158X_{1CH3COOH}X_{2A} + 0.1158X_{1CH3COOH}X_{2B} + 6.0817e\text{-}5X_3X_{2A} - 6.0817e\text{-}5X_3X_{2B} \quad \textbf{[5.1]}$$

Equation 5.1 shows that two linear coefficients (X_{2A} and X_{2B}) and some interaction factors are statistically meaningful ($X_{1CH3COOH}X_3$, $X_{1HCl}X_{2A}$, $X_{1HCl}X_{2B}$, $X_{1NaOH}X_{2A}$ and $X_{1NaOH}X_{2B}$). The negative sign of X_{2A} means that concentration A (high) has the effect of decreasing the roughness while the positive sign of X_{2B} indicates that this factor increases the roughness expressed as Rms rough. **Figure 5.3** shows the interaction plots for Rms rough. **Figure 5.3a** suggests that the effect of the chemical solution on Rms rough is dependent on the treatment time. This dependence is stronger when

using NaOH and CH_3COOH but is negligible when using HCl. On the other hand, **Figure 5.3b** indicates that the effect of the chemical solution on the response is dependent also on the concentration. This dependence is strong for HCl and CH_3COOH, while is low for NaOH.

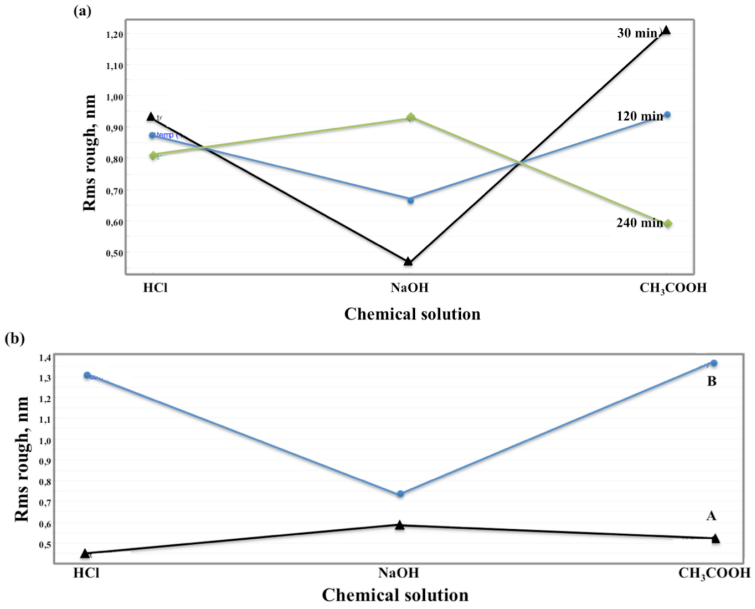

Figure 5.3. Interaction plots for Rms rough; (a) Chemical Solution/Treatment time; (b) Chemical Solution/Concentration.

5.1.2.2. Y_2, R_{p-v}

The raw data for R_{p-v} presented high reproducibility and normal distribution (after the logarithmic transformation). The model obtained presents good values of R^2, model validity and reproducibility, but a negative Q^2 value. From the analysis of residuals it was found that some experiments deviate from the normality and could be considered as possible outliers. By the removal of one of these experiments, a valid regression model (**Equation 5.2**) with good values of R^2, Q^2, model validity and reproducibility (**Table 5.3**) was obtained:

Table 5.3. Summary of fit of the regression model for R_{p-v}.

Parameter	Value
R^2	0.96
Q^2	0.77
Model validity	0.70
Reproducibility	0.97

$$Y_2 = 1.8843 + 0.2901X_{1HCl} - 0.2783X_{1NaOH} - 0.0118X_{1CH3COOH} - 0.0010X_3 - 0.0458X_{2A} + 0.0458X_{2B} - 9.3167e\text{-}5X_{1HCl}X_3 + 0.0025X_{1NaOH}X_3 - 0.0024X_{1CH3COOH}X_3 - 0.2623X_{1HCl}X_{2A} + 0.2623X_{1HCl}X_{2B} + 0.0294X_{1NaOH}X_{2A} - 0.0294X_{1NaOH}X_{2B} + 0.2329X_{1CH3COOH}X_{2A} - 0.2329X_{1CH3COOH}X_{2B} \quad \textbf{[5.2]}$$

The R_{p-v} parameter is influenced by two linear factors, the hydrochloric acid and the acetic acid, and by five interaction factors. The HCl has a positive effect, i.e., when using HCl the R_{p-v} parameter increases. On the other hand, a decrease in R_{p-v} is obtained when using acetic acid.

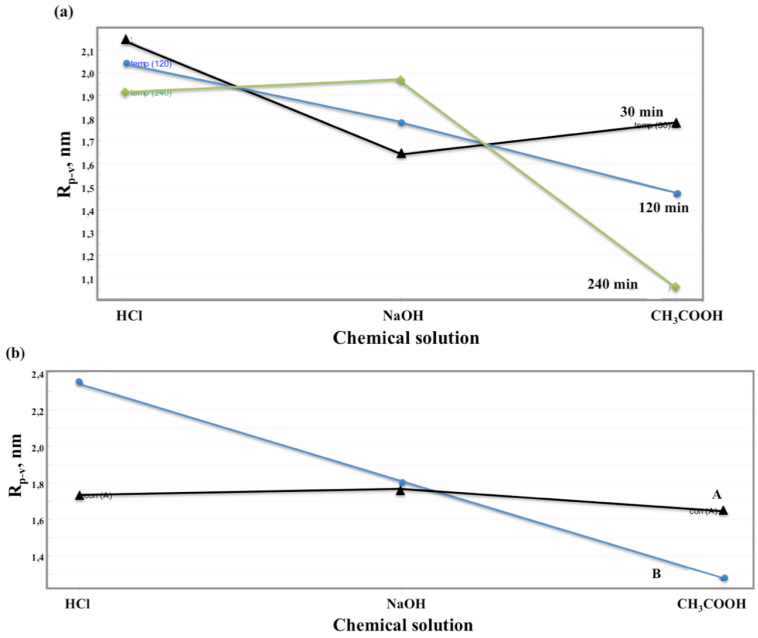

Figure 5.4. Interaction plots for Rp-v. (a) Chemical Solution/Treatment time; (b) Chemical solution/Concentraion.

The interaction plots (**Figure 5.4**) suggested that, as in previous case, the effect of the chemical solution on R_{p-v} is dependent on both the treatment time and the concentration. In particular, comparing these two plots it can be observed that the dependence of the chemical solution is stronger when varying the concentration.

5.1.2.3. Y_3, Weight loss

The analysis of the raw data for the weight loss revealed that also in this case a logarithmic transformation is necessary to obtain a Gaussian distribution in order to improve the subsequent statistical analysis. The obtained model presented non-statistically meaningful values of R^2, Q^2, model validity and reproducibility; indeed, the residual analysis shows the presence of two possible outliers. Their removal permitted to have a statistically meaningful model (**Equation 5.3**) for the weight loss.

$$Y_3 = -1.2290 + 0.6561X_{1HCl} + 0.5306X_{1NaOH} - 1.1867X_{1CH3COOH} - 0.0141X_3 + 0.0162X_{2A} - 0.0162X_{2B} - 0.0068X_{1HCl}X_3 - 0.0067X_{1NaOH}X_3 + 0.0135X_{1CH3COOH}X_2 \quad \textbf{[5.3]}$$

Equation 5.3 indicates a meaningful statistically linear factor, the treatment time (X_3) and three interaction factors, $X_{1HCl}X_3$, $X_{1NaOH}X_3$ and $X_{1CH3COOH}X_3$. The linear factor, X_3, has a negative influence on the weight loss, i.e., maximizing the treatment time and remaining constant the other factors, a decrease of the weight loss is obtained. Regard the interaction effects, the interaction plot (**Figure 5.5**) for the

weight loss revealed that the effect of the treatment time on the weight loss depends on the used chemical solution, especially at long times.

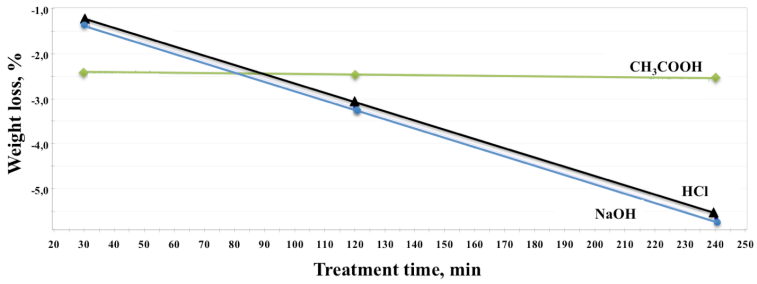

Figure 5.5. Interaction plot for Weight loss: Treatment time/Chemical solution.

5.1.3. Adhesion

Table 5.4 shows the chemical treatment, the roughness and the critical scratch loads of representative glass samples (highest, high, medium and low roughness).

Table 5.4. Roughness, scratch adhesion and WCA of some representative attacked glasses.

Sample	Roughness (nm)	Adhesion, C_L (N)	Water contact angle (WCA, °)	Observations
Reference	3.40 ± 0.01	4.56 ± 3.68	39.36 ± 1.30	At high loads the coating is detached from the substrate
Exp. 7	1.49 ± 0.02	9.17 ± 2.41	67.57 ± 2.91	The coating remains attached to the substrate in all the test
Exp. 12	13.60 ± 3.66	6.70 ± 5.33	75.88 ± 3.36	The coating remains attached to the substrate in all the test
Exp. 8	20.00 ± 10.02	3.35 ± 1.57	79.60 ± 3.41	The coating begins to detach over the track

Table 5.4 shows that the chemical treatments promote the enhancement of the WCA of the glasses. As observed in **Table 5.4**, the coated reference glass shows a non-

homogeneous low adhesion (C.L. = 4.56 ± 3.68 N). In this sample, when using high loads the coating is detached from the surface, as shown in **Figure 5.6**.

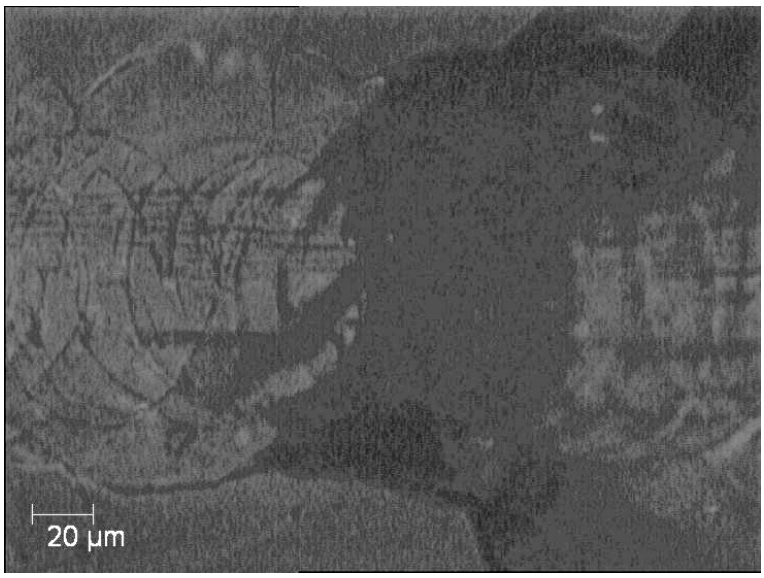

Figure 5.6. Scratch test track of Reference (as-received) glass coated with TiO_2.

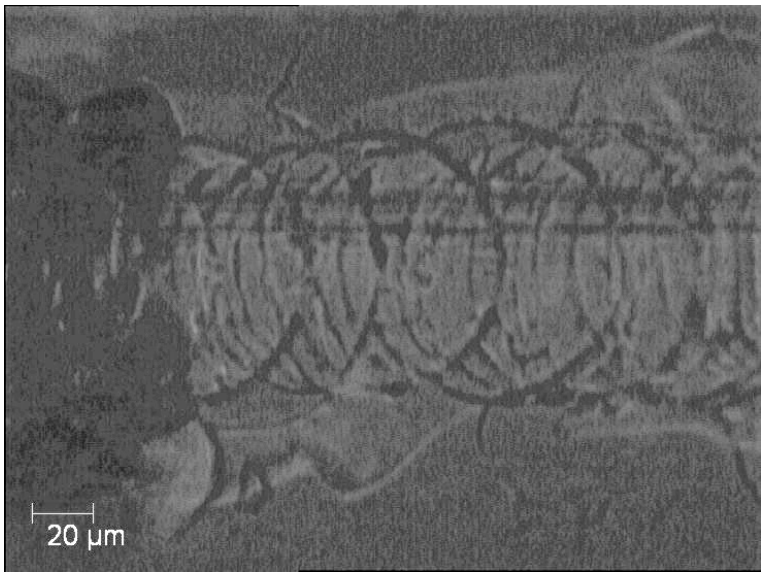

Figure 5.7. Scratch test track of Sample 8 coated with TiO_2.

Experiment 8, which presents a non-homogeneous and the roughest surface, present

one the lowest scratch adhesion, with a C.L. value of 3.35 ± 1.57 N. Therefore, this chemical treatment is not convenient for the pre-treatment of nano-coated glass substrates. Moreover, the coating begins to detach over the track, but is not completely removed from the substrate (**Figure 5.7**).

The fact that a high roughness does not improve the adhesion could be attributed to the combination of high roughness and the increase of the water contact angle of the attacked surfaces (**Table 5.4**). This combination often results in air pockets being trapped between the solid and liquid (the composite solid-liquid-air interface), thus leading to a significant decrease in the solid-liquid adhesion [1].

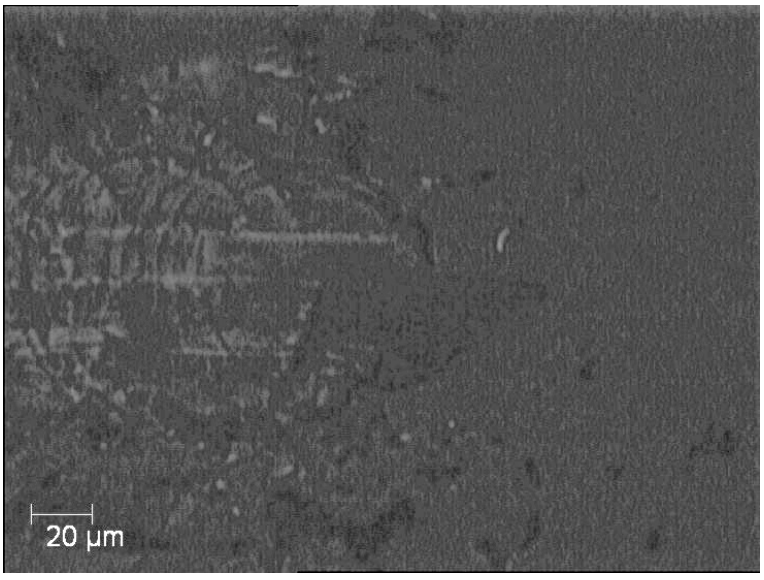

Figure 5.8. Scratch test track of Sample 12 coated with TiO_2.

Experiment 12, which presents a medium roughness value, present also a medium scratch adhesion, with a C.L. value of 6.70 ± 5.33 N. Although a medium value of adhesion was obtained, a high error is obtained. However, the coating is not

completely removed from the substrate (**Figure 5.8**).

From **Table 5.4**, it is clear that experiment 7 has the highest adhesion, since presents a critical load of 9.17 ± 2.41 N. This high value was correlated to its homogeneous smooth surface. Moreover, this sample shows one of the lowest variability of the adhesion from the sample set. In Experiment 7, the coating is not detached from the substrate; only the marks of the Rockwell tip are formed (like defects, **Figure 5.9**).

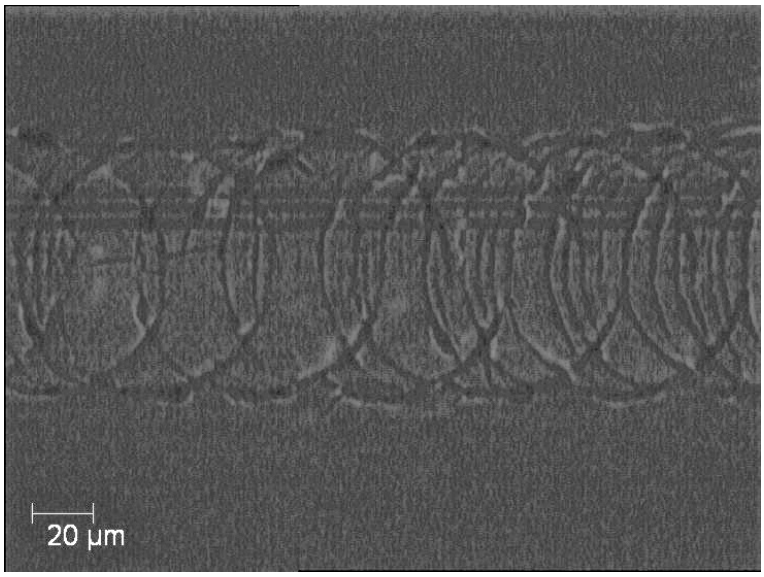

Figure 5.9. Scratch test track of Sample 7 coated with TiO_2.

5.2. Substrates that affect the PCA: soda lime glasses

Figure 5.10 shows a low magnification SEM image of the TiO_2 coating deposited from the commercial PARNASOS nano-dispersion over a soda-lime glass. As observed in this figure, some white aggregates are dispersed over the surface of the

coating. From the EDS spectrum, it was individuated that these white aggregates contains principally Ti, Na, Cl and Ca.

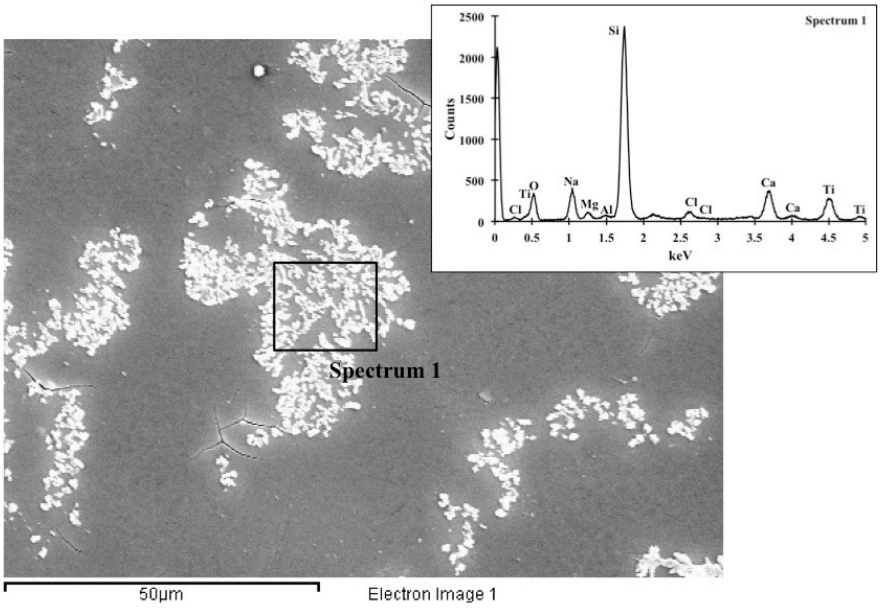

Figure 5.10 SEM image and EDS spectrum of the as-prepared TiO_2-coated glass.

This sample was further characterized by XRD with the aim to individuate the mineralogical composition of the coating. However, since the glass substrate caused signal interferences with the diffraction peaks corresponding to crystalline phases, this analysis was repeated over the same coating deposited over a silicon substrate. **Figure 5.11** shows the XRD pattern of the as-prepared TiO_2 coating deposited over a silicon substrate. As specified by the nano-dispersion producer, the TiO_2 present in the coating is in the anatase form (JCPDS N° 01-086-1155). In addition, the diffraction spectrum shows the presence of sodium chloride in the sample (JCPDS N° 01-072-1668), confirming the results obtained by EDS. The additional SiO_2 peak (JCPDS N° 00-042-1401), was attributed to the Si substrate, which was cleaned with

a H_2SO_4:H_2O_2 70:30 solution before the coating deposition, forming a surface SiO_2 layer.

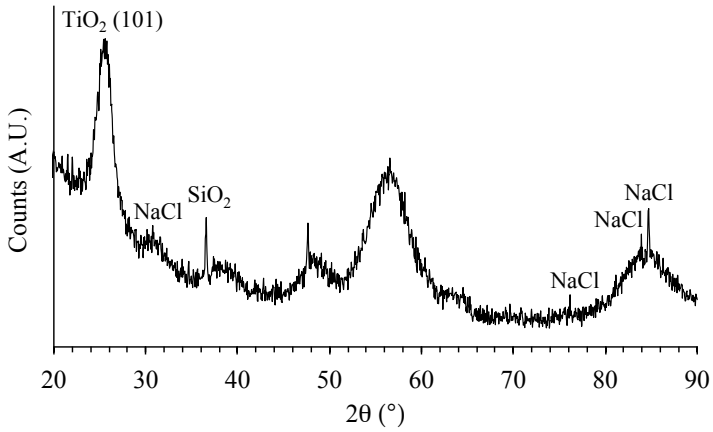

Figure 5.11. XRD pattern of the as-prepared TiO_2 coating deposited over a silicon substrate.

As stated in **Chapter 2** - **Section 2.1.2** - it has been well documented that soda-lime glasses (such as those used in this work) affect the PCA of the TiO_2 self-cleaning glasses due to diffusion of sodium and calcium ions from the substrate to the coating. This diffusion is usually attributed to the annealing process necessary to crystallize the anatase phase. Since in this work, no annealing was carried out (the as-prepared coating presented the anatase phase, see **Figure 5.11**), the ion diffusion hypothesis was rejected. To determine the source of NaCl, the original glass substrate treated with concentrated acetic acid (4 h *prior* the coating deposition) was analysed by XPS. It is important to keep in mind that this treatment was made with two objectives: (i) enhance the adhesion between the coating and the substrate (as stated in **Section 5.1.3.**) and (ii) reduce the alkaline and alkaline earth ion concentrations from the glass surface. **Figure 5.12** shows the XPS Na photoemission peaks of the

as-received and acid-treated glasses coated with the PARNASOS TiO_2 nano-suspension. **Table 5.5** shows the surface compositions of the as-received and acid treated glasses, both uncoated and coated with TiO_2.

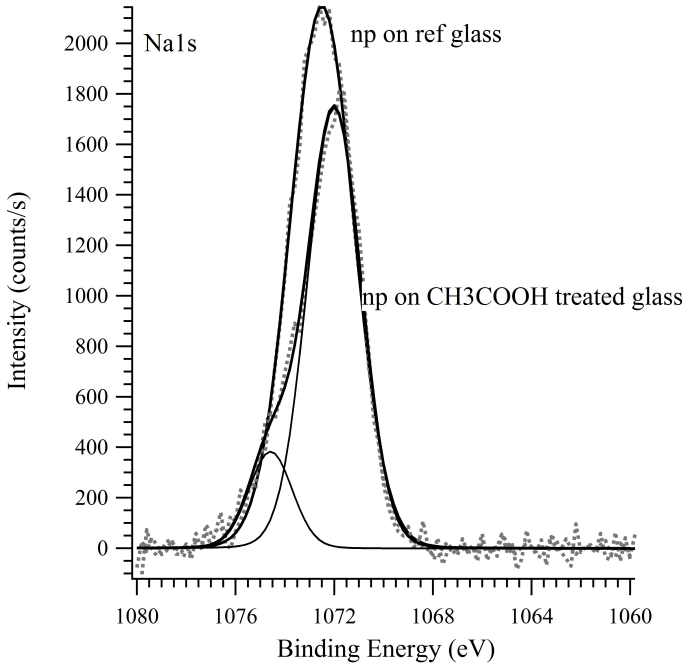

Figure 5.12. XPS Na photoemission peaks in the as-received and acid-treated glasses coated with the TiO_2 nano-suspension.

Table 5.5. Surface composition (atomic %) of the original and acid-treated glasses with and without the TiO_2 coatings, obtained from the photoemission peaks areas from the XPS spectra.

Sample	Si	O	Na	Ti	C
Original glass	21	47	3	0	29
Acid-treated glass	20	39	1	0	40
TiO_2 coatingon original glass	0	41	17	12	30
TiO_2 coating on acid-treated glass	0	44	13	13	30

From **Figure 5.12** it can be observed that the Na photoemission peak is present in the coatings deposited over both the as-received and acid-treated glasses. However, the intensity of the Na peak in the glass treated with acid is slightly lower than that of the

as-received sample. Furthermore, from **Table 5.5** it can be seen that the sodium atomic concentration of the original glass decreases after the acid treatment, and increases again when the TiO_2 coating is deposited. From these results, it was confirmed that the sodium chloride particles comes from the nano-dispersion, since this salt is used very likely in the commercial formulation as stabilization agent [2]. Then, the effect of this salt on the PCA of the final self-cleaning glass was investigated. The results are presented in the next section.

5.3. Residues from the catalyst synthesis that affects the PCA

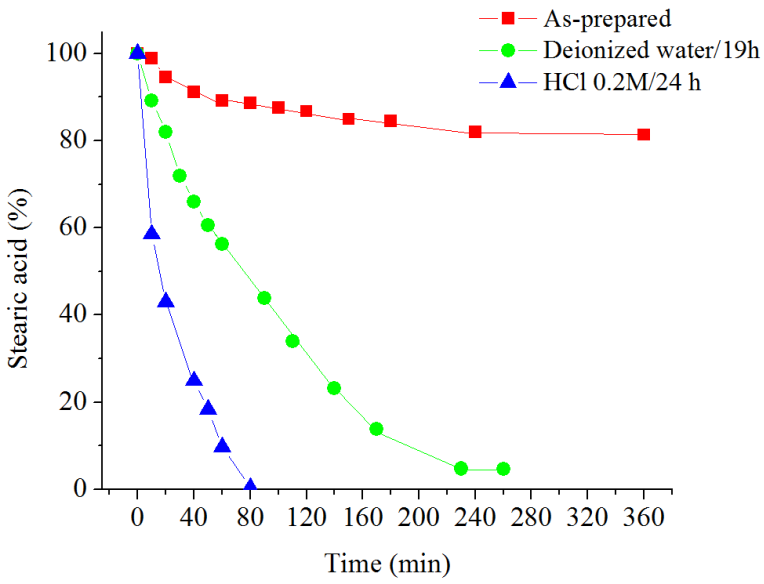

Figure 5.13. Photo-degradation of stearic acid deposited over the as-prepared, 0.02M HCl-treated and deionized water-treated TiO_2 coatings, irradiated at 365 nm.

Figure 5.13 shows the photo-degradation curves of SA deposited over the as-prepared, deionized water and HCl-treated TiO_2 self-cleaning glasses. It can be seen that in the red photo-degradation curve, corresponding to the as-prepared TiO_2

coated glass, shows that only ~20% of the deposited SA is decomposed after about 240 min of UV irradiation. This low activity was initially attributed to the sodium chloride residues contained in the TiO_2 surface.

To increase the PCA of the TiO_2 self-cleaning glass, treatments with 0.2M HCl and deionized water were carried out, and the degradation curves of the SA deposited over these treated coatings are also reported in **Figure 5.13** (green and blue curves, respectively). It is clear that treatments with an acid solution or deionized water increase both the PCA and the photo-degradation rates of the self-cleaning glasses. These rates were evaluated using the pseudo first order kinetic equation proposed by Sawunyama et al., [3] (See **Section 4.1.6**) and are 0.0010 ± 0.0007; 0.04 ± 0.01 and 0.011 ± 0.001 min^{-1} for the as-prepared, HCl-treated and water-treated self-cleaning glasses, respectively.

Figure 5.14 shows some SEM images of the as-prepared TiO_2 coating and those treated with HCl and deionized water. From **Figures 5.14a** and **5.14b** it can be noted than the treatment with HCl modifies the morphology of the coating. The nanoparticles, which are contained in aggregates of about 500-800 nm of diameter, seem more "exposed" in the coating treated with HCl than in the as-prepared one. On the other hand, the aggregates in the as-prepared sample are observed as "immersed into a matrix", probably formed by the residues from the nano-dispersion.

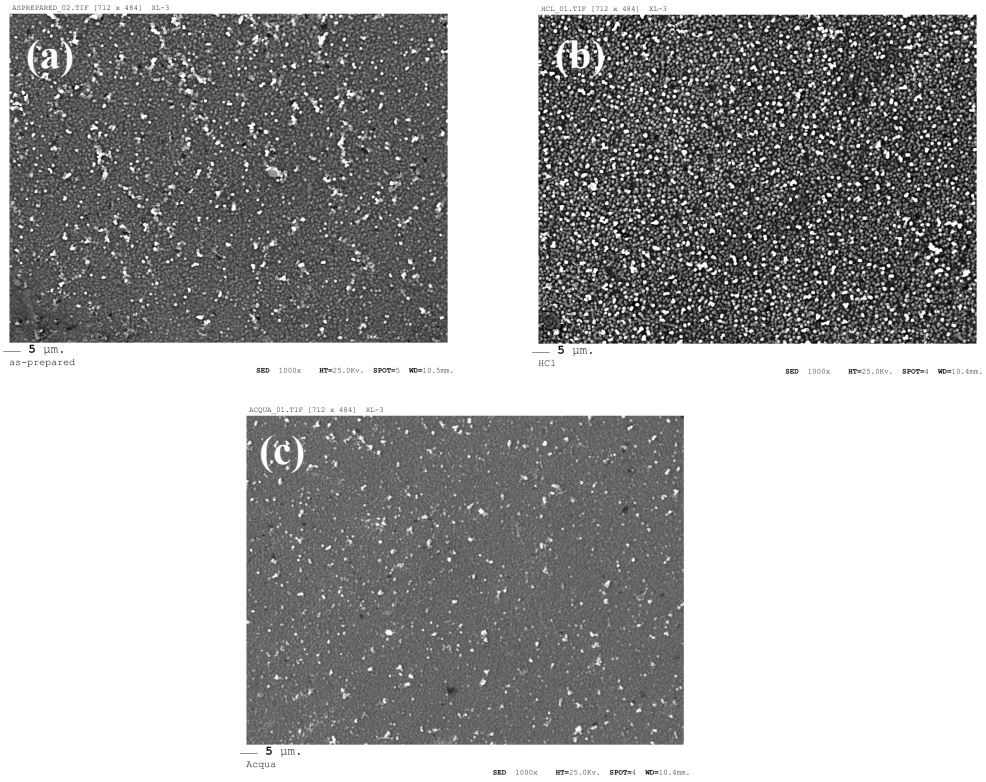

Figure 5.14. SEM images of the (a) As-prepared; (b) 0.2M HCl-treated and (c) Deionized water-treated TiO_2 coatings.

To explain this situation, we must consider the coating deposition procedure used in this work. As stated by the producer and confirmed in **Figure 5.11**, the nano-dispersion contains titania nanoparticles in the anatase form, thus thermal treatments to crystallize this phase are not required after deposition. Then again, a simple drying at 100 °C for one hour was carried out to evaporate the solvent of the nano-dispersion. This step is probably not sufficient to release or degrade the entrapped organic components coming from the dispersion used in the deposition, and the residue may compromise the PCA efficiency, as observed in the red curve of **Figure 5.13**.

Otherwise, the HCl-treated coating showed a better PCA (green curve in **Figure 5.13**) probably because this treatment removes the organic residues from the nano-dispersion. In the case of the coating treated with deionized water (blue curve in **Figure 5.13**), the morphology of the coating doesn't appear very different from that of the as-prepared coating (**Figures 5.14a** and **5.14c**). So, it can be concluded that treatments with deionized water do not promote the elimination of organic residues from the coating after the deposition.

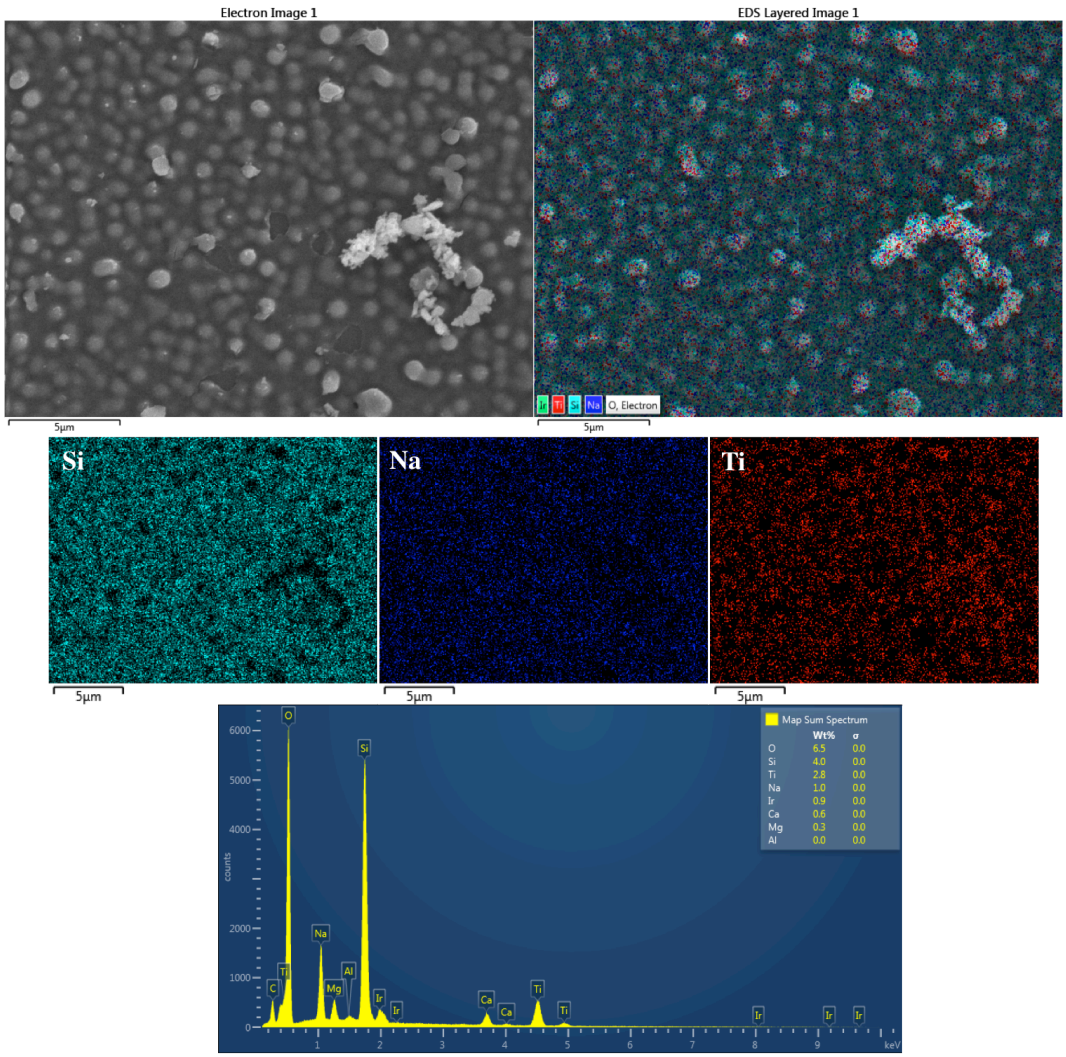

Figure 5.15. SEM image and EDS mapping of the HCl-treated TiO_2 coating deposited over a soda-lime glass.

Figure 5.15 shows a SEM image and several EDS maps corresponding to the TiO_2 coating treated with HCl. The EDS mapping was carried out for silicon, sodium and titanium elements. As observed in the EDS mapping for sodium, this is well distributed in the entire surface of the sample. Taking into account the characteristics of the electron beam of the SEM technique, it can be said that the sodium present in this sample does not correspond to the NaCl particles present over the as-prepared self-cleaning glass, but to the soda-lime glass used as substrate. In addition, this hypothesis was confirmed by the absence of chlorine in the EDS spectrum of this sample (the chlorine peak is well observed in EDS of the as-prepared TiO_2 self-cleaning glass, as shown in **Figure 5.10**).

Figure 5.16 shows the SEM image and the EDS maps corresponding to silicon, sodium and titanium elements of the TiO_2 coating treated with deionized water. Also in this case, no trace of chlorine (from NaCl) were found. So, in this sample the presence of sodium was also attributed to the soda-lime glass substrate.

The previous results indicated that environmental benefits in the production process of self-cleaning glasses from commercial coating suspensions can be obtained if the activity of residues-containing TiO_2 coatings can be enhanced just by water treatments. For example, it was seen that the treatment of the as-prepared TiO_2 coating with deionized water promotes the degradation of ~ 95% of the initial deposited SA. This value is very high compared with that of ~ 18% of the as-prepared coating. Then, although the hydrochloric acid-treated coating shows a better activity, the TiO_2 coatings prepared from this nano-dispersion do not have to be

necessary treated with acids to improve their efficiency, avoiding the generation of harmful residues. In this way, not only environmental but also economic benefits can be obtained with this method, since current TiO_2 nano-dispersions producers have not to modify completely their suspension formulas, compromising the stability of the dispersions, but just make a water treatment after the coating is deposited.

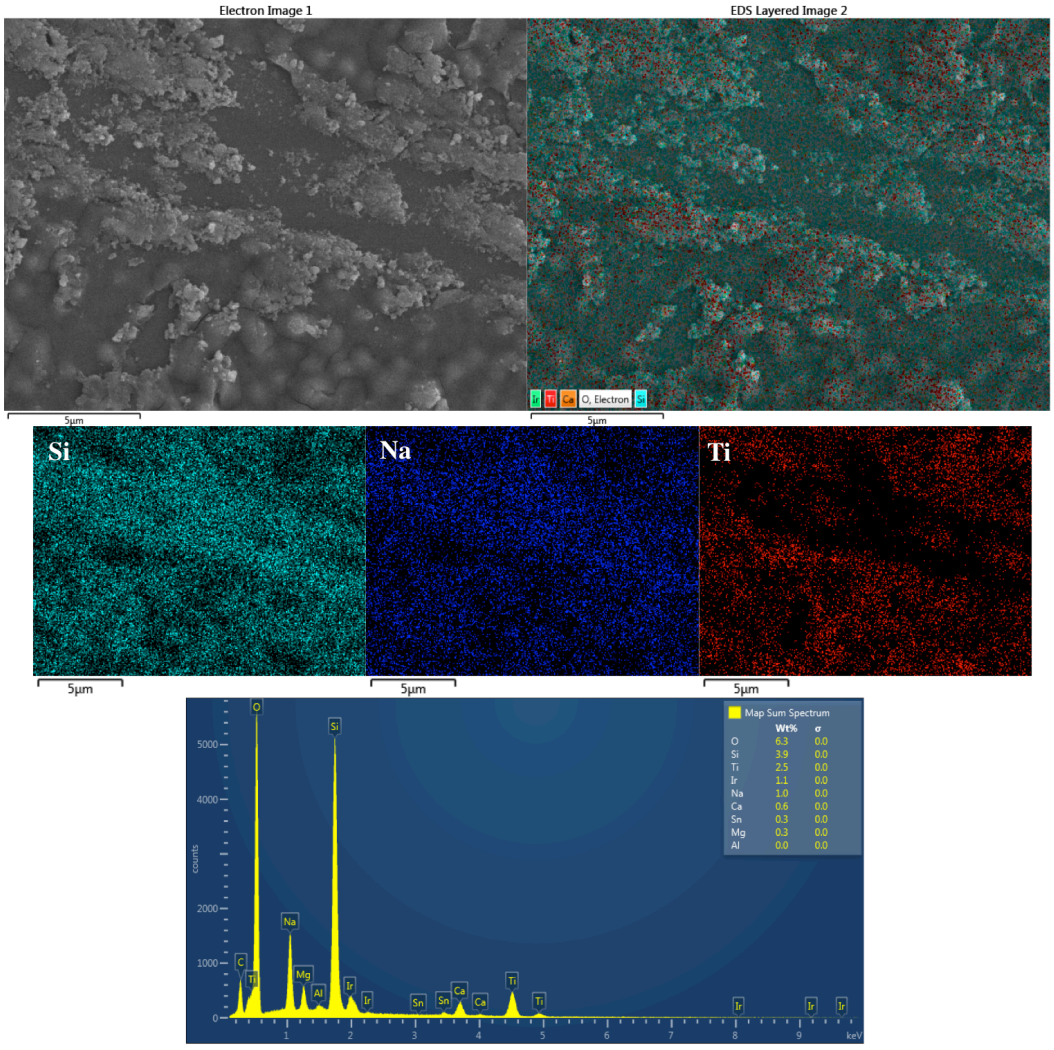

Figure 5.16. SEM image and EDS mapping of the TiO_2 coating deposited over a soda-lime glass and treated with deionized water.

5.4. References

[1]. Bhushan, B.; Nosonovsky, M. *Superhydrophobic surfaces and emerging applications: Non-adhesion, energy, green engeenering.* Curr. Opin. Colloid Interface Sci. **2009**;14:270.

[2]. Jiang J, Oberdörster, G Biswas, P. *Characterization of size, surface charge and agglomeration state of nanoparticle dispersions for toxicological studies*. J. Nanopart. Res. **2009**;11:77-89.

[3]. Sawunyama, P.; Jiang, L.; Fujishima, A.; Hashimoto, K. *Photodecomposition of a Langmuir-Blodgett film of stearic acid on TiO_2 film observed by in situ Atomic Force Microscopy and FT-IR*. J. Phys. Chem. B **1997**;101:11000.

CHAPTER 6

LIMITATIONS ASSOCIATED WITH THE UTILIZATION OF TiO_2 SELF-CLEANING COATINGS AT REAL CONDITIONS

In this Chapter, the results and discussions regards the limitations associated with the utilization of TiO_2 self-cleaning coatings at real conditions are presented. As stated in **Chapter 2**, some of these limitations include:

- *Weathering*
- *The changes in the PCA associated to the relative humidity*
- *The changes in the PCA associated to the substrate temperature*

6.1. Weathering

The effects of weathering on the durability and PCA of TiO_2 coatings was evaluated for three different morphologies: nanoparticled, mesoporous and non-porous coatings. The nanoparticled coatings were obtained from the commercial nano-dispersion, while the mesoporous and non-porous coatings were synthetized. Since during the experiments it was observed that the durability of coatings the were very

different from each, the treatments were carried out for 19 h for the nanoparticled coating and for 7 days for the mesoporous and non-porous coatings. Thus, comparisons were made only for these two latter coatings.

6.1.1. Nanoparticled coating

Table 6.1 describes the model solutions used to simulate weathering phenomena; the TiO_2 released after each treatment and the rates of stearic acid destruction for the nanoparticled TiO_2 coatings. On the other hand, **Figure 6.1** shows the SEM micrographies of the nanoparticled coatings treated as described in **Table 6.1**.

Table 6.1. Chemical treatments of the nanoparticled TiO_2 to simulate some common house hold conditions.

Treatment	Objective	TiO_2 released, %	k_{obs}, min^{-1}
Boiling water	Aging test	N.D.	0.010 ± 0.004
Deionized water	Resistance to washing	N.D.	0.012 ± 0.001
Acid rain	Resistance in places with acid rain	6.87 ± 0.75	0.004 ± 0.001
Isopropanol 5%	Resistance to glass cleaning agents	N.D.	0.042 ± 0.004
Detergent solution	Resistance to all-purpose cleaning agents	-	0.009 ± 0.002

N.D. = Not detected (lower than the instrument's detection limit). k_{obs}= Pseudo-first order rate constant as expressed in **Equation 4.1** (Chapter 4, Section 4.1.6).

From **Figure 6.1**, it can be observed that the morphology of the coatings does not change significantly after weathering. The only exception is the sample treated with acid rain.

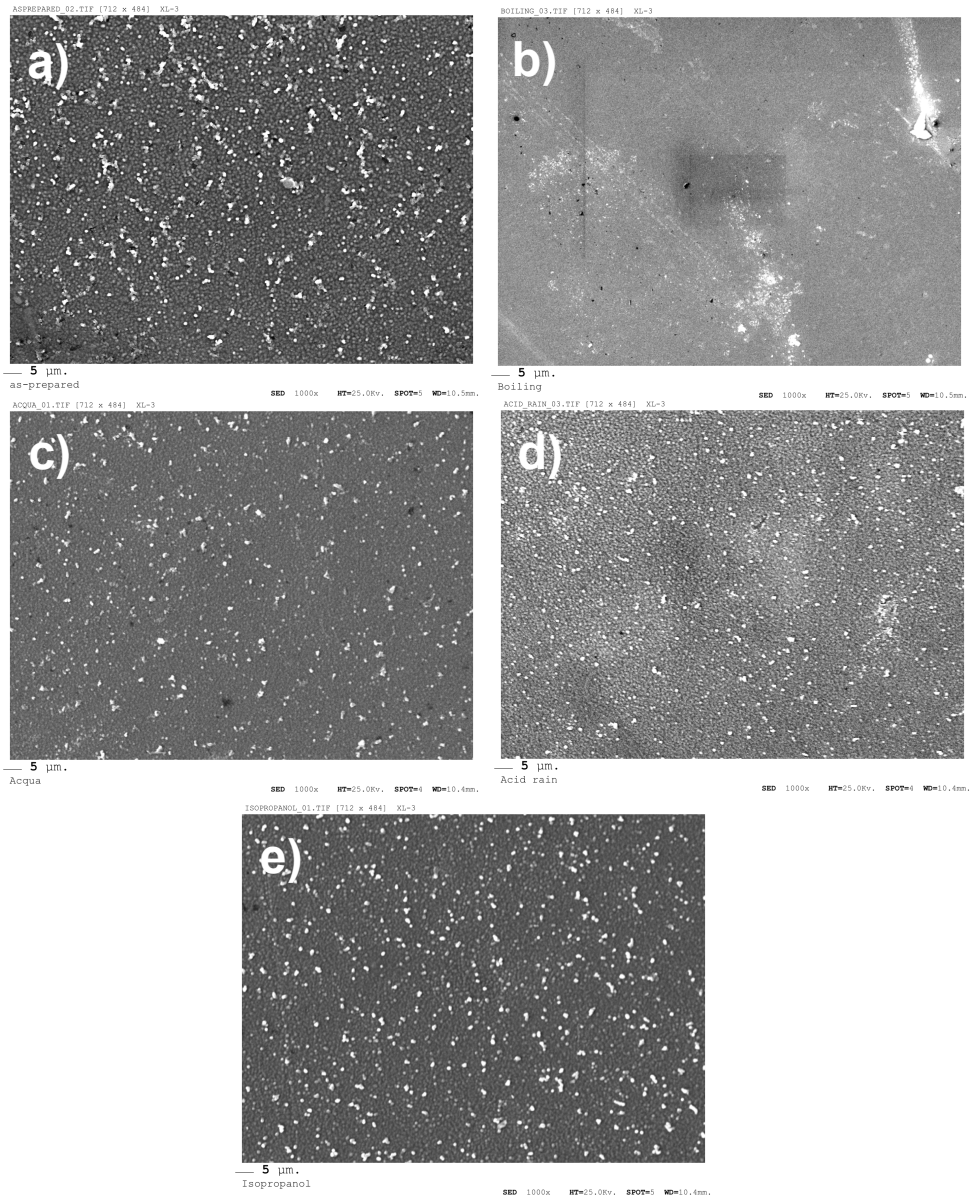

Figure 6.1. SEM micrographies of the nanoparticled TiO_2 self-cleaning glasses: (a) As-prepared; (b) Boiling water; (c) Deionized water; (d) Acid rain and (e) Isopropanol 5% (glass cleaner solution).

Figure 6.2 shows the SA degradation using the nanoparticled coatings treated as described in **Table 6.1**.

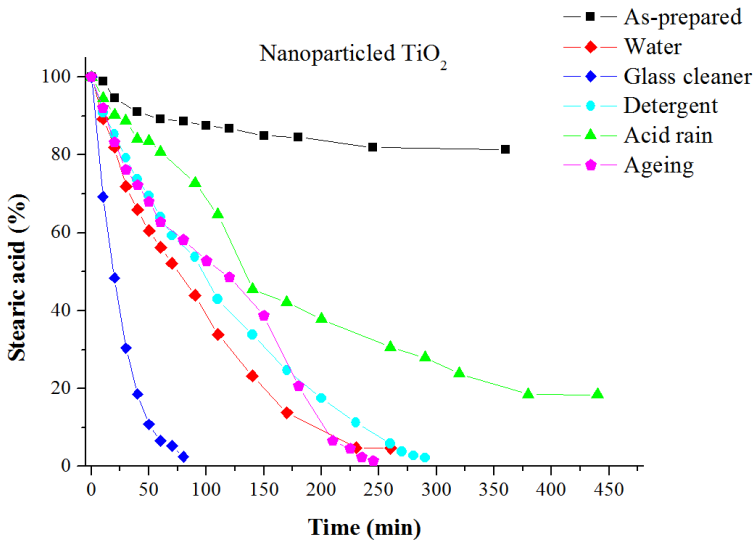

Figure 6.2. Overall photo-degradation of organic compounds deposited over the treated TiO_2 films.

From **Table 6.1** and the photo-degradation curves of **Figure 6.2**, it can be observed that the nanoparticled TiO_2 coatings possess a good chemical resistance, since there is no apparent loss of activity due to the release of TiO_2 nanoparticles. Indeed, if compared with the initial efficiency of the as-prepared TiO_2 coating (black curve), a 100% of stearic acid degradation is reached in almost all cases. From **Table 6.1**, the best photocatalytic rate is obtained when the coating is treated with the isopropanol solution. Other good and very similar rates are obtained when the coating is treated with water, boiling water and the detergent solution. As shown in **Figure 6.2** and **Table 6.1**, the coating treated with the acid rain has the lowest degradation rate and stops its PCA after 380 min of UV irradiation, very likely due to the formation of reaction intermediates [1], although in the FTIR spectra (from which the photo-degradation activity was determined) were not detected.

Figure 6.3 shows the FTIR spectra of the as-prepared and treated TiO_2 coatings. All the samples present the O-H stretching band between 3000-3600 cm^{-1} and some very small peaks between 2800-3000 cm^{-1}. These bands were attributed to the aliphatic C-H stretching vibration mode of the diethylene glycol present in the commercial nano-dispersion [2]. The darkest spectrum, corresponding to the as-prepared coating, shows the biggest O-H peak, and this was attributed to both the OH groups from the ethylene glycol and the adsorbed water, while the chemical-treated TiO_2 coating present OH bands with minor intensity. Then, the increase in the activity was related to an adequate grade of hydroxylation of the coatings, since, as will be explained in **Section 6.2** (Humidity), depending on the hydroxylation level, the adsorbed hydroxyl groups on the TiO_2 surface can both promote or inhibit the photocatalytic activity.

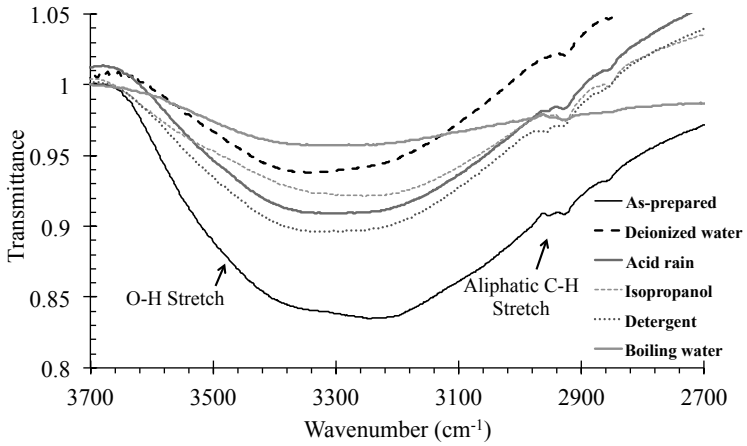

Figure 6.3. FTIR spectra of the as-prepared and TiO_2 films treated with the chemical solutions.

6.1.2. Mesoporous and non-porous TiO_2 coatings

6.1.2.1. Characterization

6.1.2.1.1. X-ray diffraction

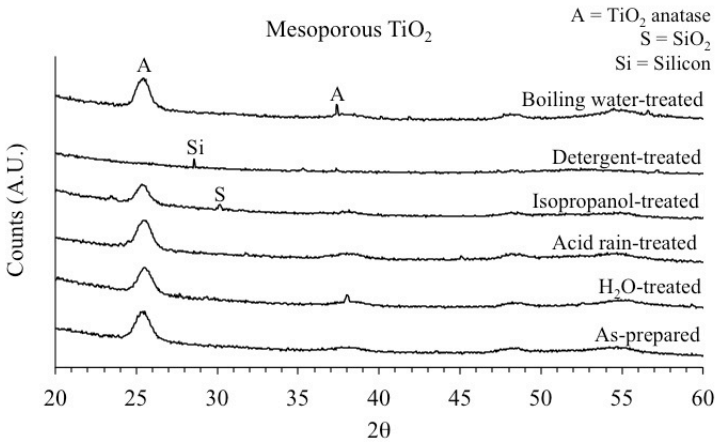

Figure 6.4. X-ray patterns of the mesoporous TiO_2 films before and after the chemical treatments.

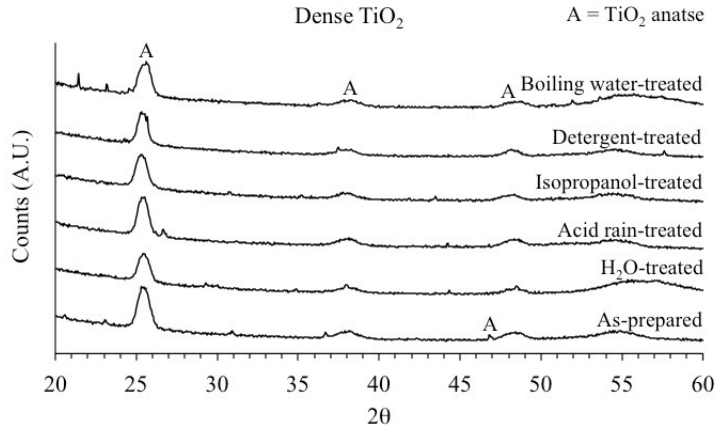

Figure 6.5. X-ray patterns of the non-porous TiO_2 films before and after the chemical treatments.

Figure 6.4 and **Figure 6.5** show the X-ray diffraction patterns of the mesoporous and non-porous (also named dense through this work) TiO_2 coatings deposited over

silicon substrates, before and after weathering. From the bottom of **Figures 6.4** and **Figure 6.5** it is observed that both as-prepared samples present the TiO_2 anatase phase. In **Figure 6.4** it is observed that the treatment with a detergent solution promotes a strong dissolution of the TiO_2 coatings, since no anatase phase peaks were detected by X-ray diffraction; only the peak of the silicon from the substrate is visible. This effect was also confirmed visually, since only the edges of the film remained after the treatment. On the other hand, **Figure 6.5** shows that after the domestic weathering of non-porous TiO_2 coatings, anatase phase peaks still remain present in the samples (25-26° main peak).

6.1.2.1.2. Scanning electron microscopy

Figure 6.6 shows the field emission-SEM images of the as-prepared mesoporous and non-porous TiO_2 coatings.

Thickness is about 121 nm and 117 nm, respectively. Top of **Figure 6.6** confirms the porous structure of the mesoporous sample, having pores of about 10 nm of diameter. On the other hand, from the bottom of **Figure 6.6**, it is observed that non-porous TiO_2 coating is formed by a continuous surface of agglomerated TiO_2 nanoparticles of about 21 nm of diameter.

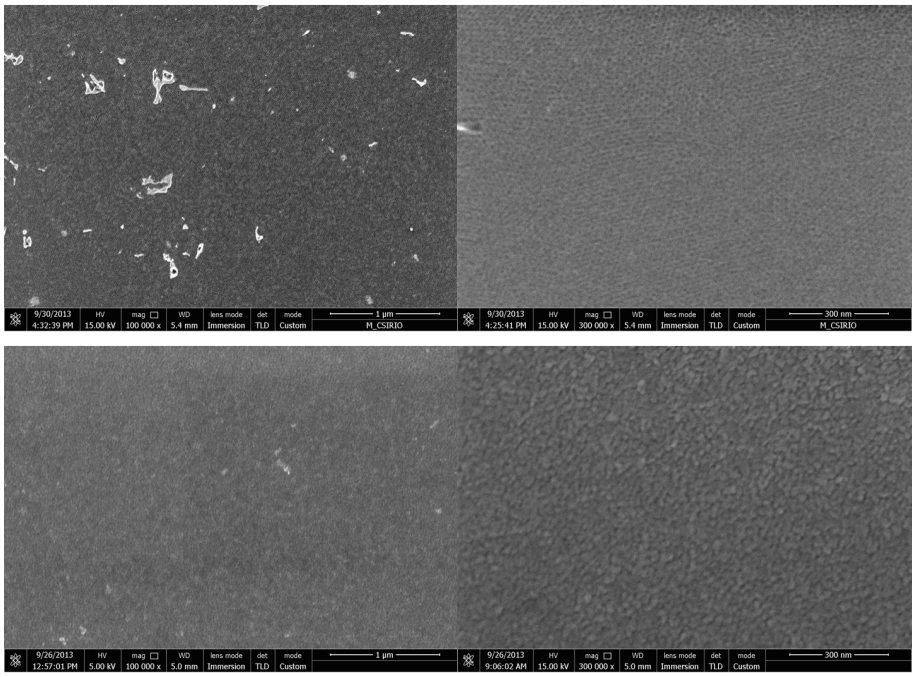

Figure 6.6. Field emission-SEM images of the as-prepared mesoporous (top) and non-porous TiO_2 (bottom) coatings.

6.1.2.1.3. Atomic force microscopy

Figure 6.7 and **Figure 6.8** show the AFM 2D images of the as-prepared and treated mesoporous and non-porous TiO_2 coatings, respectively. From both figures it can be observed that the treatment with detergent (**Figures 5.7e** and **5.8e**) is the most aggressive one, since both the mesoporous and non-porous coatings present a damaged morphology. Another treatment that seems to modify the morphology is that made with boiling water (ageing test, **Figures 5.7f** and **5.8f**).

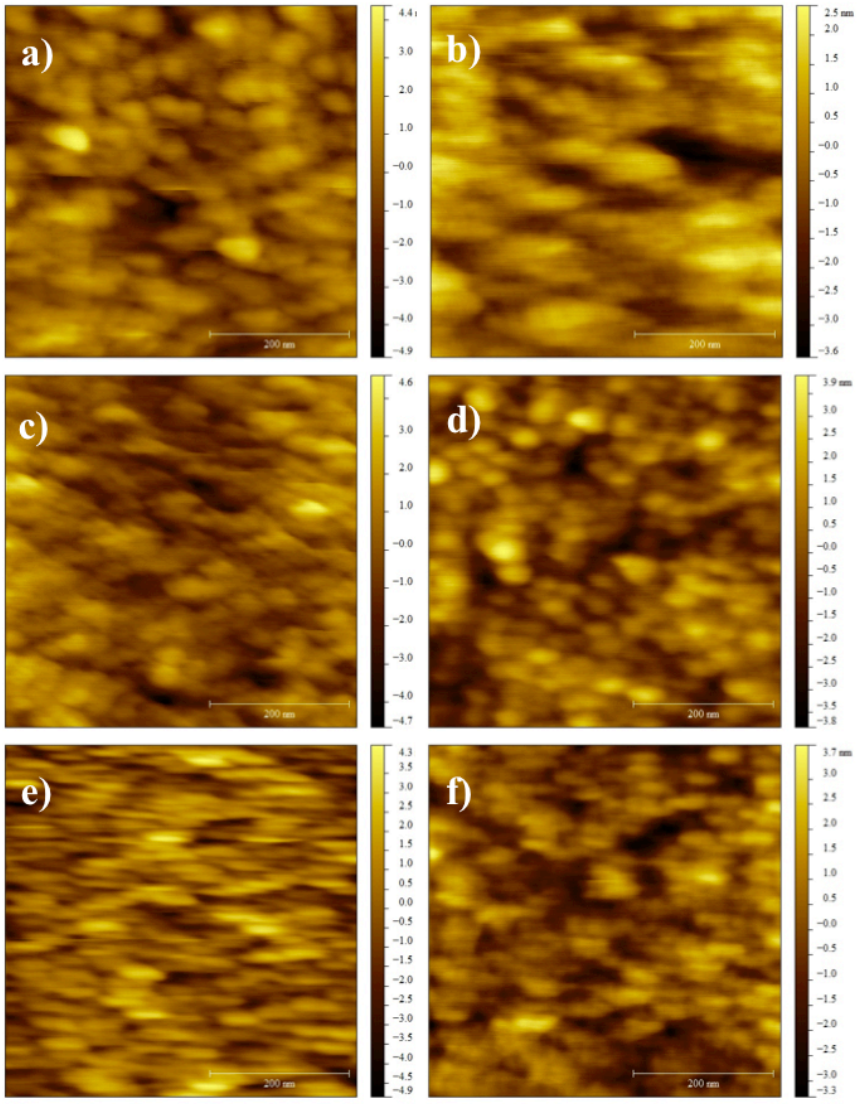

Figure 6.7. AFM 2D images of the a) As-prepared; b) water-treated; c) acid rain-treated; d) glass-cleaner treated; e) detergent-treated and f) boiling water-treated mesoporous TiO_2 films.

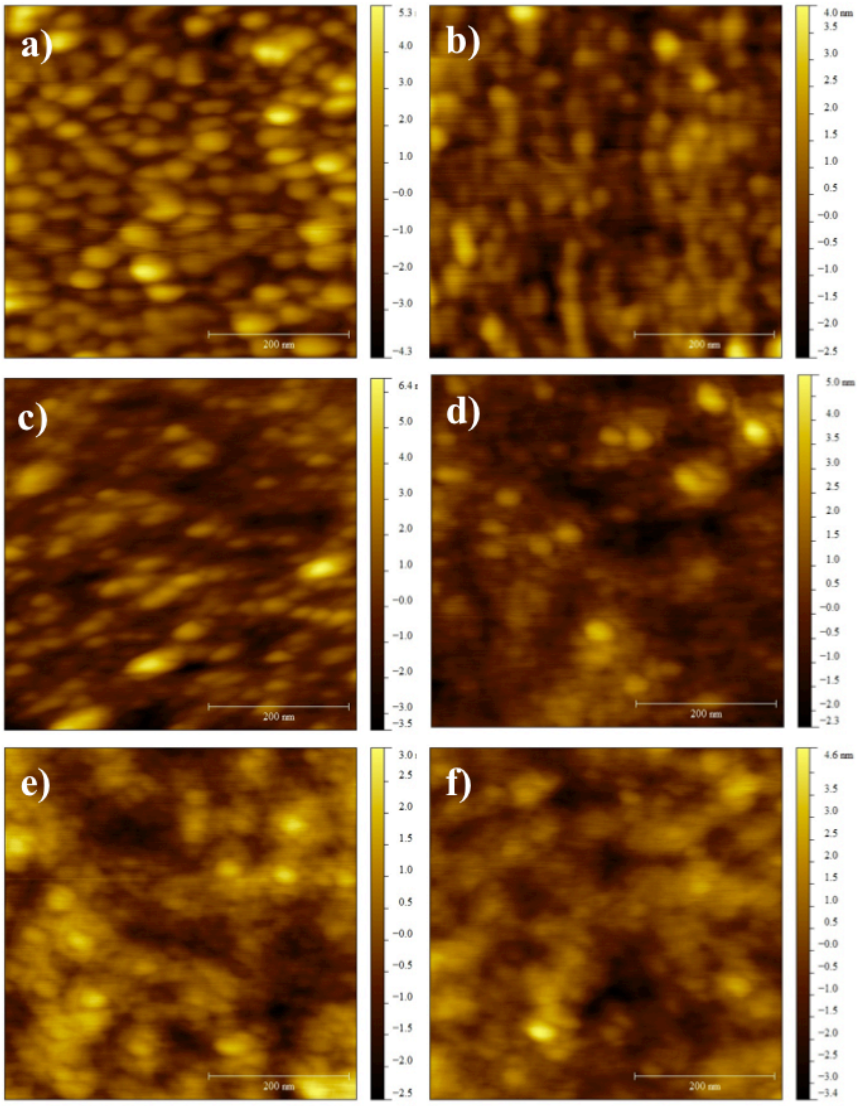

Figure 6.8. AFM 2D images of the a) As-prepared; b) water-treated; c) acid rain-treated; d) glass-cleaner treated; e) detergent-treated and f)boiling water-treated non-porous TiO_2 films.

Some properties such as the AFM roughness, the band gap energy (E_g), the water contact angle (WCA) and the scratch critical loads of the mesoporous and non-porous samples are presented in **Table 6.2**.

Table 6.2. Properties of the as-prepared and treated non-porous (dense) and mesoporous TiO_2 films.

Treatment	Roughness (nm)		E_g (eV)		WCA_i (°)		Critical load (mN)	
	Dense	Mesoporous	Dense	Mesoporous	Dense	Mesoporous	Dense	Mesoporous
As-prepared	1.02	0.88	3.35	3.18	30.8 ± 1.4	33.5 ± 2.9	112.3 ± 1.5	137.2 ± 2.2
Water	0.65	0.77	3.22	3.22	34.2 ± 1.5	28.8 ± 1.6	111.8 ± 1.6	136.3 ± 3.2
Acid rain	0.91	0.93	3.23	3.22, 3.25	50.1 ± 3.9	33.1 ± 2.5	112.5 ± 1.9	128.2 ± 9.6
Glass cleaner	0.72	0.89	3.22	3.16, 3.25	54.7 ± 0.9	41.9 ± 1.4	115.1 ± 3.9	141.5 ± 6.6
Detergent	0.68	0.96	3.76	3.22	31.4 ± 2.5	17.3 ± 4.2	117.5 ±1.3	138.1 ± 5.8
Ageing test	0.76	0.81	3.22	3.21	54.5 ± 1.6	35.4 ± 2.1	115.5 ± 0.7	131.4± 0.8

6.1.2.1.4. Band gap energy

The E_g values for all samples were calculated from the UV–Vis spectra using the **Equation 6.1**:

$$\alpha(h\nu) = A(h\nu - E_g)^{m/2} \quad \textbf{[6.1]}$$

where α is the absorption coefficient, $h\nu$ is the photon energy, A is a constant; and $m = 1$ represents a direct transition between the valence band and conduction band [3-5].

Table 6.2 shows that the E_g values do not change after the treatments of the coatings and are in well agreement with that commonly reported for TiO_2 (3.2 eV [3, 5, 6]) except in the case of the non-porous coating treated with the detergent solution.

6.1.2.1.5. Initial water contact angle (WCA_i)

The photocatalysis and the hydrophilicity of TiO_2 are two different processes that promote the overall self-cleaning property of TiO_2. It means that in order to have an

efficient self-cleaning performance, is not only necessary that TiO_2 shows good photo-oxidation performance, but also high hydrophilicity. This later property permits the wash out of dust and organic contaminants from the TiO_2 surface when raining [7] and it's commonly evaluated by the WCA of the TiO_2 samples.

In this work, the effect of domestic weathering on the WCA_i (initial water contact angle) was evaluated and results are reported in **Table 6.2**. Generally speaking, domestic weathering changes hydrophilicity of the original as-prepared coatings. These changes will be discussed and correlated to the self-cleaning performance in **Section 6.1.2.3**. In addition, mesoporous treated coatings show minor WCA_i values that the non-porous samples.

6.1.2.1.6. Adhesion

From **Table 6.2**, it is observed that the critical load (i.e., the load at which the film is detached from the Si substrate) for the as-prepared mesoporous coating is higher than that of the as-prepared non-porous one. However, critical loads of the treated non-porous coatings suggest that the adhesion does not change significantly after domestic weathering. Instead, non-porous samples treated with the glass-cleaner and detergent solutions, besides that subjected to the ageing test, present a slightly higher critical load. On the other hand, domestic weathering seems to have a negative influence on the adhesion of mesoporous coatings, especially on those treated with the acid rain and subjected to the ageing test. Although from visual inspection and XRD results it was confirmed that the detergent solution is an "aggressive" treatment

for the mesoporous coatings, the edges of the remaining coatings showed a critical load similar to that of the as-prepared coating, although the error is bigger compared to this later. Also in this case, a slightly higher critical load than that of the mesoporous as-prepared coatings was obtained for the mesoporous glass cleaner-treated sample.

6.1.2.2. TiO_2 release

The release of TiO_2 nanoparticles after domestic weathering was evaluated by ICP and results are shown in **Table 6.3**, which reports the percentage of the TiO_2 released after domestic weathering. It can be observed that the treatments that cause the highest release in both samples are the detergent and acid rain treatments, the detergent treatment being in both cases the most aggressive one. From these results it was confirmed that non-porous TiO_2 coatings resist domestic weathering better than the mesoporous coatings. Indeed, the TiO_2 releases from the mesoporous samples are the highest from all the samples set.

Table 6.3. Percentage of the original deposited TiO_2 released after domestic weathering determined by ICP analysis.

Treatment	TiO_2 released (%)	
	Non-porous	Mesoporous
Water	3.7	11.1
Acid rain	9.5	50.0
Glass-cleaner	3.3	12.5
Detergent	13.3	90.0
Ageing test	3.4	11.1

6.1.2.3. Photocatalytic activity

6.1.2.3.1. Mesoporous TiO_2 coating

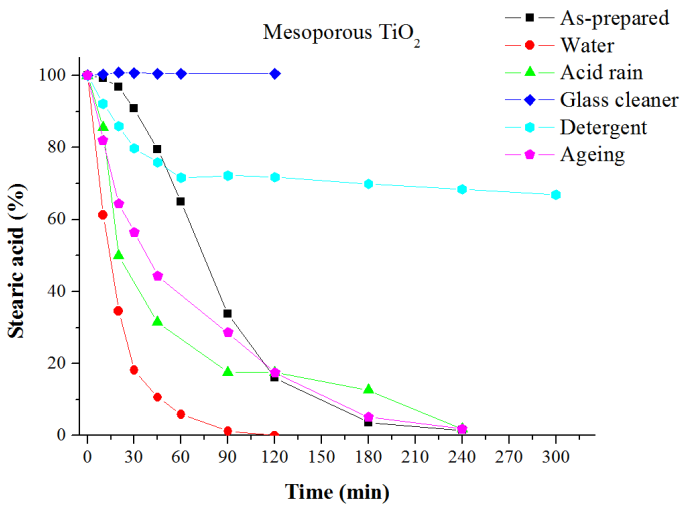

Figure 6.9. Photocatalytic efficiency of the mesoporous TiO_2 film before and after the chemical treatments.

Figure 6.9 shows the photocatalytic degradation curves of the as-prepared and subjected-to-weathering mesoporous TiO_2 coatings. It is observed that the as-prepared coating reaches total degradation of SA in 240 min of UV irradiation and the mesoporous water-treated coating shows the best performance, reaching total degradation in 90 min. The photocatalytic performance tendency for the mesoporous treated coatings is as follow: water-treated > as-prepared > ageing-treated > acid rain-treated > detergent-treated > glass cleaner-treated. **Figure 6.10** shows the SA initial degradation rates (r_i) calculated from the absorption band of the C-H bond in the FTIR spectra acquired during degradation. From this plot, it can be observed that

the mesoporous as-prepared film has the lowest r_i when compared with the treated films.

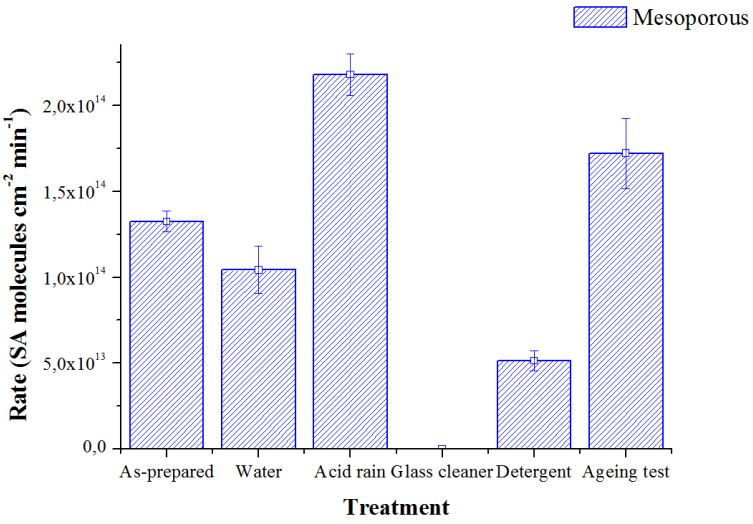

Figure 6.10. Initial degradation rates of the as-prepared and treated mesoporous TiO_2 coatings.

As it was mentioned, mesoporous water-treated film shows the best performance of the entire mesoporous sample set (**Figure 6.9**). The increased activity of this sample is very likely correlated to the high hydration grade of the film after the treatment. Since no additional components are added during the treatment, the TiO_2film just interacts with water, becoming hydrated. This hydrated state could promote a major availability of OH^- groups and thus a major availability of OH• for photo-oxidation. Since the WCA_i of this sample is lower than that of the as-prepared sample (**Table 6.2**), the self-cleaning performance of this sample can be further enhanced, since organic contaminants would easily washed out from the photocatalytic surface when raining. Furthermore, the water treatment for 7 days promotes the lowest TiO_2 release.

Although acid-treated mesoporous film releases about 50% of the original deposited TiO_2 (see **Table 6.3**), it shows the second better photocatalytic performance (**Figure 6.9**) and the highest r_i (**Figure 6.10**) of the sample set. It has been previously reported that treatments of mesoporous TiO_2 films (deposited over soda-lime glasses and fused quartz) with H_2SO_4 enhances their photocatalytic activity due to the reduction of sodium contamination -from glass substrates- and increase in the adsorbed hydroxyl content on the TiO_2 surface [8]. Since in this work there is no sodium contamination from substrates, the enhanced photocatalytic activity is due to increase in the adsorbed hydroxyl content. Furthermore, although a high roughness value is not always *directly* correlated with a high surface area [9], this characteristic could help to the promotion of a better PCA than in the mesoporous as-prepared film (0.93 and 0.88 nm, respectively, see **Table 6.2**).

The aged mesoporous sample shows almost a similar performance that the acid rain-treated sample (**Figure 6.9**). Indeed, it presents also a high r_i as observed in **Figure 6.10**. The performance of this sample was also correlated to the hydration of the film, although it was made in "more aggressive" conditions (100°C) than the simple water-treated sample (37°C) and also for less time (1 hour instead 7 days). The acid rain-treated and the aged samples are hydrophilic as the as-prepared mesoporous sample (**Table 6.2**).

From **Figure 6.9**, it is clear that the cleaning agents have the more negative effect on the PCA of mesoporous TiO_2 coatings. In the case of the glass cleaner treatment, the absence of activity of the films was attributed more to chemical deactivation instead

TiO_2 releases, since no meaningful losses of TiO_2 were detected after the treatment (**Table 6.3**). Several authors have reported that gaseous isopropyl alcohol (IPA, the main component of the glass cleaner solution) on TiO_2 at 300 K leads to the formation of three surface species: (i) strongly bonded non-dissociated IPA species on $Ti^{+\delta}$ sites; (ii) strongly dissociated adsorbed IPA according to the following reaction:

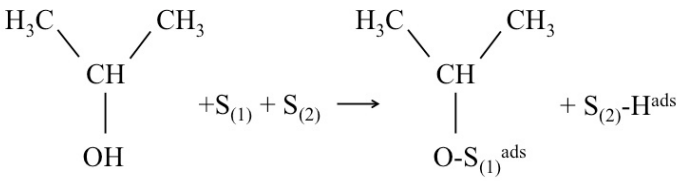

[6.2]

where $S_{(1)}$ and $S_{(2)}$ represent two different adsorption sites and (iii) weakly hydrogen-bonded IPA species on $Ti^{+\delta}$sites [10].

In this work, the inactivation of the coating was correlated with the irreversible adsorption of IPA over the TiO_2 active sites, impeding the interaction of SA with the TiO_2 surface, although from the IR spectrum of the as-prepared film did not revealed the presence of these chemical species. However, some indication of the adsorption of non-polar species on the TiO_2 surface was revealed through the increase in the WCA_i after the treatment (See **Table 6.2**). Since IPA degradation over TiO_2 has been reported [11], probably this film must be first treated with UV irradiation to free the TiO_2 active sites that were already occupied by the IPA species. This pre-irradiation treatment was not made in this work because the objective of this investigation was

to evaluate the *effect* of domestic weathering of TiO_2 films and its effect on the PCA, and not to *avoid* domestic weathering.

The mesoporous detergent-treated coating, as observed in **Table 6.3**, losses the 90% of the original deposited TiO_2 but it still shows little activity (**Figure 6.9**) and even a better r_i (**Figure 6.10**) than the as-prepared coating during the first 90 min of UV illumination. After this time, it shows no activity. This phenomenon was correlated to the low TiO_2 content. The slightly higher r_i of this sample when compared with that of the as-prepared coating was attributed to its partial hydration after the treatment (detergent *aqueous* solution), since the as-prepared sample is never in contact with any type of aqueous solution.

6.1.2.3.2. Non-porous TiO_2 coating

Figure 6.11 shows the photo-degradation curves of SA deposited over the as-prepared non-porous TiO_2 coating and those subjected to weathering.

As observed in **Figure 6.11**, the as-prepared non-porous TiO_2 coating presents the lowest photocatalytic activity compared with all the non-porous-treated coatings and with the mesoporous as-prepared sample (**Figure 6.9**). **Figure 6.12** presents the SA initial degradation rates of the non-porous sample set.

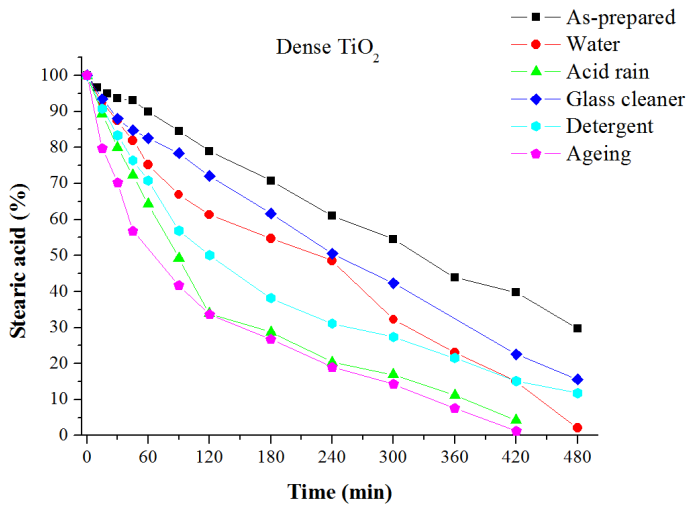

Figure 6.11. Photocatalytic efficiency of the non-porous TiO_2 film before and after the chemical treatments.

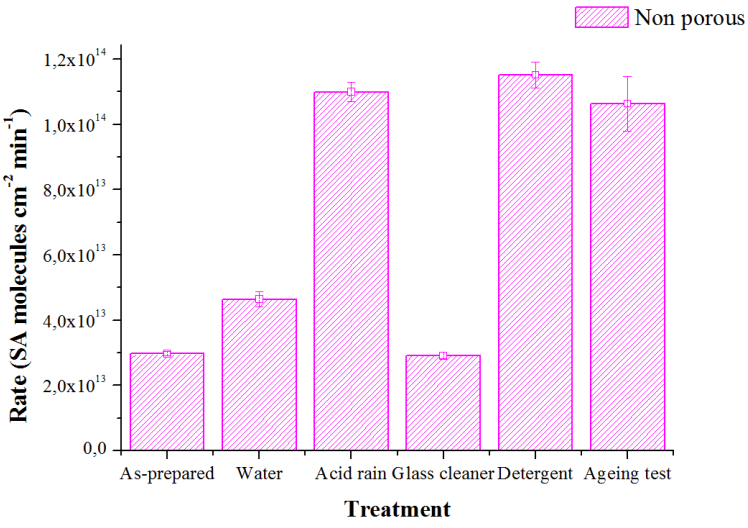

Figure 6.12. Initial degradation rates of the as-prepared and treated non-porous TiO_2 coatings.

Aged and acid rain-treated samples present the best (and very similar) photocatalytic performance. The slightly lower r_i of the acid rain sample (**Figure 6.12**) was correlated to its major release of TiO_2 (**Table 6.23**) and consequently, the minor availability of active sites for photocatalysis. As in the mesoporous sample set, the

best performance of the aged and acid rain samples was attributed to the increase in the OH^- population. The higher WCA_i could promote the adhesion of SA but could also difficult the wash off of dust or organic contaminants deposited over the TiO_2 surface.

Water-treated sample shows the second best performance of the non-porous sample set, reaching almost complete degradation at 480 min of UV irradiation. The fact that the this sample shows a slower degradation of SA than the other sample that was treated with water (i.e., the aged sample, treated with deionized water at 100 °C for 1h) was attributed to its relatively lower roughness (0.65 nm, **Table 6.2**) and hence, probably to a lower surface area than that of the aged sample (roughness = 0.76 nm, **Table 6.2**). Furthermore, water-treated film was subjected to the treatment for 7 days, having enough time to become saturated of OH^- groups. It has been reported that OH^- saturation promotes deceleration of degradation and even catalyst inhibition [12, 13]. A consequence of this saturated state was observed in the lower WCA_i of this sample when compared with those of the acid rain-treated and aged samples.

Also in this case, both the cleaning agents have a negative effect in the PCA of the non-porous TiO_2 coatings, although they degrade SA in a major grade that in the case of the mesoporous sample (**Figure 6.9**). Furthermore, the glass cleaner treatment presents the lowest r_i (**Figure 6.12**), probably due to the partial inactivation of the film, since low TiO_2 releases (compared with the detergent-treated sample) were measured (**Table 6.3**). This sample also presents the highest WCA_i, confirming the hypothesis that non-polar specie is adsorbed on the surface of the film.

6.2. Relative Humidity

In this research, the effect of humidity on the PCA of nanoparticled TiO_2 films was evaluated using stearic acid. Since humidity strongly influences the adsorption of pollutants on the TiO_2 surface, the film was pre-conditioned at the target humidity *prior* SA deposition. Although some groups have studied the influence humidity on the photocatalytic decomposition of solid SA over TiO_2 films [14-16] they do not specifies if the a pre-conditioning process of the film at a specific humidity level was carried out before SA deposition, so, the effect of humidity in a adsorption process of a solid pollutant over TiO_2 has not been fully studied [d].

6.2.1. Nanoparticled self-cleaning glass

6.2.1.1. Characterization

XRD, SEM and FTIR characterization of the nanoparticled self-cleaning glass has been already presented in **Section 5.2** (**Chapter 5**) and **Section 6.1.1**.

6.2.1.2. Photocatalytic activity

Figure 6.13 displays the photo-degradation curves of SA deposited over TiO_2 nanoparticled self-cleaning glasses at 33%, 63% and 75% relative humidities,

[d] **NOTE**: Due to instrumental limitations, the nanoparticled self-cleaning glass was tested at only three humidity values, while the mesoporous and non-porous coatings were tested at four humidity levels. Moreover, tests were carried out in different institutions and therefore, comparisons are made only between the mesoporous and non-porous TiO_2 coatings.

irradiated at 365 nm at room temperature and controlled humidity. **Table 6.4** shows the changes in the kinetic constant when the humidity value is varied.

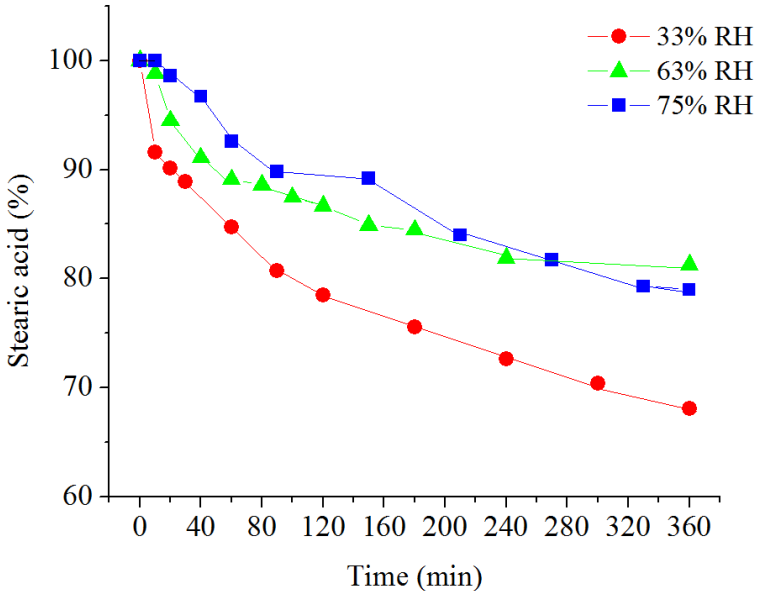

Figure 6.13. Photo-degradation curves of SA deposited over TiO_2 coatings pre-treated at 33, 63 and 75 % RH and irradiated at 365 nm. The photocatalytic tests were carried at controlled humidity and room temperature (20 °C).

Table 6.4. Rates of stearic acid destruction over nanoparticled TiO_2 film under common outdoor and indoor humidity values (T_{room} = 20 °C).

Humidity effect at T_{room} (20°C)	
R.H., %	k_{obs}, min^{-1}
33	0.003 ± 0.002
63	0.001 ± 0.0007
75	0.0008 ± 0.0004

From **Figure 6.13** it can be observed that humidity has a strong influence in the PCA of the coated glasses, although the best photodegradation rate (or highest kinetic constant) at low humidity is slightly higher than the lowest photodegradation rates at medium and high humidity values (**Table 6.4**). From **Figure 6.13** it is clear that low

humidity values promote an increase in the photodegradation rate. This can be explained by the film morphology and the humidification procedure used in this work. **Figure 6.14** shows a SEM micrography of the nanoparticled TiO_2 self-cleaning glass.

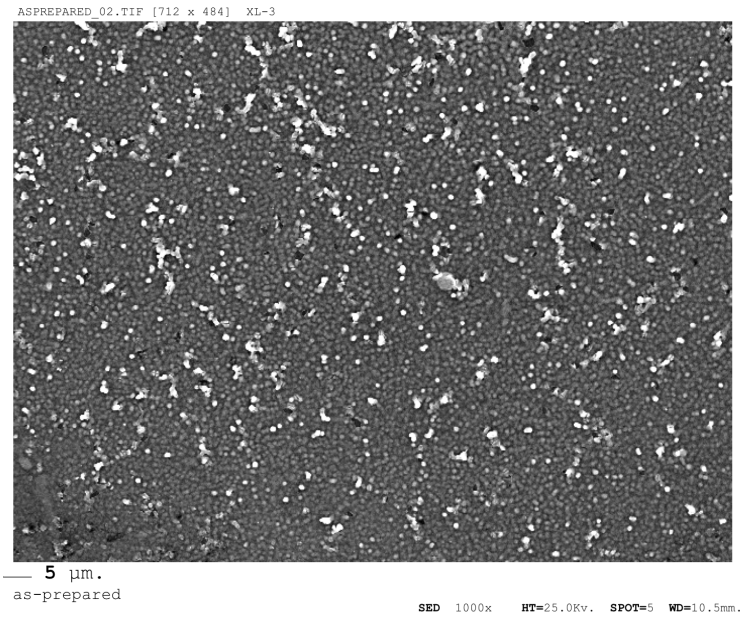

Figure 6.14. SEM micrography of the nanoparticled TiO_2 self-cleaning glass.

We can see that, although the nanoparticles form aggregates of 500-800 nm of diameter, these aggregates provide a big surface area of the film, that's it, a high availability of Ti^{4+} sites where big water quantities can be adsorbed [12, 15, 17]. This characteristic should conduct to an increase of the PCA when humidity rises. However, at the same time, it has been reported that increasing humidity levels usually decrease the PCA due to competition between water and the organic pollutant for the active sites [12, 13]. Then, since in this work the film was exposed to humidity for 12h before the deposition of SA, the adsorbed water could hindered the access of SA to the adsorption sites [12] and therefore, inhibit the PCA.

6.2.2. Mesoporous and non-porous coatings

6.2.2.1. Characterization

Figure 6.15 shows the XRD patterns of the TiO_2 coatings. TiO_2 anatase phase was identified in both samples. In addition, the diffraction peaks corresponding to silicon and silicon oxide from the substrate are visible in the non-porous sample.

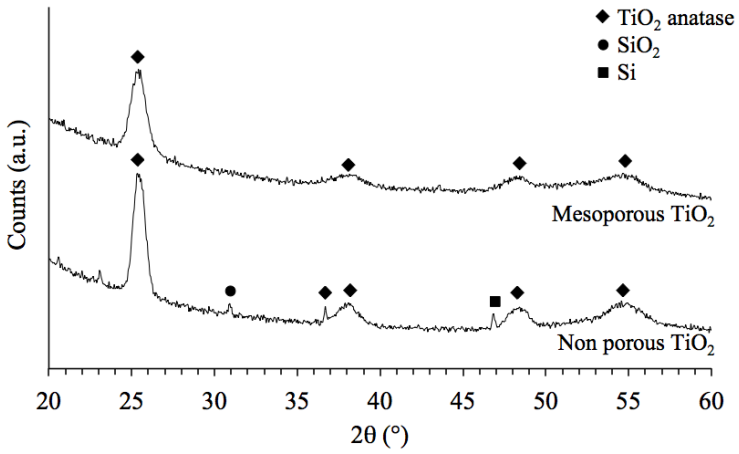

Figure 6.15. XRD patterns of the mesoporous and non-porous TiO_2 coatings.

Figure 6.16 shows the FTIR spectra of the mesoporous and non-porous TiO_2coatings. Both samples presented two absorption bands at about 433 and 636 cm^{-1}. It has been reported that absorption bands between 550-650 cm^{-1} and 435-535 cm^{-1} in the FITR spectra of TiO_2 correspond to the stretching vibrations of the Ti-O and Ti-O-Ti bonds, respectively [18]. In the mesoporous sample, the broad and slightly flat absorption band in the wavelength range from 700 to 460 cm^{-1} should be due to the quantum effect of the nanoparticle size, that is, the fine structure of the

infrared absorption band disappears [19]. The bands located around 2846-2914 cm^{-1} and 1118 cm^{-1} in the non-porous IR spectrum were respectively attributed to C-H and C-O-C bonds, probably from residual organic matter due to the incomplete calcination of the carbonaceous organic precursor.

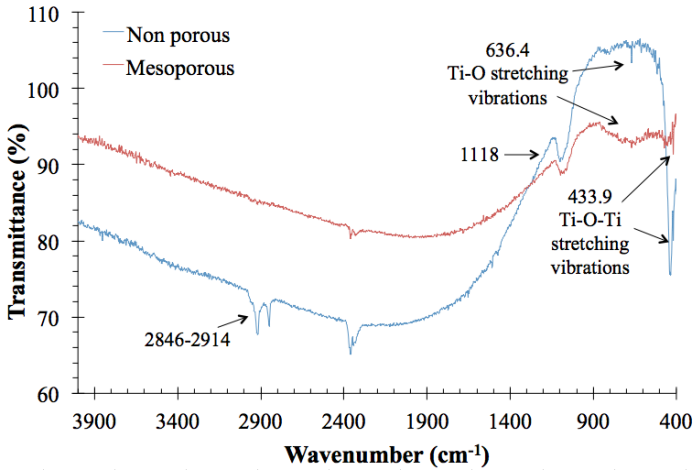

Figure 6.16. FTIR spectra of the mesoporousand non-porousTiO_2 coatings.

The band gap energy values for both samples were calculated from the UV–Vis data using **Equation 6.1** [3, 4]. The calculated E_g values for the mesoporous and non-porous TiO_2 coatings were 3.18 and 3.35 eV, respectively. The E_g value for the mesoporous coating is in well agreement with that commonly reported for TiO_2 (3.2 eV [6]). On the other hand, the non-porous TiO_2 coating presents a higher E_g value than mesoporous TiO_2, indicating that it has to be irradiated with UV light of shorter wavelength to show its better photocatalytic performance.

Figure 6.17 presents the AFM 3D images of the mesoporous and non-porous coatings. From this figure, it can be observed that the non-porous sample is rougher

than the mesoporous one. Indeed, roughness values were 0.875 and 1.02 nm, respectively. Qualitatively, one could expect that a porous surface has larger roughness than a non-porous surface, and consequently, larger surface area. However, it has been previously reported that these two properties are not clearly correlated because the relative amplitude and frequency of the asperities of the surfaces play a key role in the final material morphology [9]. Therefore, from the results of AFM roughness, it was found that roughness measurements were not indicative of the degree of surface area, since it is expected that the mesoporous sample will show higher surface area than the non-porous sample due to the presence of the pores observed in the top of **Figure 6.6** (field-emission SEM micrographies of these coatings were shown in **Section 6.1.2.1.2.**).

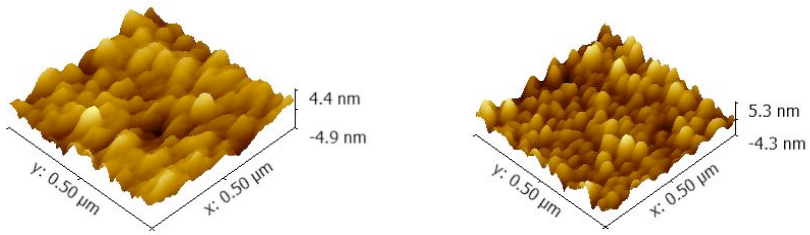

Figure 6.17. AFM 3D images of the mesoporous (left) and non porous (right) TiO_2 coatings.

6.2.2.2. Photocatalytic activity

Figure 6.18 shows the photodegradation curves of SA deposited over the mesoporous TiO_2 coating and irradiated with UV light at 11, 33, 53 and 75% RH. It is clear that as humidity increases, the activity of the mesoporous coating is not only

enhanced but also almost complete degradation in about 6 hours was promoted for humidity levels of 33 and 53% RH. Furthermore, complete degradation is reached in 5 hours when humidity is fixed at 75% RH. This behaviour was correlated with the major availability of hydroxyl radicals for SA degradation as humidity increases and to the interconnected wormhole framework of the sample, since this structure can promote not only larger availability of hydroxyl radicals for degradation but also easier diffusion of reactants and products [8].

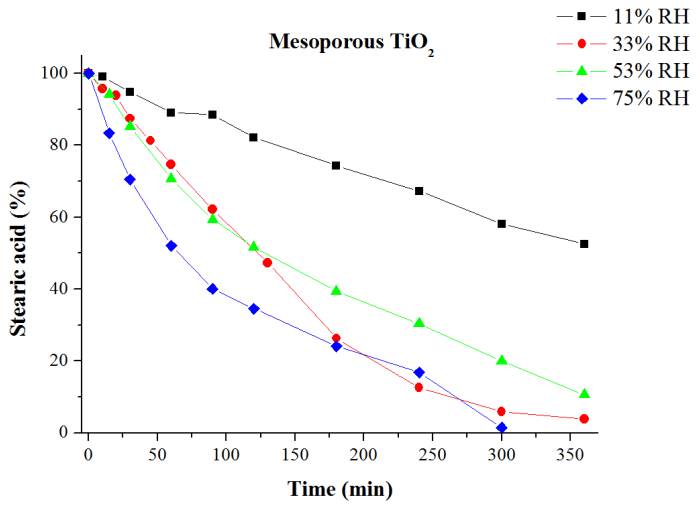

Figure 6.18. Degradation of stearic acid over mesoporous TiO_2 coating at different relative humidity values.

Figure 6.19 shows the photodegradation curves of SA deposited over the non-porous TiO_2 coating and irradiated at 11, 33, 53 and 75% RH. It is clear that this sample has a different general behaviour than the mesoporous one. At low humidity, the non-porous coating presents almost null photocatalytic activity. As humidity increases to 33% RH, photodegradation increases until it reaches complete SA degradation at

53% RH. Finally, at 75% RH, activity decreases and presents a similar behaviour than that at 33% RH.

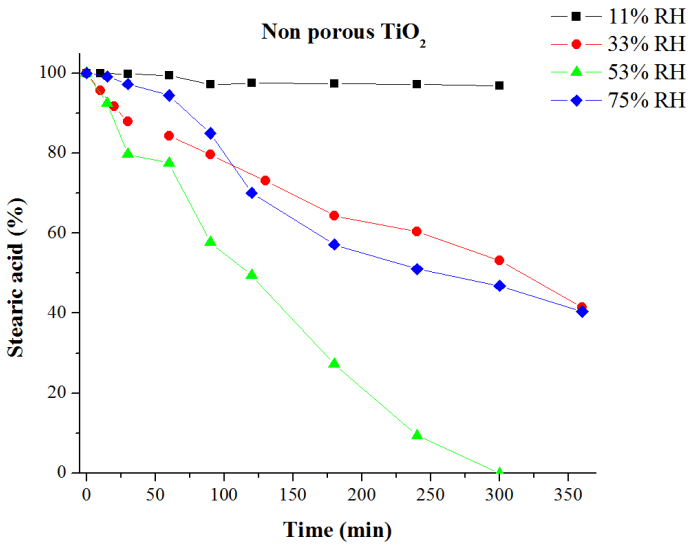

Figure 6.19. Degradation of stearic acid over non-porous TiO_2coating a different relative humidity values.

The behaviour of the SA photodegradation in **Figure 6.19** was principally attributed to the degree of hydroxylation of the non-porous TiO_2 surface at each humidity level. At low humidity levels (11% and 33% RH in **Figure 6.19**), there is not enough adsorbed hydroxyl radicals for degradation. Higher humidity values promote the increase in hydroxyl radicals and consequently, in the degradation of SA on the well-hydrated TiO_2 (53% RH in **Figure 6.19**). However, it has been widely demonstrated that there exists a suitable equilibrium between adsorption and consumption of hydroxyl radicals to keep stable photocatalytic degradation behaviour [13, 14, 17, 20-22]. If the water vapour content in the reaction mixture is raised (as in the case of the 75% RH curve in **Figure 6.19**), such equilibrium is destroyed and the increase of

adsorption of water molecules on the catalyst surface decreases the overall degradation due to competition between the water and the pollutant molecules for the TiO_2 adsorption sites [13, 14, 17, 20-22].

Figure 6.20 presents the initial degradation rates of SA deposited over the mesoporous and non-porous coatings at different humidity level.

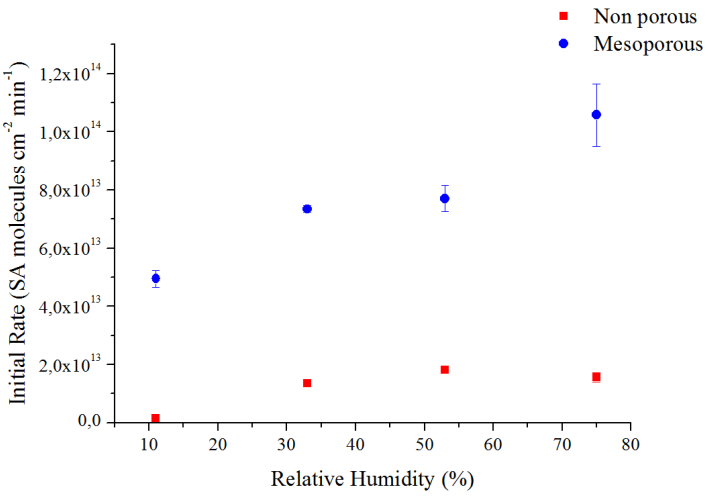

Figure 6.20. Initial degradation rates of stearic acid deposited over mesoporous and non-porous TiO_2 coatings at different relative humidity values.

The difference in the PCA and degradation rate of the mesoporous and non-porous coatings when varying humidity was attributed principally to their differences in their microstructure. As a first consideration, the large surface area of the mesoporous sample (due to the presence of porous) promotes the adsorption of larger amount of water and hydroxyl groups compared with those adsorbed on the non-porous sample at the same humidity value. Then, when samples are UV-irradiated,

the bigger quantity of adsorbed species on the mesoporous coating promotes the formation of a bigger quantity of hydroxyl radicals, permitting the oxidation of major quantity of SA in the mesoporous sample than in the non-porous sample. This explanation is especially true for all the humidity levels in the mesoporous sample (see **Figure 6.18**) and for humidity values of 33% and 53% RH in the non-porous samples (see **Figure 6.19**). Indeed, this can be confirmed from the SA initial degradation rates plotted in **Figure 6.20**. Moreover, as humidity increases, the larger amount of adsorbed water on the surface could also assist in stabilizing electron-hole pairs avoiding recombination [8].

As observed in **Figure 6.19 and Figure 6.20**, further increments of humidity up to 75% causes the decrease in activity and degradation rate for the non-porous coating. This behaviour was correlated to the small surface area of the non-porous sample, that is, the non-porous TiO_2 surface is probably water-saturated at this humidity level and competition between SA and water molecules takes place decreasing the activity.

The results resented here regards the PCA of the mesoporous TiO_2 coating at low humidity (11% R.H.) are in well with those obtained by Sitkiewitz and Heller [15] and Guillard et al. [23]. These authors demonstrated that the water originally adsorbed over a TiO_2 surface could be enough to carry out the photocatalytic degradation of SA even in the absence of additional quantity of water vapour (humidity). On the other hand, the discrepancies between the PCA at 11% RH of the non-porous coating considered in this work and those reported by Sitkiewitz and Heller and Guillard et al. clearly reflects the different behaviour induced by different

morphologies of the materials. However, this fact could not be confirmed since characteristics of the coatings in those works were not discussed in the papers.

An interesting result that was observed in this work was the importance of the pre-conditioning stage of the TiO_2 coatings before the deposition of the pollutant and the effect of this step in the PCA at fixed humidity levels. For example, Mills and co-workers [16] reported that the kinetics of SA photo-oxidation were largely invariant over the range 10-100 % RH when used Pilkington Activ^{TM} self-cleaning glass as TiO_2 surface. So, in this work, the differences between the results reported here and those reported by Mills et al. [16] were attributed to the pre-conditioning stage, since all the TiO_2 coatings were first exposed to the target RH for at least 12 hours before SA deposition. This process was carried out to promote the hydration of the TiO_2 surface before contact with the pollutant, permitting to elucidate the effect of humidity in the whole self-cleaning process. Since no pre-conditioning stage at the target RH was specified in similar works, the results presented here reveal that humidity affects the photocatalytic activity of TiO_2 coatings *versus* solid pollutants such as SA, and this influence depends not only on humidity level and the characteristics of the coating, but also on the hydration of the coating before the deposition on SA.

6.3. Substrate temperature

This project evaluated the photocatalytic efficiency of nanoparticled, mesoporous and non-porous TiO_2 coatings at the most common outdoor temperatures [e] with the aim to investigate the feasibility (in terms of efficiency) of using TiO_2 self-cleaning materials in zones with very variable temperatures (from low to relatively high).

6.3.1. Nanoparticled TiO_2 self-cleaning glass

6.3.1.1. Characterization

XRD, SEM and FTIR characterization of the nanoparticled self-cleaning glass has been already presented in **Section 5.2** (**Chapter 5**) and **Section 6.1.1**.

6.3.1.2. Photocatalytic activity

Figure 6.21 shows the photo-degradation curves of stearic acid deposited over the TiO_2 coatings and irradiated at 10, 20 and 30 °C. It is clear that an increase in the substrate temperature greatly enhances the PCA of the TiO_2 coating. **Figure 6.21** shows that the apparent reaction order for all the substrate temperatures is zero, with respect to the amount of stearic acid. So, in this case the rates were calculated using the reported concentration value of 3.17×10^{15} stearic acid molecules per cm^2 per

[e] **NOTE:** Also in this case, some instrumental limitations with the FTIR spectrometer prevented the analysis of the SA degradation over the nanoparticled self-cleaning glasses when testing at 0 °C. Then, comparisons were made only between the mesoporous and non-porous coatings.

integrated absorbance unit over this range [24] (See **Section 4.1.6**, **Chapter 4**). **Figure 6.22** presents the obtained results. It can be observed that photo-degradation rates at 10 and 20 °C are similar and lower than that at 30 °C.

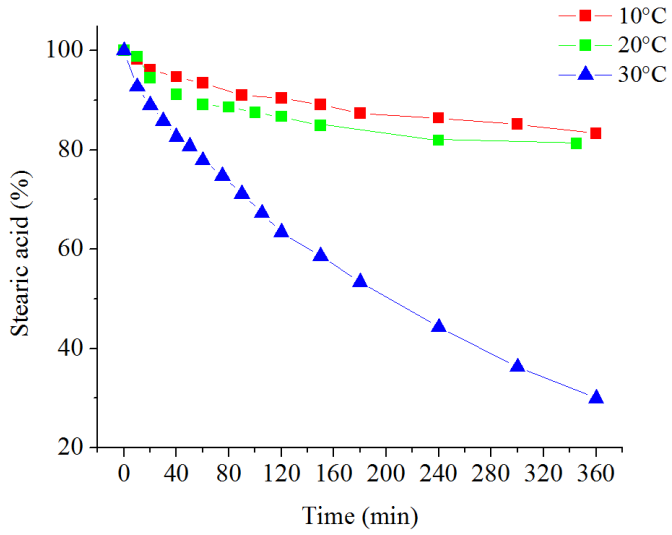

Figure 6.21. Photo-degradation curves of SA deposited over nanoparticled TiO_2 coatings at 10, 20 and 30 °C and irradiated at 365 nm.

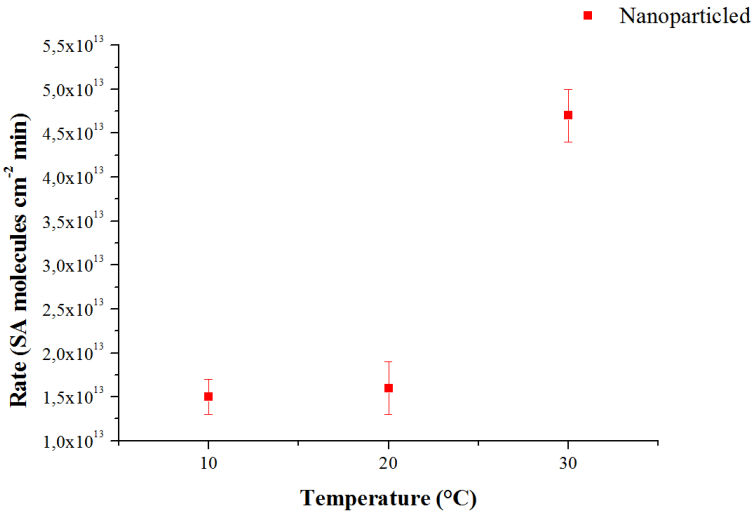

Figure 6.22. Rates of stearic acid destruction over nanoparticled TiO_2 coatings under common outdoor and indoor temperature values.

An interesting effect of increasing the substrate temperature is that an increase in PCA was observed although the photocatalytic tests were carried out at room humidity (medium level, 63-64% RH), when it has been demonstrated that this humidity levels is detrimental for the PCA of the studied coatings (**Section 6.2.1.2.**). This effect was attributed to the release of water molecules from the TiO_2 surface, enhanced by the raising temperature [22, 25].

6.3.2. Mesoporous and non-porous coatings

6.3.2.1. Characterization

The characterization of the mesoporous and non-porous TiO_2 coatings was already presented in **Section 6.2.2.1**.

6.3.2.2. Photocatalytic activity

Figure 6.23 shows that the mesoporous TiO_2 coating is photocatalytically active at all the tested temperatures. Indeed, small increments in temperature, even from 0 to 10 °C or from 10°C to 20°C, promote an increase of the SA photodegradation of ~30%. Further increments in temperature until 30 °C promotes the total photodegradation in 6 hours of UV illumination. The performance of this sample at low temperatures (0-20 °C) was correlated with the sample's structure. The mesoporous structure of this coating should favour not only the contact of the pollutant with the photocatalyst but also promote multiple reflections of the light

(highly scattering porous coating), resulting in an increased light adsorption [26] and hence increased activity. This, combined to a higher porosity (and consequently a higher surface area) of this coating are most probably the reasons of the high photocatalytic activity of this coating at low temperatures.

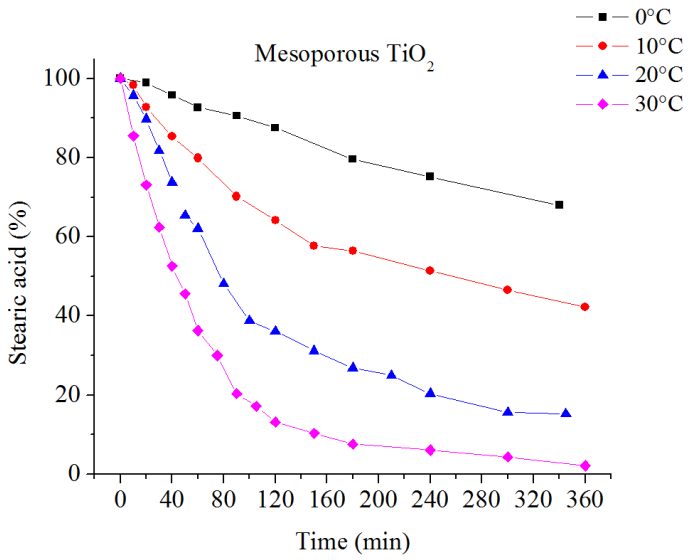

Figure 6.23. Photo-degradation curves of SA deposited over the mesoporous TiO_2 coating, irradiated with UV light (365 nm) at 0, 10, 20 and 30 °C.

Figure 6.24 shows the degradation curves of the stearic acid deposited over the non-porous TiO_2 sample and irradiated with 365 nm UV light at 0, 10, 20 and 30 °C. As first information, from **Figure 6.24** is clear that this sample is partially active at all the tested temperatures. PCA is limited for low temperatures (≤20 °C) and increments from 0 to 10 or even 20 °C causes only an increase of ~25% of stearic acid degradation. In addition, photocatalytic degradation seems to stop at ~240 min for the run carried out at 0 °C, at ~180 min for the run at 10 °C, and at ~300 min for the run at 20 °C. On the other hand, heating until 30 °C promotes a marked

increment in the PCA of the non-porous TiO_2 coating, and complete SA degradation is reached at 150 min of UV illumination.

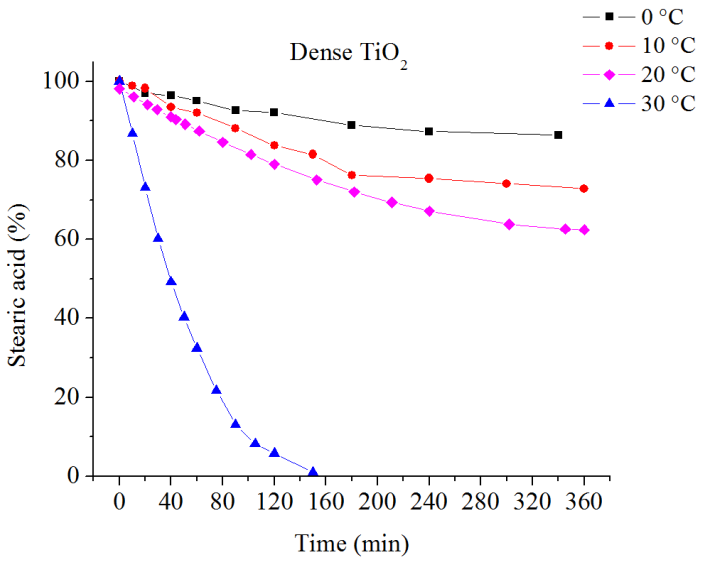

Figure 6.24. Photo-degradation curves of SA deposited over the non-porous TiO_2 coating, irradiated with UV light (365 nm) at 0, 10, 20 and 30 °C.

The effects of temperature on the PCA of the non-porous coating coating versus SA were attributed to limited release of the photo-generated H_2O and/or reaction intermediates from the TiO_2 surface. It has been reported that for an efficient photodegradation process, the TiO_2 surface must not only be able of photo-oxidize organic pollutants but also release the reaction products to free up active sites for further degradation [27]. As observed in **Figure 6.24**, the non-porous TiO_2 coating degrades in some grade SA at low temperatures (0 – 20 °C). Consequently, water molecules are formed as one of the reaction products. Since the TiO_2 surface is continuously UV irradiated, it becomes hydrophilic and then, water is hold on the photocatalyst surface. This "water-holding" condition is promoted by the low

temperatures at which tests were conducted, since water release from the surface by evaporation is impeded. In addition, some authors have reported that strong adsorption of reaction intermediates promotes deactivation of the TiO_2 surface [23]. Since it is known that both water and reaction intermediates are easily released when increasing temperature [23, 27], the better performance of the non-porous coating when tested at 30 °C was correlated to this phenomena, although no traces of intermediates or adsorbed water were observed in the FTIR spectra.

As observed in **Figure 6.23** and **Figure 6.24**, the non-porous TiO_2 coating has a better performance than the mesoporous one at 30 °C. This phenomenon was attributed to the different thermal conductivity of the samples. It is know that a thin coating with small grain size shows low thermal conductivity [28, 29]. So, in principle, both coatings (composed of small TiO_2 particles) should present low thermal conductivities. However, it has been reported that reductions of the thermal conductivity of coatings are possible when increasing porosity [28]. Since in this work both non-porous and mesoporous TiO_2 coatings have similar thicknesses (117 and 121 nm, respectively), thermal conductivity would only depend on the microstructure of the samples, being smaller that corresponding to the porous sample. Indeed, Choi et al. [28] have reported a thermal conductivity of 0.56 W/m·K at 300K for a 250 nm thick mesoporous TiO_2 thin coating deposited over a Si substrate, value that was almost eleven times smaller than that of their nonporous TiO_2 coating (6.2 W/m·K). Based in this previous report [28], the better performance of the non-porous TiO_2 coating at 30 °C could be attributed to the higher thermal conductivity than that of the mesoporous coating.

An alternative explanation for the better performance of the dense TiO_2 coating at 30 °C can be made considering the morphology of both coatings and the differences in the overall degradation process in these two samples as a consequence of their morphology. As demonstrated by Carretero-Genevrier et al. [30], the diffusion of mobile species (such as pollutants or radical species) in a *Im3m* mesoporous structure occurs not only toward the bulk of the film, but also toward its surface, by means of its 3D interconnected pores that are open to both the substrate and the coating-air interface [30]. Moreover, Carretero-Genevrier et al. also proved that there is an efficient photocatalytic activity (or pollutant degradation) inside the pores of a mesoporous film. In this work, the synthesis of the film was made with the aim to obtain the same cubic *Im3m* organization of the pores in the mesoporous TiO_2 sample. In this case, if SA degradation on the mesoporous sample takes place inside the pores, water or other degradation products such as reaction intermediates are generated also inside the pores and consequently, they must diffuse toward the surface of the film to allow more SA degradation [27]. Aversely, over the dense TiO_2, there is no diffusion of SA toward the bulk of the sample before degradation and both degradation and generation of products takes place at the surface of the coating. These phenomena are the same at all the tested temperatures and the major availability of active sites for degradation of the mesoporous sample with respect to the dense one can be easily intuited from the major PCA shown in **Figure 6.23** and **Figure 6.24** over the 0-20 °C interval and from the r_i's of both samples presented in **Figure 6.25**. In the 0-20 °C interval, the overall degradation process over the mesoporous sample (which includes diffusion of the pollutant, degradation and diffusion of products) its faster than the same process over the dense coating

(although in this case, there is no diffusion step). It has been suggested that water (or other reaction products) are easily released when increasing temperature [27, 31]. However, when heating until 30 °C, although the overall degradation process over the mesoporous sample is even faster than that at other temperatures, it is not as faster as the same process over the dense sample (see **Figure 6.25**).

These results can thus be also attributed to the additional diffusion step that takes place over the mesoporous TiO_2. When degradation takes place inside the pores, diffusion of products toward the surface must take place to allow more SA degradation. On the other hand, over the dense sample, degradation products release just from the surface of the coating, and this process begins to be faster at temperatures higher than 20 °C.

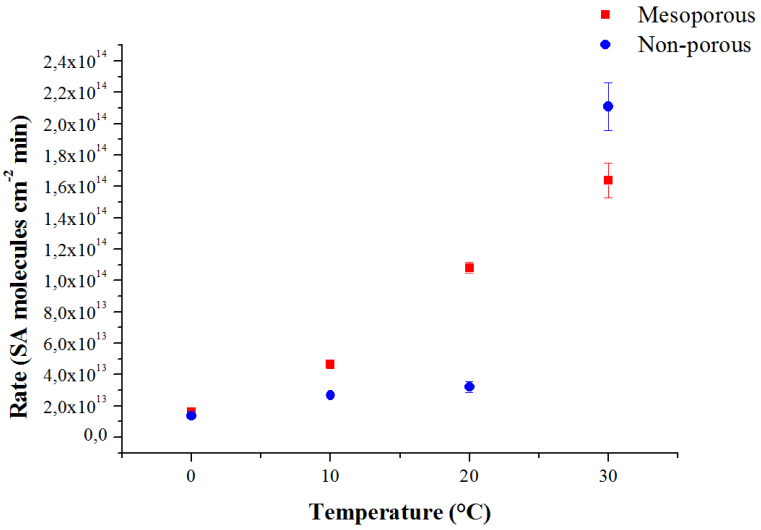

Figure 6.25. Photocatalytic reaction rates for stearic acid over mesoporous and non-porous TiO_2 coatings.

6.4. References

[1]. Minabe, T.; Tryk, D. A.; Sawunyama, P.; Kikuchi, Y.; Hashimoto, K.; Fujishima, A. *TiO_2-mediated photodegradation of liquid and solid organic compounds*. J. Photochem. Photobiol. A **2000**;137:53.

[2]. Pini, M.; Cedillo-González, E. I.; Neri, P.; Siligardi, C.; Ferrari, A. M. *Life cycle assessment of nanoTiO_2 coated self-cleaning float glass*. Technical Proceedings of the 2013 NSTI Nanotechnology Conference & Expo, NSTI-Nanotech 2013. Vol. 3, **2013**, 728.

[3]. Garza-Tovar, L.L.; Torres-Martínez, L. M.; Bernal Rodríguez, D.; Gómez, R.; del Angel, G. *Photocatalytic degradation of methylene blue on Bi_2MNbO_7 (M = Al, Fe, In, Sm) sol-gel catalysis*. J. Mol. Catal. A **2006**;247:283.

[4]. Murphy, A. B. *Band-gap determination from diffuse reflectanse measurements of semiconductor films, and application to photoelectrochemical water-splitting.* Solar Energy Mater. Solar Cells **2007**;91:1326.

[5]. Torres-Martínez, L. M.; Cruz-López, A.; Juárez-Ramírez, I.; Meza-de la Rosa, Ma. E. *Methylene blue degradation by $NaTaO_3$ sol-gel doped with Sm and La.* J. Hazard. Mater. **2009**;165:774.

[6]. Hashimoto, K.; Irie, H.; Fujishima, *A. TiO_2 Photocatalysis: A Historical Overview and Future Prospects*. Jpn. J. Appl. Phys. **2005**;44:8269.

[7]. Fujishima, A.; Zhang, X. *Titanium dioxide photocatalysis: present situation and future approaches*. C. R. Chimie **2006**;9:750.

[8]. Yu, J. C; Yu, J.; Zhao, J. *Enhanced photocatalytic activity of mesoporous and ordinary TiO_2 thin films by sulphuric acid treatment*. Appl. Catal. B **2002**;36:31.

[9]. Best, C. H. *Significance of test and properties of concrete and concrete making materials*. ASTM International, **1978**.

[10]. Sivachandiran, L.; Thevenet, F.; Gravejat, P.; Rousseau, A. *Isopropanol satured TiO_2 surface regeneration by non-thermal plasma: Influence of air relative humidity*. Chem. Eng. J. **2013**;214:17.

[11]. Larson, S. A.; Widegren, J. A.; Falconer, J. L. *Transient studies of 2-Propanol photocatalytic oxidation on titania*. J. Catal. **1995**;157:611.

[12]. Coronado, J. M.; Zorn, M. E.; Tejedor-Tejedor, I.; Anderson, M. C. *Photocatalytic oxidation of ketones in the gas phase over TiO_2 thin films: a kinetic study on the influence of water vapor*. Appl. Catal. B **2003**;43:329.

[13]. Raillard, C.; Héquet, V.; Le Cloirec, P.; Legrand, J. *Kinetic study of ketones photocatalytic oxidation in gas phase using TiO_2-containing paper: effect of water vapour*. J. Photochem. Photobiol. A **2004**;163:425.

[14]. Dibble, L. A.; Raupp, G. B. *Kinetics of the gas-solid heterogeneous photocatalytic oxidation of trichloroethylene by near UV illuminated titanium dioxide*. Catal. Lett. **1990**;4:345.

[15]. Sitkiewitz, S.; Heller, A. *Photocatalytic oxidation of benzene and stearic acid on sol- gel derived TiO_2 thin films attached to glass*. New J. Chem. **1996**;20:233.

[16]. Mills, A.; Lepre, A.; Elliot, N.; Bhopal, S.; Parkin, I. P.; O'Neill, S. A. *Characterisation of the photocatalyst Pilkington Activ^{TM}: a reference film photocatalyst?*. J. Photochem. Photobiol. A **2003**;160:213.

[17]. Obee, T. N.; Brown, R. T. *TiO_2 photocatalysis for indoor air applications: effects of humidity and trace contaminant levels on the oxidation rates of formaldehyde, toluene and 1,3-butadiene.* Environ. Sci. Technol. **1995**;29:1223.

[18]. Wang, J.; Li, R.; Zhang, Z.; Sun, W.; Wang, X.; Xu, R. *Degradation of hazardous dyes in wastewater using nanometer mixed crystal TiO_2 powders under visible light irradiation*. Water Air Soil Pollut. **2008**;189:225.

[19]. He, Z.; Que, W.; Chen, J.; He, Y.; Wang, G. Surface chemical analysis on the carbon-doped mesoporous TiO_2 photocatalysts after post-thermal treatments: XPS and FTIR characterization. *J. Phys. Chem. Solids* **2013**;74:924.

[20]. Kim, S. B.; Hong, S. C. *Kinetic Study for Photocatalytic Degradation of Volatile Organic Compounds in Air Using Thin Film TiO_2 Photocatalyst*. Appl. Catal. B **2002**;35:305.

[21]. Kim, S. B.; Hwang, H. T.; Hong, S. C. *Photocatalytic Degradation of Volatile Organic Compounds at the Gas-Solid Interface of a TiO_2 Photocatalyst*. *Chemosphere* **2002**;48:437.

[22]. Fu, X.; Clark, L. A.; Zeltner, W. A.; Anderson, M. A. *Effects of reaction temperature and water vapour content on he heterogeneous photocatalytic oxidation of ethylene*. J. Photochem. Photobiol. A **1996**;97:181.

[23]. Guillard, C.; Herrmann, J. M.; Puzenat, E.; Peruchon, L. *Photocatalytic efficiencies of self-cleaning glasses. Influence of physical factors*. Photochem. Photobiol. Sci. **2009**;8:1040.

[24]. Paz, Y.; Luo, Z.; Rabenberg, L.; Heller, A. *Photooxidative self-cleaning transparent titanium dioxide films on glass.* J. Mater. Res. **1995**;10:2842.

[25]. Obee, T. N.; Hay, S. O. Effects of moisture and temperature on the photooxidation of ethylene on titania. Environ. Sci. Technol. **1997**;31:2034.

[26]. Kalyanasundaram, K.; Grätzel, M. *Applications of functionalized transition metal complexes in photonic and optoelectronic devices*. Coord. Chem. Rev. **1998**;177:247.

[27]. Yu, H.; Zhang, K.; Rossi, C. *Experimental Study of the Photocatalytic Degradation of Formaldehyde in Indoor Air Using a Nano-Particulate Titanium Dioxide Photocatalyst*. Indoor Built Environ. **2007**;16:529.

[28]. Choi, S. G.; Ha, T.-J.; Yu, B.-G.; Shin. S.; Cho, H. H.; Park, H.-H. *Application of mesoporous TiO_2 as a thermal isolation layer for infrared sensors*. Thin Solid Films **2007**;516:212.

[29]. Kim, D. J.; Kim, D. S.; Cho, S.; Kim, S. W.; Lee, S. H.; Kim, J. C. *Measurement of thermal conductivity of TiO_2 thin films using 3ω method*. Int. J. Thermophys. **2004**;25:281.

[30]. Carretero-Genevrier, A.; Boissiere, C.; Nicole, L.; Grosso, D. *Distance dependence of the photocatalytic efficiency of TiO_2 revealed by in situ ellipsometry*. J. Am. Chem. Soc. 2012:134:10761.

[31]. Peruchon, L.; Puzenat, E.; Herrmann, J. M.; Guillard, C. *Photocatalytic efficiencies of self-cleaning glasses. Influence of physical factors*. Photochem. Photobiol. Sci. 2009;8:1040.

CHAPTER 7

CONCLUSIONS

7.1. Conclusions

In this thesis, aspects correlated with the production and application of TiO_2 coatings for building materials (particularly, self-cleaning glasses) were investigated.

Regard the issues associated with the production of such materials, from the D-optimal experimental design there were individuated the factors that affect the roughness of soda-lime glasses and at what levels these factors must be kept to generate smooth surfaces (those that presented the better adhesion of coatings formed by dip coating from a commercial TiO_2 nano-suspension). So, it was found that the treatment of the soda-lime glass surface with 96% acetic acid for 4 h generates a smooth surface (with Rms roughness of about 1.49 nm), and this latter promotes the best adhesion of the TiO_2 coatings. The fact that high roughness values did not improve the adhesion (as it was expected) was attributed to the combination of high roughness and the increase of the water contact angle of the attacked

surfaces. This combination often results in air pockets being trapped between the solid and liquid, thus leading to a significant decrease in the solid-liquid adhesion.

In addition to the enhancement of the adhesion between TiO_2 coatings and the glass substrate, the pre-treatment of the glass with acetic acid also lead to the reduction of sodium ion from the surface. This side effect can thus low the risk of diffusion of this ion from the glass to the coating, phenomenon that has been proved to affect negatively the PCA of the final self-cleaning glasses.

The last issue correlated with the production of self-cleaning glasses was the effect of residues from the photocatalyst synthesis (from the industrial synthesis). It was observed that NaCl residues deposited together with the TiO_2 coating from the commercial PARNASOS nano-dispersion and their presence compromises the PCA. Treatment of the self-cleaning glasses with an acid solution increases the activity and the stearic acid (SA) initial degradation rate (r_i). On the other hand, a good activity and degradation rate were also obtained when the self-cleaning glasses were treated only with deionized water. This characteristic could carry environmental benefits in the TiO_2 materials production process, since no acid residues will be generated and disposed to the environment.

In the second part of this research, the limitations associated to the application of TiO_2 coatings at real conditions were investigated.

From the weathering study, it was found that the nanoparticled (commercial) coating has lower chemical resistance than the mesoporous and non-porous coatings.

Individually, the nanoparticled TiO_2 coating has good chemical resistance to common household factors like cleaning agents or rain. Furthermore, an increase in PCA was observed after the film was treated with the model solutions, due to hydroxylation of the TiO_2 surface. Only the treatment with acid rain seemed to promote the poisoning of the film after 380 min of UV irradiation, although the FTIR spectra does not shown the presence of any intermediate, and the activity of this sample was better than that of the as-prepared one. Meanwhile, the mesoporous coating presented better activities and higher r_i's than the non-porous ones when subjected to domestic weathering. The characteristic structure of the mesoporous coating (that favours the adsorption of the pollutant and its contact with the photocatalyst) combined to its higher porosity, are most probably the reasons of their superior PCA. On the other hand, domestic weathering has a stronger effect over mesoporous TiO_2 coatings. Indeed, mesoporous samples treated with the glass cleaner and detergent solutions shown null or limited activity. Furthermore, in the case of the detergent treatment, the mesoporous coating was almost completely detached from the silicon substrate. Contrary, the non-porous coating seem to be less affected by domestic weathering, instead, weathering promotes an increase of r_i in almost all the cases. Regard nanoparticles release, the treatments that cause the highest TiO_2 releases in both samples are the acid rain and the detergent treatments. In both cases, the detergent treatment was the most aggressive one.

A variable that strongly affect the PCA of self-cleaning materials during their life cycle is the relative humidity. In this work, it was found that humidity has a strong influence in the PCA of nanoparticled TiO_2 self-cleaning glasses and that better activities are obtained at low humidity levels (33% R.H.).

The mesoporous TiO_2 coating is photocatalytically active at all the tested R.H. levels (11, 33, 53 and 75% R.H.) and both activity and SA r_i increases as humidity rises. On the other hand, the non-porous coating shows almost no activity at the lower RH level tested (11% R.H.), and its PCA and r_i are enhanced when RH is increased up to 53%, for then decreasing again when RH is fixed at 75%. These behaviours were correlated to the differences in surface area between the mesoporous and non-porous samples and to the water competition phenomena. The results obtained here suggested that humidity affects the PCA of TiO_2 coatings *versus* solid pollutants such as SA, and that its influence depends not only on humidity level and the characteristics of the coating, but also on the hydration of the coating before stearic acid deposition.

Finally, the effect of the substrate temperature over the PCA of all the TiO_2 coatings was investigated. From the obtained results, it was found that the substrate temperature influences greatly the activity of nanoparticled TiO_2 self-cleaning glasses, and increasing temperature leads to the desorption of water from TiO_2 surface with a consequent improvement of the PCA. On the other hand, both non-porous and mesoporous TiO_2 coatings are photocatalytically active at all the tested temperatures (0, 10, 20 and 30 °C). The non-porous coating is only partially active

when tested at 0, 10 and 20 °C while the mesoporous coating showed higher activity at the same temperatures. The better performance of this latter sample at low temperatures (0-20 °C) was correlated with its mesoporous structure that should favour the contact of the pollutant with the photocatalyst and higher light adsorption. An interesting effect when increasing substrate temperature up to 30°C was observed for the non-porous coating. At that temperature, it showed better PCA than that of the mesoporous sample at the same condition. The better performance of the non-porous TiO_2 coating at 30 °C was attributed to the higher thermal conductivity than that of the mesoporous one.

7.2. Some tips for application of TiO_2 coatings in the building industry

Based in the obtained results, it was concluded that nanoparticled TiO_2 self-cleaning glasses can be applied in houses without risk of looses of efficiency due to weathering from common cleaning agents or atmospheric factors like rain or acid rain. Non-porous TiO_2 coatings can be applied in domestic environments with few risk of release of nanoparticles although with a low photocatalytic activity, while highly active mesoporous TiO_2 coatings cannot be exposed to environments in which domestic cleaning agents are commonly used. These coatings do not only loose the self-cleaning properties but also release nanoparticles to the environment. Furthermore, although acid rain promotes an increase in the initial SA degradation, long exposures (of 7 days or more) of mesoporous coatings to this environment promote the release of TiO_2 nanoparticles.

It is also suggested that nanoparticled TiO_2 self-cleaning glasses are appropriate for their commercialization in dry and hot geographic zones. Self-cleaning building materials composed by non-porous TiO_2 coatings are appropriate for geographical zones with medium humidity levels (53% RH) and relatively high temperature values (30 °C). On the other hand, self-cleaning materials based in mesoporous TiO_2 coatings can be applied and commercialized in zones with both variable humidity (from 11 to 75%) and temperature (from 0 to 30 °C). The best performance of mesoporous-based materials could be reached in environments characterized by humidity values ranging from 33 to 75 % and temperature values between 20 – 30 °C.

APPENDIX A

PHOTOCATALYTIC EFFICIENCY PLOTS

The photo-degradation of stearic acid (SA) - used as model pollutant - was followed monitoring the disappearance of the vibrational bands between 2700-3000 cm^{-1} in the FTIR spectra. These bands correspond to the aliphatic C-H stretching modes of the SA molecules. **Figure A.1** shows an example of the FTIR spectra of the stearic acid (SA) deposited over a mesoporous TiO_2 coating and irradiated with UV light (365 nm) at 30 °C and $R.H._{room}$ (63%) for 360 min.

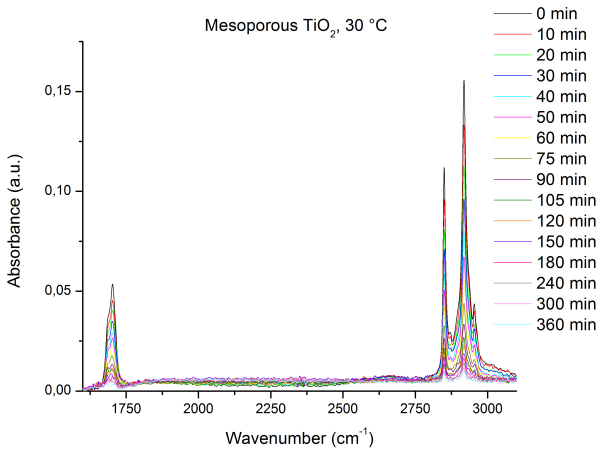

Figure A.1. FTIR spectra of the SA deposited over a mesoporous TiO_2 coating and irradiated with UV light at 30 °C and $R.H._{room}$.

The photocatalytic efficiency plots were obtained by integrating the area under the C-H peaks, using the software OPUS 6.0 from Bruker. **Figure A.2** shows the 2800-3000 cm^{-1} section of the FTIR spectra presented in **Figure A.1**.

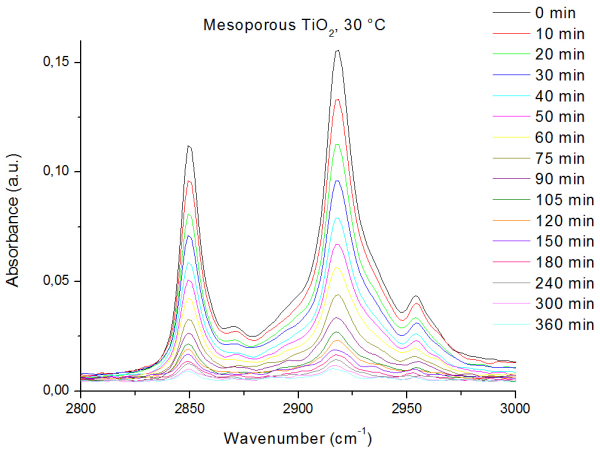

Figure A.2. 2700-3000 cm^{-1} section of the FTIR spectra shown in **Figure A.1**.

After integrating the area of the C-H peaks, the concentration of the SA at each time was determined applying the reported concentration value of 3.17 x 10^{15} stearic acid molecules per cm^2 per integrated absorbance unit over the 2700-3000 cm^{-1} interval in the FTIR spectrum [1].

With the aim to facilitate the comparisons between different samples, the SA concentration was expressed as percentage (%) in the photocatalytic efficiency plots. **Table A.2** presents the integrated area and concentration of stearic acid at each time and **Figure A.3** shows the final photocatalytic efficiency plot made from data of **Table A.1**. All the photocatalytic efficiency plots reported in this thesis were made using the same procedure.

Table A.1. Integrated area and SA concentration.

Time (min)	Area 2700-3000 cm^{-1}	SA molecules/cm^2	SA %
0	8.6109	2.73×10^{16}	100.00
20	6.7554	2.14×10^{16}	78.39
40	5.2519	1.66×10^{16}	60.81
60	4.1794	1.32×10^{16}	48.35
90	3.0631	9.71×10^{15}	35.57
120	2.5186	7.98×10^{15}	29.23
150	2.4094	7.64×10^{15}	27.99
180	2.0286	6.43×10^{15}	23.55
240	1.8555	5.88×10^{15}	21.54
300	1.6841	5.34×10^{15}	19.56
360	0.0017	5.39×10^{12}	0.002

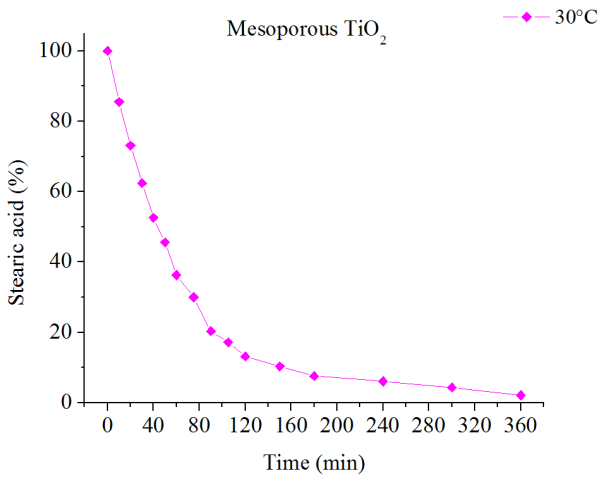

Figure A.3. Photocatalytic efficiency plot of a mesoporous TiO_2 coating tested at 30 °C and $R.H._{room}$

Reference

[1]. Paz, Y.; Luo, Z.; Rabenberg, L.; Heller, A. *Photooxidative self-cleaning transparent titanium dioxide films on glass*. J. Mater. Res. **1995**;10:2842.

APPENDIX B

DETERMINATION OF INITIAL DEGRADATION RATES

Depending of the trends in SA photodegradation observed in the different processes evaluated in this work, the kinetic modelling was obtained using two methods:

(i) Calculation of the degradation rate through the slope of the plot SA concentration *vs.* time or

(ii) Using the pseudo first order kinetic equation proposed by Sawunyama et al., 1997.

As stated in **Chapter 4**, it is difficult to develop a model for the dependence of the photocatalytic degradation rate on the experimental parameters for the whole treatment time [1] so, kinetic modelling of the photocatalytic processes was restricted to the analysis of the *initial rate* of photocatalytic degradation, r_i.

B.1. Calculation of the degradation rate through the plot SA concentration *vs.* time or

This methodology was utilized when the initial trend from the photocatalytic efficiency plot revealed a zero apparent reaction order with respect to the stearic acid concentration [2, 3]. An example of this trend is shown in **Figure B.1** (note that only the first 90 min of reaction are considered and that for this calculation the SA concentration is expressed in molecules cm^{-2}).

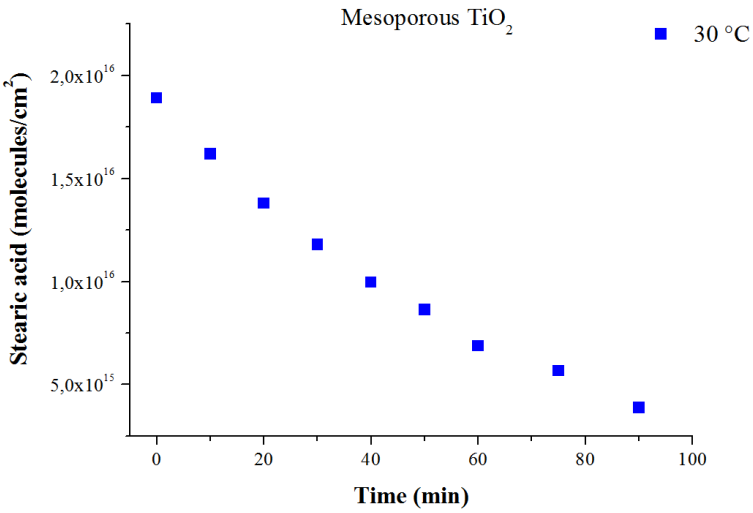

Figure B.1. Photocatalytic efficiency plot of the mesoporous TiO_2 coating tested at 30 °C and $R.H._{room}$. SA concentration has been expressed as molecules cm^{-2}.

The slope of the line, i.e., r_i, was calculated using the software Origin Pro 8. **Figure B.2** displays the obtained results.

From the results displayed in **Figure B.2**, it can be concluded that the r_i of a mesoporous TiO_2 coating tested at 30 °C and $R.H._{room}$ using SA is $1.64 \times 10^{14} \pm 1.12 \times 10^{13}$ SA molecules cm^{-2} min^{-1}.

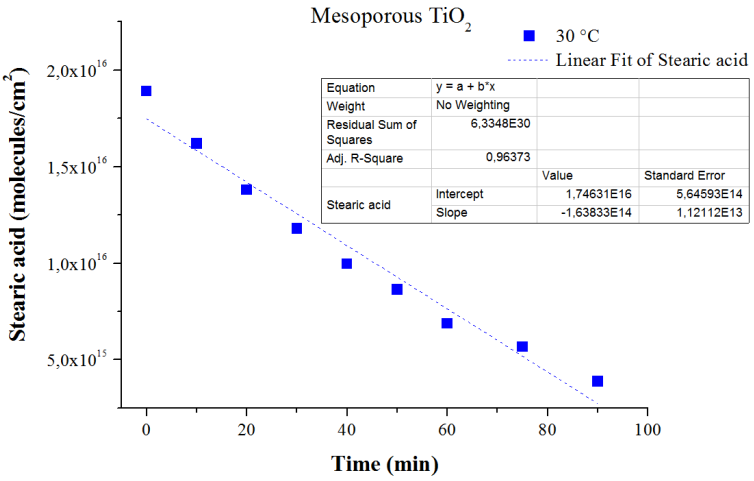

Figure B.2. Calculation of the r_i through the slope of the plot SA concentrations *vs* time.

B.2. Calculation of the degradation rate through the pseudo first order kinetic equation proposed by Sawunyama et al.

As stated in **Chapter 4**, the pseudo first order kinetic equation proposed by Sawunyama et al. [4] incorporates the reactivity of TiO_2 film and film disorganization phenomenon during the photodegradation process:

$$[SA]_t = [SA]_{initial}\exp(-k_{obs}t) \quad \textbf{[B.1]}$$

where $[SA]_t$ is the concentration of stearic acid at time t, $[SA]_{initial}$ is the initial concentration of stearic acid, and k_{obs} is the pseudo first order rate constant.

The calculation of r_i through **Equation B.1** was made when the data contained in the photocatalytic efficiency plots were not accurately modelled by the slope approach. **Figure B.3** presents the photocatalytic efficiency plot of the mesoporous TiO_2 coating tested at 10 °C and RH_{room}. It can be seen that in this case, the data do not follow an apparent zero-order with respect to the stearic acid concentration.

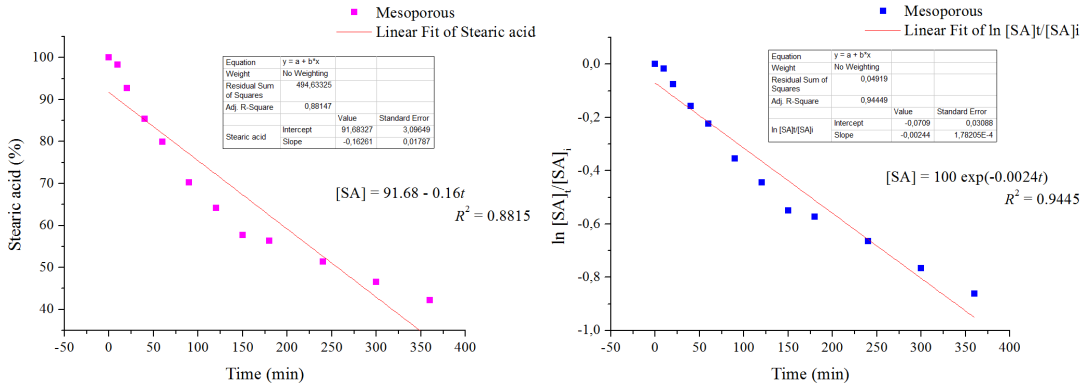

Figure B.3. Photocatalytic efficiency plots of the mesoporous TiO_2 coating tested at 10 °C and RH_{room}. SA concentration has been expressed as %.

In this case, the r_i (expressed as k_{obs}) was calculated from **Equation B.1**. For the example shown in **Figure B.3**, $r_i = 0.0024 \pm 0.0002$ min^{-1}.

References

[1]. Kim, S. B.; Hong, S. C. *Kinetic study for photocatalytic degradation of volatile organic compunds in air using thin film TiO2 photocatalyst*. Appl. Catal. B **2002**;35:305.

[2]. Paz, Y.; Luo, Z.; Rabenberg, L.; Heller, A. *Photooxidative self-cleaning transparent titanium dioxide films on glass*. J. Mater. Res. **1995**;10:2842.

[3]. Mills, A.; Lepre, A.; Elliot, N.; Bhopal, S.; Parkin, I. P.; O'Neill, S. A. *Characterisation of the photocatalyst Pilkington Activ^{TM}: a reference film photocatalyst?*. J. Photochem. Photobiol. A **2003**;160:213.

[4]. Sawunyama, P.; Jiang, L.; Fujishima, A.; Hashimoto, K. *Photodecomposition of a Langmuir-Blodgett film of stearic acid on TiO_2 film observed by in situ Atomic Force Microscopy and FT-IR*. J. Phys. Chem. B **1997**;101:11000.

APPENDIX C

DETERMINATION OF BAND GAP ENERGY VALUES

The E_g values for all samples were calculated from the UV–Vis spectra using the **Equation C.1**:

$$\alpha(h\nu) = A(h\nu - E_g)^{m/2} \qquad \textbf{[C.1]}$$

where α is the absorption coefficient, $h\nu$ is the photon energy, A is a constant; and $m = 1$ represents a direct transition between the valence band and conduction band [1-3].

For the estimation of E_g from the UV-Vis spectra, a straight line is extrapolated from the adsorption curve to the abscissa axis, as shown in the example of **Figure C.1**. When α has a value of 0, then $E_g = h\nu$.

The signal interferences observed in the UV-Vis spectrum of **Figure C.1** are due to organic residues from the photocatalyst synthesis that probably remained entrapped in the sample and were not calcined during the annealing process.

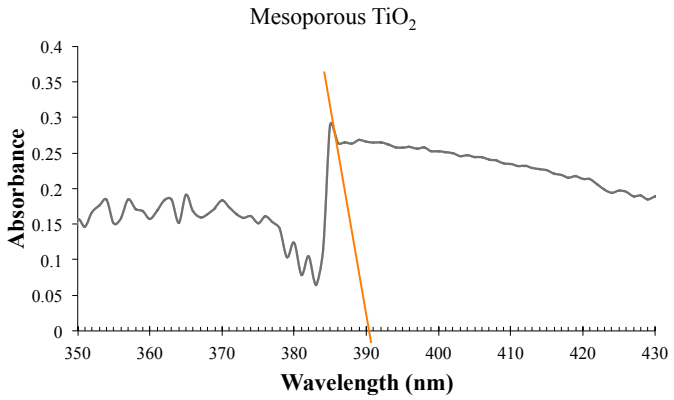

Figure C.1. UV-Vis spectra of the mesoporous TiO_2 coating.

The calculated E_g value for this example (TiO_2 coating) is 3.18 eV. This value is in well agreement with that commonly reported for TiO_2 (3.2 eV (Hashimoto et al., 2005; Garza-Tovar et al., 2006)).

References

[1]. Garza-Tovar, L.L.; Torres-Martínez, L. M.; Bernal Rodríguez, D.; Gómez, R.; del Angel, G. *Photocatalytic degradation of methylene blue on Bi_2MNbO_7 (M = Al, Fe, In, Sm) sol-gel catalysis*. J. Mol. Catal. A **2006**;247:283.

[2]. Murphy, A. B. *Band-gap determination from diffuse reflectanse measurements of semiconductor films, and application to photoelectrochemical water-splitting.* Solar Energy Mater. Solar Cells **2007**;91:1326.

[3]. Torres-Martínez, L. M.; Cruz-López, A.; Juárez-Ramírez, I.; Meza-de la Rosa, Ma. E. *Methylene blue degradation by $NaTaO_3$ sol-gel doped with Sm and La.* J. Hazard. Mater. **2009**;165:774.